

EFFECTS OF AQUATIC VEGETATION ON SEDIMENT TRANSPORT

Àlex Ros i Sala

Per citar o enllaçar aquest document:
Para citar o enlazar este documento:
Use this url to cite or link to this publication:
<http://hdl.handle.net/10803/401629>



<http://creativecommons.org/licenses/by-nc/4.0/deed.ca>

Aquesta obra està subjecta a una llicència Creative Commons Reconeixement-
NoComercial

Esta obra está bajo una licencia Creative Commons Reconocimiento-NoComercial

This work is licensed under a Creative Commons Attribution-NonCommercial licence



DOCTORAL THESIS

EFFECTS OF AQUATIC VEGETATION ON
SEDIMENT TRANSPORT

Àlex Ros i Sala

2016

Doctoral Programme in Experimental Sciences and Sustainability

Supervisors:

Teresa Serra Putellas

Xavier Casamitjana Vila

Thesis submitted for the degree of Doctor of Philosophy by the University of Girona

La Dra. Teresa Serra Putellas, professora Titular del Departament de Física, i el Dr. Xavier Casamitjana Vila, professor Catedràtic del Departament de Física de la Universitat de Girona,

CERTIFIQUEN:

Que aquest treball, titulat “effects of aquatic vegetation on sediment transport”, que presenta l'Àlex Ros i Sala per a l'obtenció del títol de doctor, ha estat realitzat sota la seva direcció.

I perquè així consti, signen aquest certificat el 30 d'abril de 2016.

Dra. Teresa Serra Putellas Dr. Xavier Casamitjana Vila

Agraïments

Aquesta tesi ha estat possible gràcies a la col·laboració de moltíssimes persones que m'han recolzat al llarg del camí.

Els meus tutors de tesi, la Dra. Teresa Serra i el Dr. Xavier Casamitjana, del Departament de Física, per confiar en mi, per l'interès que han mostrat en tot moment pels progressos que feia, i que mai no han tingut un no per resposta. Ells han sabut animar-me en els moments on les coses no sortien, gràcies!

També del Departament de Física, el Dr. Jordi Colomer i la Dra. Marianna Soler, que m'han ajudat amb els experiments i en l'anàlisi dels resultats.

M'agradaria agrair la tasca del Personal d'Administració i Serveis de la Universitat de Girona. La seva feina moltes vegades no és gaire sabuda, però ha estat del tot necessària per poder realitzar aquesta tesi. Molt especialment a l'Anna Espígol, en Xevi Baca, en Pere Bellvehí, ... sempre hi han estat quan els he necessitat.

Els meus companys de "camarote", amb qui tots els dies he compartit alegries i penes al despatx o al laboratori: la Dra. Dolors Pujol, la Dra. Montse Costa, la Dra. Nazha El Allaoui i el Dr. Aarón Enríquez.

Moltes són les persones que en un moment o un altre m'han donat un cop de mà i han vingut al laboratori per ajudar-me amb els experiments: Maria Sànchez (Sussa), Maria Casellas, Dídac Palma, Albert Palomer, David Faulon, Ramon Jové, Andrea Mercadé, Guillem Arrufat, Pol Giribet i Joan Martell. I els que des de casa sempre m'han escoltat i animat quan he parlat dels meus alts i baixos fent la tesi: Anna, Carlota, Judit i Pau.

La Colla Castellera Xoriguers de la UdG, els Óssos Rentadors, el Consell d'Associacions, i tot el personal de Rectorat amb qui tants anys he compartit la meva vida extra acadèmica, que també m'han ensenyat molt. Especialment la Dra. Sílvia Font, el Dr. Sergi Bonet, la Núria Rigau i l'Oriol Carreras. Gràcies pels moments compartits.

Vull donar les gràcies a totes les persones amb qui he compartit tants anys a la universitat i que també és gràcies a tots ells que he acabat fent aquesta tesi a la Universitat de Girona. Del pas per la UPC la Clàudia, l'Ester i en Guillem. La llicenciatura de geologia no hauria estat el mateix sense l'Anna, l'Albert i en Lisard. A tots els que em van acollir durant la meva estada a la Universidad Nacional Autónoma de México, gràcies Danae, Emilio, Rodrigo i Rebeca. I finalment els companys del màster de l'aigua, Marta i Lluís.

I per acabar vull agrair molt especialment el suport que he rebut i l'interès que sempre ha mostrat la meva família, els meus pares Maria dels Àngels i Òscar, els meus tiets Glòria, Lluïsa i Eduard, i tota la família de Mèxic, molt especialment la tieta Pepi i el tiet Louis, amb qui també he compartit una part important de la meva carrera.

Contents

Abstract	i
Resum	iii
Resumen	v
List of Abbreviations	vii
List of Figures	viii
List of Tables	xii
Publications and communications related to the thesis	xiii
Peer-reviewed papers (published/accepted)	xiii
Oral communications	xiii
<i>Chapter 1: Introduction</i>	1
1.1. Wetlands sediment characteristics	2
1.2. Previous studies describing turbulence inside meadows	3
1.2.1. Waves	3
1.2.2. Oscillating grid turbulence	4
1.2.3. Gravity currents produced by instantaneous releases	5
1.3. Research objectives	6
1.4. Organization	6
<i>Chapter 2: Materials and methods</i>	9
2.1. LISST	9
2.2. Acoustic Doppler Velocimetry	10
2.3. Turbidity sensors	12
2.4. Sediment characteristics	12
<i>Chapter 3: Experimental observations on sediment resuspension within submerged model canopies under oscillatory flow</i>	15
3.1. Background	16
3.2. Procedure	17
3.2.1. Experimental setup	17
3.2.2. Vegetation models	18
3.2.3. Measuring techniques	20
3.2.4. Methods of analysis	21
3.2.5. Sediment characteristics	22
3.3. Results	25
3.3.1. Physical basis of hydrodynamics within a canopy under progressive waves	25
3.3.2. Sediment resuspension within canopy models	31
3.4. Discussion	36
3.4.1. Canopy scale turbulence distribution	36
3.4.2. Sediment resuspension within canopies	39
3.5. Conclusions	40

<i>Chapter 4: Sediment resuspension within submerged vegetation model canopies in an oscillating grid chamber</i>	41
4.1. Background	41
4.2. Procedure	44
4.2.1. Experimental setup	44
4.2.2. Vegetation models	44
4.2.3. Sediment bed emplacement	49
4.2.4. Turbulence measurements	50
4.2.5. Sediment entrainment measurements	52
4.3. Results and discussion	52
4.3.1. Turbulent field in the presence of a bottom canopy	52
4.3.2. Sediment resuspension in the presence of a bottom canopy	57
4.4. Conclusions	61
<i>Chapter 5: Influence of extreme flooding events on wetlands</i>	63
5.1. Background	63
5.2. Procedure	66
5.2.1. Experimental set up	66
5.2.2. Vegetation models	66
5.2.3. Theory	68
5.2.4. Turbulence measurements	69
5.2.5. Sediment characteristics	69
5.2.6. Sediment measurements	69
5.2.7. Calculation of the mean flow and the turbulent kinetic energy	70
5.3. Results and discussion	71
5.3.1. Turbulent field in the presence of a canopy.....	71
5.3.2. Sediment transport.....	76
5.4. Conclusions	79
<i>Chapter 6: General discussion</i>	81
6.1. Hydrodynamics	81
6.1.1. Plant density effects.....	81
6.1.2. Plant flexibility effects	82
6.2. Sediment transport	83
6.2.1. Plant density effects.....	83
6.2.2. Plant flexibility effects	84
6.3. Ecological implications	84
6.4. Future perspectives	85
<i>Chapter 7: Conclusions</i>	87
<i>Chapter 8: References</i>	89
<i>Appendix</i>	99

Abstract

In the margins of continents there are the coastal zones, regions of remarkable biological productivity. Coastal zones include, among others, wetlands, that are land areas inundated permanently or seasonally, characterized by the presence of aquatic vegetation adapted to the hydric soil. Therefore it is necessary to consider the effect of aquatic canopies in wetlands investigations. These areas are governed by physical forces originated from tidal currents, waves, winds, night convection and floods. The aim of this thesis is to study the sediment transport in wetlands in which fluid is dominated by a) progressive waves, b) nearly isotropic turbulence and c) extreme flooding events.

The study of sediment transport under progressive waves corresponds to Chapter 3. The experiments were conducted on a laboratory channel, and three vegetation models (rigid, flexible and real plants of *Ruppia maritima*) were considered with different plant densities. Also different wave frequencies were used. The aim of the study was to understand the relation between the morphology of canopies (flexibility and density) in front of the physical forcing, and its effect on sediment resuspension from a bed of cohesive sediment. The experiments showed that the sediment resuspension is related to TKE. Some of the canopy densities (real and flexible plants, and rigid plants at high density and high wave frequencies) reduce TKE, and thus reduce sediment resuspension, in contrast to the sparse rigid canopies at low wave frequencies, that increase TKE and enhance sediment resuspension.

Chapter 4 describes the effect of canopies on sediment resuspension by nearly isotropic turbulence. The experiments were conducted on an oscillating grid chamber, with either submerged rigid and flexible canopies with different plant densities. This chapter was aimed to investigate the protecting capacity of soil erosion by submerged canopies, in front of turbulence. The concentration of suspended sediment is a linear function of the TKE. All of the canopies used in the experiment reduce sediment resuspension, except sparse canopies of flexible plants that increase TKE by the freely movement of its blades.

The third part of this thesis (Chapter 5) is the study of extreme flooding events of different intensities. The experiments were made with emergent rigid vegetation on a laboratory

channel, and floods were simulated by discharging particle-laden water into water free of particles. The flood was composed by a mean flow and a gravity current that advanced through the channel across the vegetated area. The aim of this study was to understand the effect of canopies in flooding events and the depositional rates from this particle-laden gravity current. The canopies can reduce the maximum velocity of the flow. The progression of the gravity current that follows the mean flow is modified by the presence of plants from an inertial-dominated regime to a viscous-dominated regime. Emergent plants also enhance sediment deposition.

Chapter 6 illustrates the general discussion, and Chapter 7 presents the overall conclusion of this thesis.

Chapter 3 is an adaptation of the published article in *Continental Shelf Research*. A copy of this article can be found in the appendix.

Resum

Als marges dels continents hi ha les zones costaneres, regions d'altra productivitat biològica. Les zones costaneres inclouen, entre d'altres, els aiguamolls, que són zones terrestres inundades permanentment o estacionalment, caracteritzades per la presència de vegetació aquàtica adaptada a sols hídrics. És per tant necessari considerar l'efecte de les praderies aquàtiques en les investigacions en aiguamolls. Aquestes àrees estan governades per forces físiques originades per corrents de mareas, ones, vent, conveccions nocturnes i inundacions. L'objectiu d'aquesta tesi és estudiar el transport de sediments en aiguamolls on el fluid és dominat per a) ones progressives, b) turbulència gairebé isòtropa i c) inundacions extremes.

L'estudi del transport de sediments per ones progressives correspon al Capítol 3. Els experiments es van realitzar en un canal de laboratori, i es van utilitzar tres models de vegetació (plantes rígides i flexibles, i plantes reals de *Ruppia maritima*) amb diferents densitats de plantes. També es van considerar diferents freqüències d'oscil·lació. L'objectiu d'aquest estudi era entendre la relació entre la morfologia de les praderies (flexibilitat i densitat) davant de les forces físiques, i el seu efecte en la resuspensió de sediments d'un llit de sediments cohesius. Els experiments mostren que la resuspensió de sediments està relacionada amb la TKE. Algunes de les densitats de plantes (flexibles i reals, i rígides a altes densitats de plantes i altes freqüències de les ones) redueixen la TKE, i per tant redueixen la resuspensió de sediments, contràriament al que passa amb les plantes rígides espaiades i baixes freqüències de les ones, que incrementen la TKE i afavoreixen la resuspensió de sediments.

El Capítol 4 descriu els efectes de les praderies en la resuspensió de sediments degut a turbulència gairebé isòtropa. Els experiments es van fer en una cambra amb xarxa oscil·lant, tant amb vegetació submergida rígida com flexible, amb diferents densitats de plantes. Aquest capítol pretén investigar la capacitat de protecció contra l'erosió del sòl de les praderies submergides, davant de la turbulència. La concentració de sediment en suspensió és una funció lineal amb la TKE. Totes les praderies utilitzades en els experiments redueixen la resuspensió de sediments, excepte les praderies de plantes flexibles a baixes densitats de plantes que incrementen la TKE degut al moviment lliure de les fulles.

La tercera part de la tesi (Capítol 5) és l'estudi dels esdeveniments d'inundacions extremes de diferents intensitats. Els experiments es van realitzar amb vegetació emergent en un canal de laboratori, i les inundacions van ser simulades mitjançant descàrregues d'aigua carregada de partícules en aigua sense partícules. La inundació estava composta per un corrent principal i un corrent de gravetat que avançava pel canal a través de la zona vegetada. L'objectiu d'aquest estudi era entendre l'efecte de les praderies en els esdeveniments d'inundacions extremes i la quantitat de sediment dipositat pel corrent de gravetat. Les praderies poden reduir la velocitat màxima del flux. La progressió del corrent de gravetat que segueix el corrent principal es modifica per la presència de plantes, i passa d'un règim dominat per la inèrcia a un règim viscos. Les plantes emergents també afavoreixen la deposició de sediments.

El Capítol 6 il·lustra la discussió general, i el Capítol 7 presenta unes conclusions generals d'aquesta tesi.

El Capítol 3 és una adaptació de l'article publicat a *Continental Shelf Research*. Es pot trobar una còpia de l'article als annexos.

Resumen

En los márgenes de los continentes se encuentran las zonas costeras, regiones de alta productividad biológica. Las zonas costeras incluyen, entre otros, los humedales, que son zonas terrestres inundadas permanentemente o estacionalmente, caracterizadas por la presencia de vegetación acuática adaptada a los suelos hídricos. Por lo tanto es necesario considerar el efecto de las praderas acuáticas en las investigaciones en humedales. Estas áreas están gobernadas por fuerzas físicas originadas por corrientes de mareas, olas, viento, convecciones nocturnas e inundaciones. El objetivo de ésta tesis es estudiar el transporte de sedimento en humedales en donde el fluido está dominado por a) olas progresivas, b) turbulencia casi isótropa y c) inundaciones extremas.

El estudio del transporte de sedimentos por olas progresivas corresponde al Capítulo 3. Los experimentos se realizaron en un canal de laboratorio, y se hicieron servir tres modelos de vegetación (plantas rígidas y flexibles, y plantas reales de *Ruppia maritima*) con distintas densidades de plantas. También se consideraron diferentes frecuencias de oscilación. El objetivo de este estudio era entender la relación entre la morfología de las praderas (flexibilidad y densidad) frente a las fuerzas físicas, y su efecto en la resuspensión de sedimentos desde una cama de sedimentos cohesivos. Los experimentos mostraron que la resuspensión de sedimentos está relacionada con la TKE. Algunas densidades de las praderas (plantas flexibles y reales, y plantas rígidas a altas densidades de plantas y altas frecuencias de las olas) reducen la TKE, y por lo tanto reducen la resuspensión de sedimentos, contrariamente a lo que sucede con las praderas de plantas rígidas a bajas densidades de plantas y frecuencias de las olas bajas, que incrementan la TKE y favorecen la resuspensión de sedimentos.

El Capítulo 4 describe los efectos de las praderas en la resuspensión de sedimentos debido a la turbulencia casi isótropa. Los experimentos se realizaron en una cámara con una red oscilante, tanto con vegetación sumergida rígida como flexible, con distintas densidades de plantas. Éste capítulo pretende investigar la capacidad de protección contra la erosión del suelo de las praderas sumergidas, frente a la turbulencia. La concentración de sedimentos en suspensión es una función lineal de la TKE. Todas las praderas que se han hecho servir en los experimentos

reducen la resuspensión de sedimentos, excepto las praderas de plantas flexibles a baja densidad de plantas, que incrementan la TKE debido al movimiento libre de las hojas.

La tercera parte de la tesis (Capítulo 5) es el estudio de los eventos de inundaciones extremas de distintas intensidades. Los experimentos se realizaron con vegetación emergente en un canal de laboratorio, y las inundaciones fueron simuladas mediante descargas de agua cargadas de partículas en agua sin partículas. La inundación estaba compuesta por una corriente principal y una corriente de gravedad que avanzaba por el canal a través de la zona vegetada. El objetivo de éste estudio era entender el efecto de las praderas en los eventos de inundaciones extremas y la cantidad de sedimento depositado por la corriente de gravedad. Las praderas pueden reducir la velocidad máxima del flujo. La progresión de la corriente de gravedad que sigue al flujo principal se modifica por la presencia de plantas, desde un régimen dominado por la inercia a un régimen viscoso. Las plantas emergentes también favorecen la deposición de sedimentos.

El Capítulo 6 ilustra la discusión general y el Capítulo 7 presenta unas conclusiones generales de ésta tesis.

El Capítulo 3 es una adaptación del artículo publicado en *Continental Shelf Research*. Se puede encontrar una copia del artículo en los anexos.

List of Abbreviations

ADV	Acoustic Doppler Velocimeter
ERV	Emergent Rigid Vegetation
Fig.	Figure
LISST	Laser in situ scattering and transmissometry
OGT	Oscillating Grid Turbulence
PVC	Polyvinyl chloride
rms	Root mean square
Rup	<i>Ruppia maritima</i>
SFV	Submerged Flexible Vegetation
SPF	Solid Plant Fraction (%)
SRV	Submerged Rigid Vegetation
SREV	Submerged Real Vegetation
TKE	Turbulent Kinetic Energy ($\text{m}^2 \cdot \text{s}^{-2}$)
TSS	Total Suspended Sediment ($\text{g} \cdot \text{L}^{-1}$)
TURB	Turbidity sensor
WP	Without plants

List of Figures

Fig. 1.1. States of cohesive sediments (Whitehouse et al., 2000).....	3
Fig. 1.2. a. Low wave penetration, b. High wave penetration.	4
Fig. 1.3. Schematic of a gravity current within a canopy. h_w is the water depth, ρ_1 and ρ_2 are the densities of the denser (gray) and the lighter (white) fluids, respectively.	5
Fig. 2.1. (a) LISST-100X (Sequoia scientific, Inc., Washington, USA). (b) Scheme of the sample volume and the ring detectors.	10
Fig. 2.2. (a) SonTek 16-MHz MicroADV. (b) Scheme of the acoustic transmitter and the three acoustic receivers.	11
Fig. 2.3. Seapoint Turbidity Meter.....	12
Fig. 2.4. (a) Location of Empordà Marshes Natural Park and Baix Ter Natural Park in NE Catalonia. (b) Empordà Marshes Natural Park. (c) Baix Ter Natural Park.	13
Fig. 2.5. Particle size distribution for the sediment used in Chapter 3 experiments (a) and Chapters 4 and 5 experiments (b).....	13
Fig. 3.1. (a) Scheme of the experimental set-up. Experiments were conducted in a 6 m long flume. The streamwise coordinate is denoted by x , with x positive in the downstream direction, and $x = 0$ at the mean position of the wave maker. The vertical coordinate is z , with $z = 0$ at the bed. The mean water depth, h , is 30 cm. The plant height in still water is $h_v = 14$ cm. The model meadow was 250 cm long. The horizontal dashed lines indicate the position of the velocity (ADV) and sediment concentration measurements, both turbidity and particle sediment concentration (TURB+LISST). The beach slope at the end of the tank is not scaled. (b) Picture of the submerged rigid canopy. (c) Picture of the submerged flexible canopy. (d) Picture of the submerged real canopy (<i>R. maritima</i>).	19

Fig. 3.2. Particle size distribution for the salt marsh sediment used in the experiments. Vertical dashed lines in the figure represent the classification by van Rijn (2007) where range a (small particles) corresponds to the particle range of clay and very fine silts (very cohesive sediment), range b (large particles) corresponds to the particle range of fine, coarse silts and fine sands (weakly cohesive sediment) and range c corresponds to fine sands.....24

Fig. 3.3. Wave velocities at $z/h_v = 0.4$ for the different SPF studied and for rigid (a) and flexible (b) canopies. The solid line represents the theoretical value predicted for the no canopy case by the linear wave theory and calculated from equation 3.4 for the range of the wave frequencies studied.....26

Fig. 3.4. Relation between ΔTKE (%), calculated using equation 3.6, with the wave frequency for different canopy densities (SPF). Results for submerged rigid canopy models (SRV) are presented in the left hand panels (a, c and e), while results for submerged flexible canopy models (SFV) are presented in the right hand panels (b, d and f). Top panels (a and b) correspond to the results for $z/h_v = 1.6$, middle panels (c and d) correspond to the results for $z/h_v = 1.1$ and bottom panels correspond to the results for $z/h_v = 0.4$. Results for *R. maritima* (Rup) were included in all the plots. Vertical error bars are presented for the lowest and largest frequencies and for 1% and 10% canopy densities.....30

Fig. 3.5. Relationship between ΔC (%), calculated using equation 3.7, for the particle range of diameters from 2.5 to 6.0 μm with the frequency for the different canopy densities (SPF). The representation of the results was the same like that used in Fig. 3.4.32

Fig. 3.6. Relationship between ΔC (%), calculated using equation 3.7, for the particle range of diameters from 6.0 to 100 μm with the frequency for the different canopy densities (SPF). The representation of the results was the same like that used in Fig. 3.4.....33

Fig. 3.7. Ratio between $u'w'$ for vegetated experiments and $u'w'$ for the vegetation-free experiments against ΔC , for experiments carried out with the three canopy models. (a) 2.5 to 6.0 μm particles and (b) 6.0 to 100 μm particles.....35

Fig. 3.8. TKE/U_w^2 vs. A_w/S , calculated at $z/h_v = 0.4$ for both rigid and flexible vegetation. ...37

Fig. 3.9. Relationship between ΔTKE and the stem Reynolds number (Re_p) for the different canopy models used at $z/h_v = 0.4$.	38
Fig. 4.1. Scheme of the experimental set-up. A and B represents the position of the water velocity measurements.	45
Fig. 4.2. Illustration of the submerged aquatic vegetation models: (a) submerged rigid vegetation; (b) submerged flexible vegetation; and plots of plants distributions: (c) SPF = 0.5 %; (d) SPF = 1 %; (e) SPF = 1.5 %; (f) SPF = 2.5 %; (g) SPF = 5 %; (h) SPF = 7.5 %; (i) SPF=10 %	46
Fig. 4.3. Plot of the lateral obstruction percentage: (a) Submerged flexible vegetation, (b) Submerged rigid vegetation.	47
Fig. 4.4. Particle size distribution for the salt marsh sediment used in the experiments. Vertical dash line represent the classification by Rijn (2007). The smaller particles ($d_p < 6 \mu m$) correspond to the particle range of clay and very fine silts (very cohesive sediment). Vertical dashed lines represent the limits between different particle size ranges	50
Fig. 4.5. TKE profiles for experiments carried without plants, and flexible and rigid vegetation with SPF = 5 %, and $F = 4.8$ Hz	53
Fig. 4.6. Relationship between the TKE the SPF for different oscillating frequencies for both rigid (a) and flexible (b) canopies.	55
Fig. 4.7. Turbulent kinetic energy spectrums above the canopy ($z = 11$ cm) and within the canopy ($z = 22$ cm) for the experiments: (a) without plants; (b) submerged rigid vegetation (SPF = 7.5 %); (c) submerged flexible vegetation (SPF = 7.5 %); (d) submerged flexible vegetation (SPF = 1 %)	56
Fig. 4.8. Time evolution in the sediment concentration for experiments carried out for both rigid and flexible canopies for SPF = 5 %. The dashed line shows the evolution of the oscillating frequency in a set of experiments	58
Fig. 4.9. Relationship between the suspended sediment concentration at the steady state (C_{ss}) and the SPF for different oscillating frequencies for both rigid (a) and flexible (b) canopies.	59

Fig. 4.10. Relationship between the total suspended sediment (TSS) and Turbulent Kinetic Energy (TKE) for either rigid, flexible and the without plants experiments. The dashed line shows the results for this relationship found by Orlins and Gulliver (2003). The thick black line shows the results of the experiments of this thesis.....60

Fig. 5.1. Scheme of the experimental set-up.67

Fig. 5.2. u_{\max} profiles along the channel for the different discharge heights (H). (a) without plants. (b) SPF = 1%. (c) SPF=2.5%. (d) SPF=5%.....71

Fig. 5.3. TKE profiles along the channel for the different discharge heights (H). (a) without plants. (b) SPF = 1%. (c) SPF=2.5%. (d) SPF=5%.....72

Fig. 5.4. Theoretical velocity compared to maximum velocity, at $x = 120$ cm. (a) SPF = 1 %. (b) SPF = 2.5 %. (c) SPF = 5 %.73

Fig. 5.5. u^* profiles along the channel for the different discharge heights (H). (a) without plants. (b) SPF = 1 %. (c) SPF = 2.5 %. (d) SPF = 5 %.74

Fig. 5.6. u_{\max} profiles along the channel for the differents discharge heights (H) and for the without plants experiments. (a) u_{\max} calculated following (Çengel and Cimbala, 2006). (b) u^*75

Fig. 5.7. Soil roughness (y_0) vs. SPF.....76

Fig. 5.8. Relationship between x/H and t/t^* . (a) SPF=5%. (b) Without plants.77

Fig. 5.9. Sediment rate deposited in the traps ($x = 120, 180$ and 240 cm) for both experiments without plants and with plants (SPF = 5 %). (a) $H = 5$ cm. (b) $H = 10$ cm. (c) $H = 15$ cm.78

List of Tables

Table 3.1. Wave and vegetation parameters for the experiments carried out: solid plant fraction (SPF), number of stems per square meter, wave frequency, the corresponding wavelengths calculated from the dispersion equation (Dean and Dalrymple, 1991) and the A_w/S parameter measured at $z/h_v = 1.1$, where $A_w = U_w/(2\pi F)$ and S is the plant-to-plant distance.	27
Table 4.1. Vegetation parameters for the experiments carried out: solid plant fraction, number of stems per square meter, oscillating grid frequency.....	48
Table 4.2. Summary of TKE, dissipation (ϵ), Kolmogorov scale (η), Taylor scale (λ_T) and integral length scale (l).	56
Table 5.1. Vegetation parameters for the experiments carried out: solid plant fraction, number of stems per square meter and H	67
Table 5.2. Soil roughness (y_0) and grain diameter (d_p).....	76

Publications and communications related to the thesis

Peer-reviewed papers (published/accepted)

Ros, À., Colomer, J., Serra, T., Pujol, D., Soler, M., Casamitjana, X., 2014. Experimental observations on sediment resuspension within submerged model canopies under oscillatory flow. *Continental Shelf Research*. 91, 220-231.

Oral communications

Ros, À., Colomer, J., Serra, T., Pujol, D., Soler, M., Marín, D., Casamitjana, X., 2013. Motion of phytoplankton patches due to periodic wind forcing. *SedNet Conference 2013, 8th International SedNet Conference (Lisbon, Portugal)*.

Soler, M., Colomer, J., Serra, T., Ros, À., El-Allaoui, N., Pujol, D., Casamitjana, X., 2013. Estructura hidrodinámica de humedales y praderas de posidonia. Modificaciones causadas por GAPS y efectos en el transporte de sedimentos. Centro de investigación científica y educación superior de Ensenada (CICESE), Ensenada, BC, México.

Ros, À., Colomer, J. Serra, T., Pujol, D., Soler, M., Casamitjana, X., 2014. Sediment resuspension within submerged model canopies under oscillatory flow. *International Workshop on Physical Processes in Natural Waters (Trento, Italy)*.

Chapter 1: Introduction

Coastal ecosystems, found along continental margins, are regions of remarkable biological productivity and high accessibility. Coastal ecosystems provide a wide array of goods and services: they host the world's primary ports of commerce; they are the primary producers of fish, shellfish, and seaweed for both human and animal consumption; and they are also a considerable source of fertilizer, pharmaceuticals, cosmetics, household products, and construction materials. However, these areas are one of the most threatened ecosystems, due to the high accessibility and the economic activity (Halpern et al., 2008; Lotze et al., 2006). The coastline of the European Union extends more than 170 000 km, and host more than 70 million inhabitants (Ondiviela et al., 2014). Most of this coastline is highly populated and threatened by erosion and flooding (Alcamo et al., 2007). Coastal ecosystems include seagrasses, mangroves, grasslands and wetlands.

A wetland is an ecological community that is inundated either year around or seasonally. Two general categories of wetlands are recognized: coastal or tidal wetlands, and inland or non-tidal wetlands. Tidal (coastal) marshes occur along coastlines and are influenced by tides and often by freshwater from runoff, rivers, or groundwater. Salt marshes are the most prevalent types of tidal marshes and are characterized by salt tolerant plants such as *Spartina alterniflora*, *Salicornia europaea*, and *Ruppia maritima*. Salt marshes have one of the highest rates of primary productivity associated with wetland ecosystems because of the inflow of nutrients and organics from surface and/or tidal water. Wetlands cover around 4% of the Earth's land surface, and produce 22.6% of the net primary production, 2000 g·m⁻² every year.

Besides its ecological importance, wetlands and salt marshes are particularly important in protecting the coastline, because they serve a buffering function between sea and land, dissipating the energy of tidal currents and waves (Coulombier et al., 2012). The vertical position of salt marsh surfaces is controlled by the sediment deposition, to which the persistence of the coastal wetlands depends (Reed, 1995). One of the main mechanisms

behind the reductive effect of macrophytes on sediment movement is their effect on hydrodynamics. Macrophytes can substantially reduce water flow velocity and turbulence compared with macrophyte-free areas (Vermaat et al., 2000; Madsen et al., 2001; Pujol et al., 2010).

The following sections in this introduction give a brief overview of the wetlands sediment characteristics and the previous studies about turbulence inside meadows. The research objectives and the thesis structure are detailed in later on this introduction.

1.1. Wetlands sediment characteristics

Cohesive sediments occur commonly in wetlands and salt marshes. The cohesive properties of sediment are exhibited with sediments containing more the 10% by mass of fine material (finer than 63 μm). Whereas the mobility and transport of sandy sediments are controlled by the particle size of the bed sediment, in cohesive sediments are the bulk properties that determine the behavior of the sediment (Whitehouse et al., 2000).

The complexity of cohesive sediment may be demonstrated by reference to a characterization of cohesive sediment (Hayter and Mehta, 1982). It includes a considerable number of parameters that need to be determined to completely describe cohesive sediments (type of material, nature of clay structure, particle size distribution, cation exchange capacity, among others). However, to make prediction of the cohesive sediment behavior not all the parameters are needed.

Four states can be considered to describe cohesive sediments (Fig. 1.1), a mobile suspended sediment layer, a high concentration near bed layer (fluid mud), a newly deposited or partially consolidated bed, and a settled or consolidated bed. The processes of cohesive sediment dynamics are erosion, transport, deposition and consolidation. *Erosion* (or resuspension) is the removal of sediment from the surface of the bed due to the stress of the moving water above the bed. *Transport* is the movement of suspended mud and high concentration layers on or near the bed by the flow. *Deposition* involves the settling through the water column and on to

the bed of flocculated sediment. *Consolidation* of a deposit is the gradual expulsion of interstitial water by the self-weight of the sediment accompanied by an increase in both density of the bed and its strength with time.

This research takes in account two of these states: the mobile suspended particles and the newly deposited bed layer, as well as the processes between them (erosion or resuspension, and deposition).

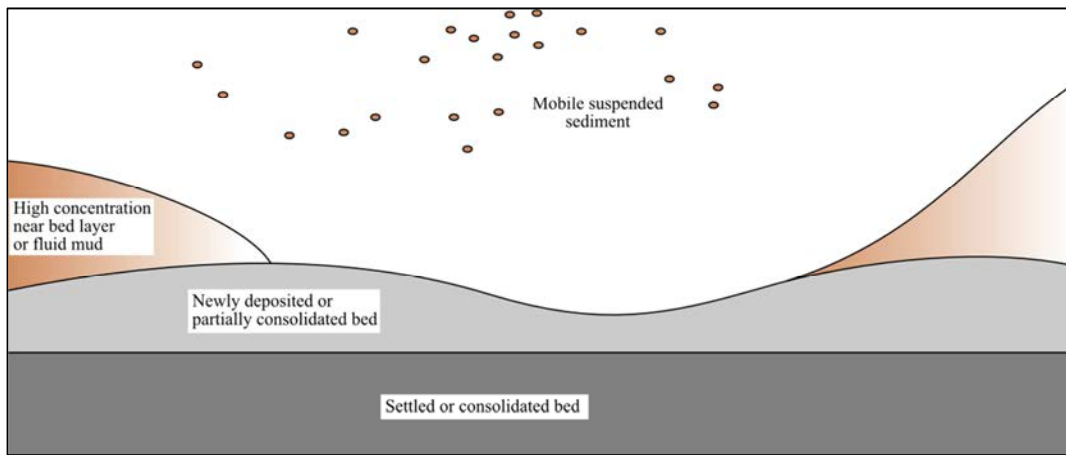


Fig. 1.1. States of cohesive sediments (Whitehouse et al., 2000).

1.2. Previous studies describing turbulence inside meadows

1.2.1. Waves

Some previous studies have described turbulence generated by waves inside meadows. As a first approach, Granata et al. (2001) and Türker et al. (2006) found that seagrasses and salt marshes attenuate wave velocities. Nepf et al. (2007) demonstrated that turbulence cannot penetrate deep into a dense canopy, and flushing is controlled by the stem-scale turbulence. Near-bed turbulence levels within seagrass canopies have been found lower than those on bed without plants (Granata et al., 2001; Hendriks et al., 2008; Pujol et al., 2013b).

The wave velocity inside a canopy is always lower than above the canopy (Lowe et al. 2005a, 2005b). The flow attenuation inside the canopy is related to the canopy geometry, such as the height and spacing of the stems, and it was found to depend on the non-dimensional parameter A_w/S where A_w is the wave orbital excursion length and S is defined as the edge-to-edge average distance between closest elements in any direction. High A_w/S indicates a low wave penetration within the canopy (Fig. 1.2 a) whereas a low A_w/S indicates a high wave penetration within the canopy (Fig. 1.2 b, Lowe et al., 2005a; Pujol et al., 2013b).

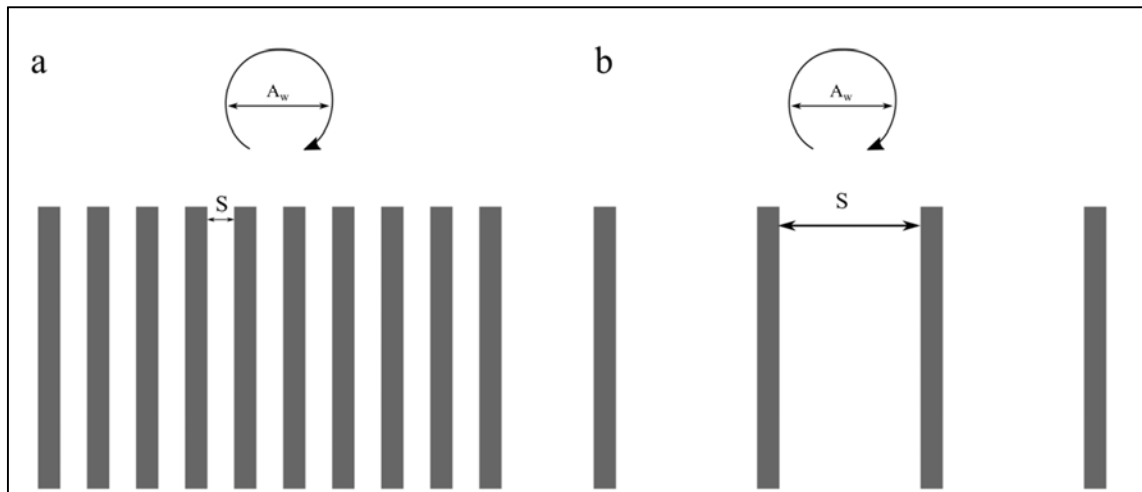


Fig. 1.2. a. Low wave penetration, b. High wave penetration.

1.2.2. Oscillating grid turbulence

Oscillating grid devices have been used since 1950s to study near isotropic turbulence without a main current associated. The geometry of the oscillating grid determines the properties of the turbulence generated (Holzner et al., 2006; Nokes, 1988). Some previous studies with sediment transport by oscillating grid turbulence (OGT) have been made, particularly by Orlins and Gulliver (2003), who related the sediment resuspension to the turbulent kinetic energy (TKE) levels and the consolidation time of the sediment. Tsai and Lick (1986) and Huppert et al. (1995) also experimented with OGT devices, for cohesive and non-cohesive

sediments, respectively. For the experiments with cohesive sediments, the resuspended sediment concentration was proportional to the oscillation frequency of the grid. For the experiments with non-cohesive sediment it was found that an amount of particles can be kept in suspension indefinitely, above a critical oscillation frequency. A steady state of resuspended particles was found after 30 minutes of oscillations.

1.2.3. Gravity currents produced by instantaneous releases

A gravity current of a fluid is a horizontal flow driven by density or by difference in height, into another fluid of different density. Experiments with gravity currents have been done in laboratory channels, removing a vertical separation between two fluids with different densities but with the same water height. Most of those experiments used salt water to produce a gravity current flowing into fresh water (Huppert and Simpson, 1980; Keulegan, 1957; O'Brien and Chernov, 1934; Simpson and Britter, 1979; Yih, 1947). These experiments showed that there are different phases in the progression of the leading edge. The initial phase follows an inertial adjustment, where the velocity decreases as t^{-1} , where t is the time measured from the release. In the second phase, it varies with $t^{1/2}$. Gravity currents may transition to a third phase in which the dominant force balance is between viscous and buoyancy forces and the front velocity varies with $t^{2/3}$ (Rottman and Simpson, 1983).

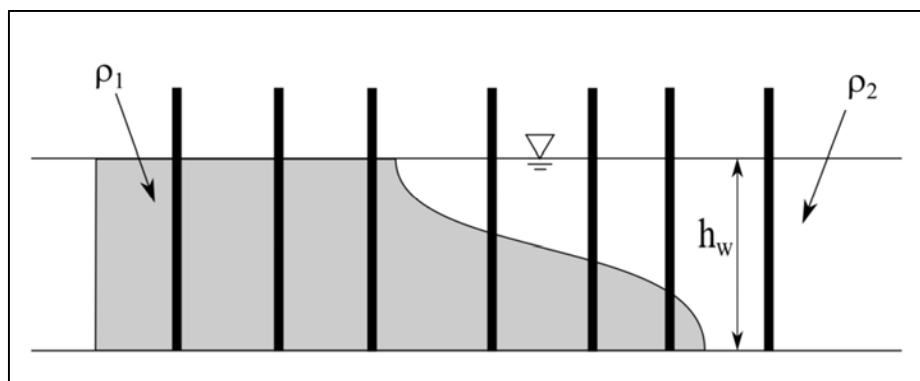


Fig. 1.3. Schematic of a gravity current within a canopy. h_w is the water depth, ρ_1 and ρ_2 are the densities of the denser (gray) and the lighter (white) fluids, respectively.

1.3. Research objectives

The main objective of this thesis is to investigate the effect of aquatic canopies on cohesive sediment resuspension and transport, using experimental observations. Various mechanisms transport sediments in wetlands, such as waves, turbulence and extreme flooding events.

The specific objectives are related to each process:

-Understanding the relationship between the turbulence generated by waves and sediment resuspension, within three types of submerged canopies (rigid, flexible and natural vegetation models) in view of the canopy properties such as the canopy density and flexibility of plants.

-To use an OGT set-up to investigate the relationship between the resuspension of natural cohesive sediment in vegetated environments and the amount of isotropic shear-free turbulence, with the aim of gaining understanding of this relationship by studying it in isolation from other phenomena such as a mean or an oscillating flow, and mimicking field situations dominated by turbulence.

-Understanding the influence of canopies in extreme flooding events under different storm event intensities. To my understanding these situations have not been studied yet. The aim is to determine the effect on hydrodynamics and the depositional rate of sediments compared with the case without plants for different canopy densities of emergent vegetation.

1.4. Organization

This research of this Thesis is organized as follows. In Chapter 2, the materials and methods, including the measuring instruments, are described. The specific procedure for each experiment has been presented in detail in each chapter and in Chapter 2, the measuring techniques used in this research are presented.

Chapter 3 corresponds to the investigations of sediment resuspension in submerged vegetation under a wave dominated regime. The section is entitled “Experimental observations on

sediment resuspension within submerged model canopies under oscillatory flows”, and it deals with the relation between sediment transport and waves in different models of submerged canopies. This section is adapted from a paper published in Continental Shelf Research (Ros et al., 2014) presented in the Appendix. Chapter 4 is entitled “Sediment resuspension within submerged vegetation model canopies in an oscillating grid chamber”. This section is related to the study of flow dominated by nearly isotropic turbulence with zero mean flow, and its relation with the sediment resuspension inside canopies models of submerged vegetation. Chapter 5 is entitled “Influence of extreme flooding events on wetlands”. Flooding events have been reproduced on a laboratory channel to understand the effect of a canopy in the attenuation of the flow produced by a particle laden discharge with different intensities.

Chapter 6 presents a general discussion of the results of the present Thesis, summarizing the main findings of this work, and the general conclusions are presented in Chapter 7.

Chapter 2: Materials and methods

The experimental set up, and specific procedure, of each of the experiments will be detailed in Chapters 3, 4 and 5. In this chapter the instruments used in the experiments are described; the laser in situ scattering and transmissometry (LISST), the acoustic Doppler velocimeter (ADV) and the turbidity sensors. The sediment used in the experiments is also described.

2.1. LISST

A Laser in Situ Scattering and Transmissometry probe, LISST-100X (Sequoia scientific, Inc., Washington, USA) has been used to measure the particle size distribution in the experiments. The LISST-100X (Fig. 2.1) consists on a laser beam, an array of 32 detector rings to analyze the light received, a data storage unit and a battery system. The LISST-100X measures the particle volume concentration of particles for 32 size classes logarithmically spaced in the range $d_p = 2.5 - 500 \mu\text{m}$, by using a procedure based on the laser diffraction theory. By integrating over the whole spectra of size classes and considering particles as spheres (Mikkelsen et al., 2005), one can obtain the total particle volume concentration of the suspension. Previous studies have demonstrated that the LISST-100X is an appropriate instrument to determine the concentration of suspended particles in water (Serra et al., 2002).

The LISST-100X determine the diameters distribution of a particles set, through the dispersion of light at different angles. The resolution of the angles range is 1.7-340 mrad. For such small angles, the dispersion of light does not depend on the refraction index of the particles neither its composition, it only depends on the particle size. The instrument emits a laser beam that interacts with suspended particles, which produce the dispersion of light. The dispersed light is centered by a lens on the detectors rings located at the focal plane of the lens. The light is dispersed with an angle that is related to the size of the particle. The detector is composed by 32 concentric silica rings and every ring can detect the light dispersed with a short range of angles. The intensity of the light measured by the detectors is related to the

particle concentration. Light intensity received by small rings corresponds to the light dispersed by large particles and the light intensity received by large rings corresponds to the light dispersed by small particles.

The LISST can be used in the field, sampling in situ, by submerging the instrument into water or it can be used in the laboratory by using a special chamber to analyze the sample. The samples under study were introduced into this chamber that requires a minimum volume of 100 mL. Afterwards, the sample is spanned by the laser.

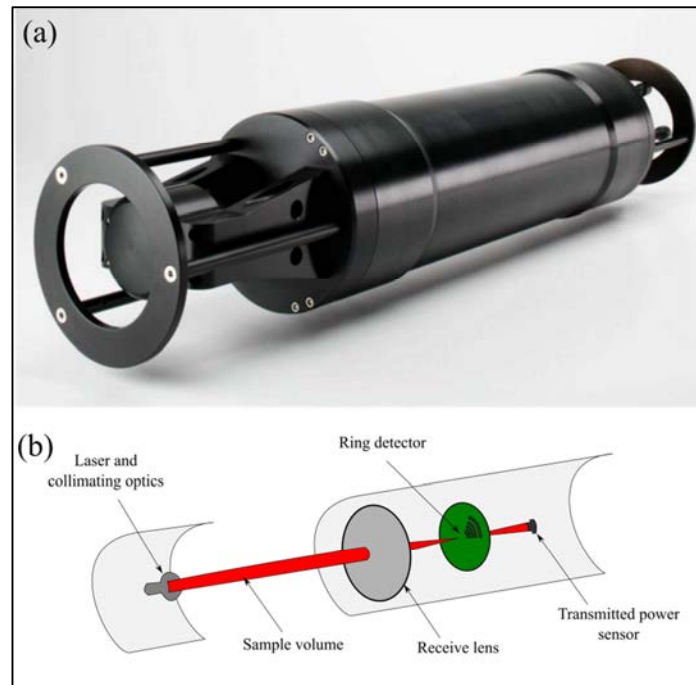


Fig. 2.1. (a) LISST-100X (Sequoia scientific, Inc., Washington, USA). (b) Scheme of the sample volume and the ring detectors.

2.2. Acoustic Doppler Velocimetry

The Acoustic Doppler velocimetry (ADV) is a popular technique for quantifying turbulent fluid flows in aquatic, marine and laboratory environments. The instrument is used to measure

the velocity of a fluid. The technique relies on the Doppler shift principle to measure the velocity of suspended particles that are assumed to move passively with the flow. Acoustic systems use travel times and acoustic intensities of sound waves reflected off suspended particles in water to determine the velocity of the flow that transports the particles. The SonTek 16-MHz MicroADV was used in the experiments of this study. This ADV instrument has a small sampling unit that makes it suitable for being used in laboratory experiments.

The instrument consists of an acoustic transmitter and three acoustic receivers (Fig. 2.2). The transmitter emits acoustic waves with a frequency of 16 MHz. This acoustic instrument has a sampling volume (located at the intersection of the transmitting and receiving beams) of 0.09 cm^3 , at a distance of 5 cm from the acoustic transmitter. Acoustic Doppler Velocimetry has been employed in a range of flow conditions, including wave environment (Pujol et al., 2013b), oscillatory grid turbulence (Pujol et al., 2010) and unidirectional flows (Folkard, 2005).

The highest sampling frequency allowed by the instrument (50 Hz) was chosen in all measurements. This high frequency was needed to determine the turbulent velocity.

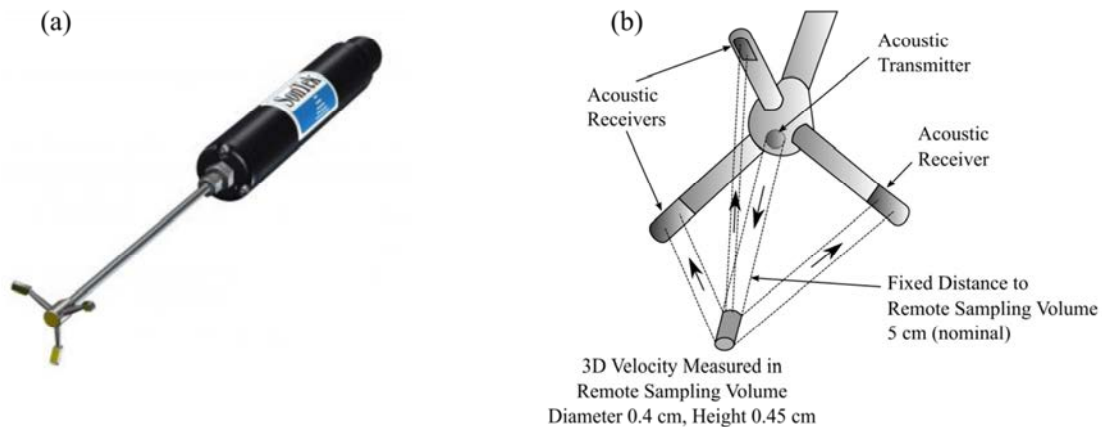


Fig. 2.2. (a) SonTek 16-MHz MicroADV. (b) Scheme of the acoustic transmitter and the three acoustic receivers.

2.3. Turbidity sensors

The Seapoint Turbidity Meter (Seapoint Sensors Inc., NH, USA) detects light scattered by particles suspended in water, generating an output voltage proportional to turbidity or suspended solids. The low power requirements make it ideal for applications where battery drain is a concern. Range is selected by two digital lines which can be hard wired or microprocessor controlled, thereby choosing the appropriate range and resolution for measurement of extremely clean to very turbid waters. The offset voltage is within 1 mV of zero and requires no adjustment across gains. The unique optical design confines the sensing volume to within 5 cm of the sensor allowing near-bottom measurements and minimizing errant reflections in restricted spaces. The sensor is easily interfaced with data acquisition packages; a 5 ft pigtail is supplied.



Fig. 2.3. Seapoint Turbidity Meter

2.4. Sediment characteristics

The sediment used in the experiments was collected from natural salt marshes in the North-East of Catalonia (NE Spain). For the experiments made in wave environments (Chapter 3), the sediment was taken from 4 field sites in the Empordà Marshes Natural Park. For the experiments with oscillating grid turbulence (Chapter 4) and extreme flooding events (Chapter 5), the sediment was collected from the Baix Ter Natural Park (Fig. 2.4).

Previous to the experiments, the sediment was sieved and cleaned to remove traces of organic matter and particles larger than $500\ \mu\text{m}$. As the sediment was collected in two different areas of the salt marsh, two sediment distributions were obtained. The first (Fig. 2.5 a) corresponds to the sediment used for the experiments with waves (Chapter 3). The second sediment distribution (Fig. 2.5 b) was used for the experiments with oscillating grid turbulence (Chapter 4) and extreme flooding events (Chapter 5). Although the different particle distribution of sediments used in this thesis, all the sediments samples were characterized by a mixture of clays, silts and very fine sands, according to the classifications proposed by Van Rijn (2007) and Blott and Pye (2012).



Fig. 2.4. (a) Location of Empordà Marshes Natural Park and Baix Ter Natural Park in NE Catalonia. (b) Empordà Marshes Natural Park. (c) Baix Ter Natural Park.

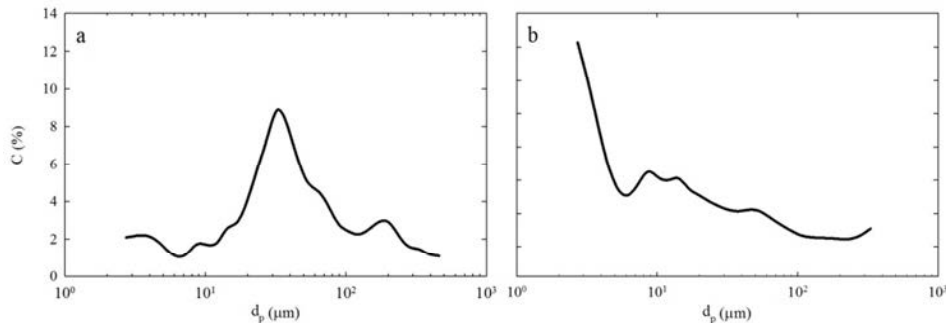


Fig. 2.5. Particle size distribution for the sediment used in Chapter 3 experiments (a) and Chapters 4 and 5 experiments (b).

Chapter 3: Experimental observations on sediment resuspension within submerged model canopies under oscillatory flow

A set of laboratory experiments were conducted to study the effect of submerged aquatic vegetation in sediment resuspension under progressive waves. Three vegetation models (rigid, flexible and real plants of *Ruppia maritima*), six wave frequencies (in the range $F = 0.6 - 1.6$ Hz) and four plant densities (Solid Plant Fractions, SPF in the range of 1 - 10%) were used. The sediment bed properties corresponded to a salt marsh wetland with a bimodal particle size distribution with two particle populations (population 1: particle diameters in the range of 2.5 to 6.0 μm , and population 2: particle diameters in the range of 6.0 to 100 μm).

Within the canopy, wave velocities were attenuated for all the canopies studied and for all the frequencies analyzed. The change in the TKE (ΔTKE) compared with the case without plants was studied. For the rigid canopy model, in comparison to the unimpeded experiment, an increase in ΔTKE inside the canopy for smaller frequencies ($F = 0.6-1.2$ Hz) was observed together with stem Reynolds numbers Re_p above 250. As a result, sediment resuspension for both sediment populations was higher than that of the unimpeded experiment. However, at higher frequencies ($F = 1.4$ and 1.6 Hz) and higher plant densities (SPF = 5%, 7.5% and 10%), the ΔTKE inside the canopy decreased, coinciding with stem Reynolds number Re_p below 250. As a result, sediment resuspension for larger canopy densities and larger frequencies was reduced.

For the flexible vegetation model, in comparison with the unimpeded experiment, a reduction in the ΔTKE inside the canopy was nearly always found. Resuspended sediment concentrations were found to decrease as flexible canopy densities increased. For the flexible vegetation the stem Reynolds number was $\text{Re}_p < 250$ and no production of ΔTKE was observed. The real case of a canopy of *R. maritima* behaved similarly to the flexible model canopy.

3.1. Background

Seagrasses and salt marshes are ecosystem engineers with the well-known function of reducing the action of waves and storm surges (Granata et al., 2001; Türker et al., 2006). Sheltering is characteristic of dense canopies, where turbulence cannot penetrate deep into the canopy, and flushing is controlled by the stem-scale turbulence (Nepf et al., 2007). Under wave-dominated flows, near-bed turbulence levels within seagrass canopies are lower than those on bare soils (Granata et al., 2001; Hendriks et al., 2008; Pujol et al., 2013b). As a consequence, wave energy and sediment resuspension are reduced by seagrasses (Bouma et al., 2005; Infantes et al., 2012; Paul et al., 2012; Terrados and Duarte, 2000). In addition, the reduction in sediment resuspension improves water clarity, which in turn, provides greater light penetration and consequently an increase in productivity, thus creating a positive feedback for the sea and wetland grasses growth (Koch, 2001; Ward et al., 1984).

The reduction of sediment resuspension within the canopy is directly linked to the modification of currents, wave velocity and turbulence (Neumeier, 2007; Pujol et al., 2013b) as well as to the intrinsic properties of the canopy itself, canopy density and flexibility of plants. As pointed out by van Katwijk et al. (2010) at the relatively wave-exposed, sandy sites, dense vegetation cause muddification (increase in fine sediments and organic content) of the sediments. In contrast, in sheltered sites with muddy sediments, dense vegetation has no effect on the sediment composition. In sparse sheltered vegetation, contrary to non-sheltered canopies, with muddy sediments, sandification (decrease in fine sediments and organic content) prevails. In events where the flow level is above the vegetation, sedimentation decreases with distance, from the seaward marsh edge and from the creeks, in parallel with a grain-size fining or muddification (Neumeier and Amos, 2006). Coastal zones present a large variety of clay, silt and sand composition. Different particle sizes compose the sediment bed in view of their density and settling velocity and are prone to differential resuspension when facing an external physical forcing. Therefore sediment resuspension will highly depend on the characteristics of plants as well as on the intensity of reduction of wave velocity by the canopies and the generation of turbulent kinetic energy through the interaction between waves and the canopy.

The attenuation of the flows inside canopies has been studied by Lowe et al. (2005a, 2005b). The authors conducted laboratory experiments and developed an analytical model to investigate the flow structure inside a submerged canopy, such as a coral reef. Their model was developed by considering the momentum balance around individual canopy elements within a larger canopy. They demonstrated that the flow inside a canopy was always lower than above the canopy, and that the degree of flow attenuation varied as a function of canopy geometry parameters, such as the height and spacing of the elements, as well as coefficients that parameterize the effects of various forces exerted by the canopy element. The canopy flow attenuation was found to depend on the non-dimensional parameter A_w/S where A_w is the wave orbital excursion length and S is defined as the edge-to-edge average distance between closest elements in any direction. This ratio has been called the Keulegan-Carpenter number (Monismith, 2007), although for Mendez and Losada (2004) the definition of this number is slightly different (S was defined as the plant area per unit height of each vegetation stand normal to the wave velocity). The two definitions of S are proportional and give account of the density of the canopy. When A_w/S is large, the flow is drag dominated and velocities inside the canopy are much lower than in the free stream. In contrast, when A_w/S is small, the interstitial flow is inertia dominated and interior velocities more nearly match exterior ones, and total mass transfer is enhanced over that of steady flows. This experiment aims at understanding the relationship between the turbulent kinetic energy, the shear stress and sediment resuspension in terms of the canopy density and depending on whether the stem is flexible or rigid. The environmental flow under study is a field of monochromatic waves. The wave frequency is also a key parameter that will be analyzed in the present chapter.

3.2. Procedure

3.2.1. Experimental setup

The study was conducted in a 6 m x 0.5 m x 0.5 m wave flume. A scheme of the setup is shown in Fig. 3.1. The mean water depth, h , was 0.3 m. A plywood beach, with a slope of 1:3 and covered with a 7 cm layer of foam rubber, was located at the end of the flume. A vertical paddle, called a flap type wavemaker, was placed at the front of the flume and was driven by

a variable-speed motor with a constant stroke of 5 cm and a variable frequency F in the range from 0.6 to 1.6 Hz (Table 3.1). Since $\lambda/2$ was always larger (Table 3.1) than the water depth (of 30 cm), the generated waves always reached the bottom of the flume (where λ is the wave length). Furthermore, since $\lambda/20 < h < \lambda/2$, these waves corresponded to waves in transitional waters, i.e. intermediate to shallow waves, which are in accordance with the typical waves in vegetated coastal regions. We defined the longitudinal direction as x , and $x = 0$ was the longitudinal position at the wavemaker. $y = 0$ at the centerline of the tank and z is the vertical direction, $z = 0$ corresponded to the depth at the flume bed. Wave conditions in the present study corresponded to the laminar regime, i.e. to wave Reynolds number, $Re_w = U_{w,\infty} A_\infty / \nu < 10000$, where $U_{w,\infty}$ represents the orbital wave velocity unaffected by the canopy roughness (i.e. the wave velocity far above the canopy, here considered at $z = 22$ cm above the bottom), called free-stream velocity, and A_∞ is the wave orbital excursion length of the free-stream potential flow. The submergence ratio, defined as h_v/h (where h_v is the plant height), was 0.47, which falls in the upper limit of those used in other studies (Manca et al., 2012).

3.2.2. Vegetation models

The rigid canopy model consisted of rigid PVC cylinders 1 cm in diameter and 14 cm long. Different canopy densities were also considered in the experiments. According to Pujol et al. (2010), the canopy density can be defined as the solid plant fraction at the bottom occupied by stems, $SPF = 100 \cdot n\pi(d/2)^2/A$, where n is the number of plants, d is the diameter of the model plant, and A is the planform area. SPF of 1%, 5%, 7.5% and 10% were used for experiments with submerged rigid vegetation, SPF of 1%, 5% and 10% were used for those experiments with submerged flexible vegetation and 1% for those with real plants (Table 3.1). The vegetation pattern for each SPF was made at random by means of a computer function (Pujol et al., 2013b). A plastic board was regularly perforated with holes of 1 cm with a distance of 1.5 cm between the centers of two neighbor holes. The random pattern of vegetation was made filling the corresponding holes with the cylinders and leaving some holes at the bottom that where afterwards filled with small dowels with the length equal to the bottom board thickness. The same procedure was repeated for each SPF.

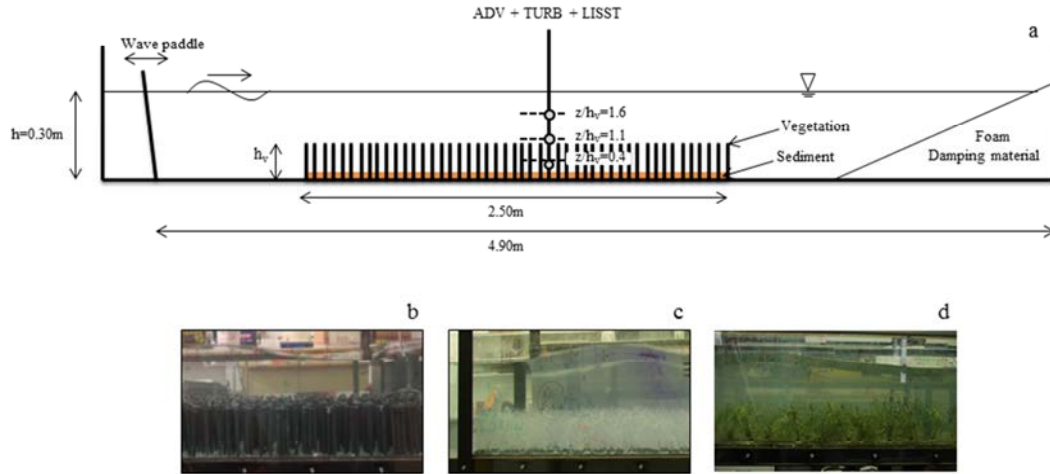


Fig. 3.1. (a) Scheme of the experimental set-up. Experiments were conducted in a 6 m long flume. The streamwise coordinate is denoted by x , with x positive in the downstream direction, and $x = 0$ at the mean position of the wave maker. The vertical coordinate is z , with $z = 0$ at the bed. The mean water depth, h , is 30 cm. The plant height in still water is $h_v = 14$ cm. The model meadow was 250 cm long. The horizontal dashed lines indicate the position of the velocity (ADV) and sediment concentration measurements, both turbidity and particle sediment concentration (TURB+LISST). The beach slope at the end of the tank is not scaled. (b) Picture of the submerged rigid canopy. (c) Picture of the submerged flexible canopy. (d) Picture of the submerged real canopy (*R. maritima*).

The flexible canopy model was constructed with implants of polyethylene (high density) blades attached with a plastic band to a PVC dowel 2 cm long and 1 cm in diameter. Each plant had eight plastic blades of 4 mm width. The model plants were dynamically and geometrically similar to typical seagrasses, as described by Ghisalberti and Nepf (2002), Folkard (2005) and Pujol et al. (2013b). The canopy density for flexible plants was calculated based on the area occupied by the dowels that fixed the plants at the bed.

The real plant model consisted of *R. maritima*, which is a typical plant found in salt marshes and especially abundant in the Mediterranean coastal areas. It produces long, narrow, straight leaves and is characterized by seasonally contrasting growth of tall flowering reproductive shoots in mid-summer and shorter vegetative roots during the remainder of the growing

season. The plants for the model were cut to a height of $h_v = 14$ cm, so that results could be compared with those obtained rigid and flexible canopy models. The real plant blades were attached to the same PVC dowels used for the flexible canopy model.

3.2.3. Measuring techniques

The Eulerian velocity field was defined as (u, v, w) in the (x, y, z) directions, respectively. The three components of the velocity were recorded with a downwards looking Acoustic Doppler Velocimeter (Sontek/YSI16-MHzMicroADV). The acoustic frequency was 16 MHz, the sampling volume was 0.09 cm^3 and the distance to the sampling volume was 5 cm. The ADV sampled at 50 Hz, limiting the velocity spectra to 25 Hz due to Nyquist frequency. The ADV was mounted on a movable vertical frame that allowed it to be manually situated at working depths of $z = 5$ cm (i.e., $z/h_v = 0.4$), well inside the canopy model, $z = 15$ cm (i.e. $z/h_v = 1.1$) and $z = 22$ cm (i.e. $z/h_v = 1.6$), these two last depths corresponding to the layer above the canopy models. It measured during 20 minutes at each depth. After measuring at one depth it was moved vertically and left for 15 minutes before measuring again. Each experiment lasted 120 minutes. To avoid spikes due to poor correlations, ADV measurements with beam correlations below 80% along and outlier instantaneous velocities higher than two standards deviations were discarded for the analysis.

The longitudinal measurements of the velocity were taken at an antinode, in order to eliminate the lower-order spatially periodic variation in wave and velocity amplitude associated with a maximum of 10% of reflection measured in the flume (Luhar et al., 2010; Pujol et al., 2013b). Then, the model bed was shifted longitudinally along the flume to measure at 150 cm from the vegetation edge. To obtain valid data acquisition within the canopy, some stems were removed to avoid blocking the pathway of the ADV beams, as was done by Neumeier and Ciavola (2004), Pujol et al. (2010) and Pujol et al. (2013b). To minimize the effect of this 'hole', its shape was specifically designed to allow the ADV acoustic receivers and the acoustic transmitter to perform properly.

3.2.4. Methods of analysis

For general wave flows, the instantaneous velocity e.g. U_i , can be decomposed as:

$$U_i = U_c + U_w + u' \quad (3.1)$$

where U_c is the steady velocity associated with the current, U_w is the unsteady wave motion which represents spatial variations in the phase averaged velocity field, and u' is the turbulent velocity, that is the instantaneous velocity fluctuation in the x direction. As in Lowe et al. (2005a) and Luhar et al. (2010), U_c is the space and phase-averaged velocity found as:

$$U_c = \frac{1}{2\pi} \int_0^{2\pi} U_i(\varphi) d\varphi \quad (3.2)$$

where $U_i(\varphi)$ is the instantaneous velocity, according to the phase. Wave velocity, U_w , was obtained by using a phase averaging technique. The Hilbert transform was used to average oscillatory flow velocities with a common phase (Pujol et al., 2013b). The root mean square (rms) of $U_i(\varphi)$ was considered as the characteristic value of the orbital velocity U_w at each depth and was calculated according to the following operation:

$$U_w = \sqrt{\frac{1}{2\pi} \int_0^{2\pi} (U_i(\varphi) - U_c)^2 d\varphi} \quad (3.3)$$

In absence of vegetation, the linear wave model leads to the following equation for the horizontal wave velocity component,

$$U_w = a\omega \frac{\cosh kz}{\sinh kh} \cos(kx - \omega t) \quad (3.4)$$

where a is the wave amplitude, k is the wave number and ω is the wave radian frequency.

Then, the Turbulent Kinetic Energy (TKE) was calculated as:

$$TKE = \frac{1}{2} \left(\langle u'^2 \rangle + \langle v'^2 \rangle + \langle w'^2 \rangle \right) \quad (3.5)$$

where $\langle \rangle$ denotes the time average. The TKE difference between measurements with and without plants, expressed as a percentage, was calculated according to:

$$\Delta TKE(z) = \left(\frac{TKE_c(z) - TKE_{wc}(z)}{TKE_{wc}(z)} \right) \cdot 100 \quad (3.6)$$

where the TKE_c is the TKE measured at z with the presence of canopy model, and the TKE_{wc} is the TKE measured at z without the presence of canopy model. Negative ΔTKE indicate a reduction of TKE, while positive values of ΔTKE imply TKE generation.

3.2.5. Sediment characteristics

For each experiment, the bottom of the flume was covered with sediment by uniformly seeding the same amount of sediment over the entire bottom of the flume, resulting in a homogeneous sediment bed of 3-5 mm height. The seeding was performed manually using a tube connected to a container with the sediment mixture. The tube was moved 1 cm above the bed along the bottom of the flume through the vegetation and also in the region without vegetation. The seeding resulted in a homogeneous bottom cloud of ~ 5 cm in height, whose particles were left to deposit by gravity. Therefore experiments commenced 1 day after the seeding. Bedforms at the bottom were not observed and it was not necessary to flatten the surface.

The concentration of suspended sediment, without the canopy, C_{wc} , or with the canopy, C_c , was measured at the same longitudinal position where velocity was measured at three points in the vertical (Fig. 3.1), at one point well inside the canopy ($z/h_v = 0.4$) and at two vertical positions above the canopy ($z/h_v = 1.1$ and $z/h_v = 1.6$). Between experiments a lag time of 8 hours was considered, so as to minimize the effect of residual sediment concentration in suspension in the flume. This time was calculated as 5 times the time needed for the sediment

to settle through the whole water column based on the settling speed considering the diameter of the smallest particles. No bedforms appeared after the tests therefore it was not necessary to flat the sediment bed. The sediment concentration was measured at $t = 0$ for each experiment, and subtracted from the sediment concentration measured at the steady state, $t = t_{ss}$, at all depths of measurements.

Three turbidity sensors (Seapoint Turbidity Meter, Seapoint Sensors Inc., NH, USA) and a Laser in Situ Scattering and Transmissometry probe, LISST-100 (Sequoia Scientific, Inc., WA, USA), were used to measure the suspended sediment concentration. Turbidity meters were located at 5, 15 and 21 cm above the bed and measured at a frequency of 10 Hz. The 3 time turbidity series analyses were used to determine the time needed for the sediment resuspension to attain the steady state, which was ~ 15 min after the initiation of the wave generation. Oguz et al., (2013) also found the same time lag for a case of sediment resuspension in a wave dominated regime. In this study, experiments lasted for a period of 120 min, when sediment samples were collected from the water column. When the steady state was reached, water samples were collected at different depths and at different times. Samples were collected with a pipette for being afterwards analyzed by the LISST-100 to obtain the particle size distribution. The LISST-100 consists of a laser beam and an array of 32 detector rings to analyze the light received, from which it determines the particle volume concentration, C , of particles for 32 size classes logarithmically distributed in the range of 2.5 - 500 μm , by using a procedure based on the laser diffraction theory. By integrating the whole spectra of size classes, the total particle volume concentration of the suspension was obtained (Serra et al., 2005, 2002). C was measured at $t = 0.5, 1$ and 2 hours, and the mean of the last hour measurements is given as the particle volume concentration at the steady state.

The sediment to seed the tank bottom was taken from 4 field sites in the Empordà Marshes Natural Park, located at the North-East of Spain, and is characterized by a mixture of clays silts and very fine sands. Given the range analysis of the particle analyzer, and based on the classification by Van Rijn (2007) and Blott and Pye (2012), the sediment presented a bimodal shape with the first range between 2.5 and 6.0 μm , i.e., corresponding to clay and very fine silts (very cohesive), and the second range between 6.0 and 100 μm ; i.e., mainly corresponding from fine to coarse silts and small sand particles (weakly cohesive) (Fig. 3.2).

From Fig. 3.2, the peak in the particle volume concentration distribution of the largest diameters above 100 μm was assumed to represent the role of just a few particles with a large volume. For this reason, these large particles were not considered in the analysis.

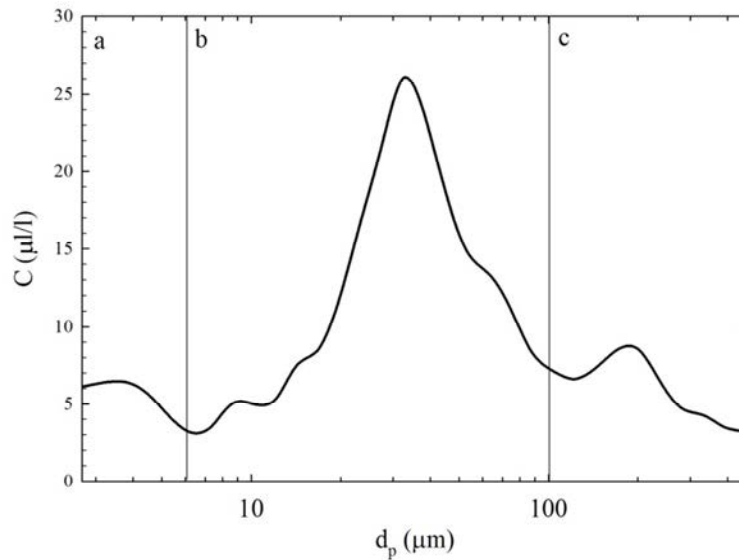


Fig. 3.2. Particle size distribution for the salt marsh sediment used in the experiments. Vertical dashed lines in the figure represent the classification by van Rijn (2007) where range a (small particles) corresponds to the particle range of clay and very fine silts (very cohesive sediment), range b (large particles) corresponds to the particle range of fine, coarse silts and fine sands (weakly cohesive sediment) and range c corresponds to fine sands.

The same procedure was followed to ensure the same sediment characteristics for each run. The natural sediment mixture of sediments was sift to separate the coarse particles and root fragments, and then was kept in a tank in its hydrated form. A constant volume of 0.3 L of the dense homogeneous sediment mixture was taken, added to a container with 4 L of water, and agitated during a time lapse of 30 minutes to obtain a completely homogeneous mixture. Afterwards, the whole mixture was immediately introduced on the bottom of the flume.

3.3. Results

3.3.1. Physical basis of hydrodynamics within a canopy under progressive waves

Previous studies using rigid and flexible vegetation models have successfully described the turbulence structure for submerged vegetation subjected to unidirectional flows (Infantes et al., 2012; Nepf and Vivoni, 2000), however, a few of them explore the turbulent structure in a canopy dominated by progressive waves (Pujol et al., 2013b). In this section we present the results of the wave velocities and the TKE for different values of the canopy density and the wave frequency.

The wave velocity, U_w , at $z/h_v = 0.4$ increased with the frequency for $F \leq 1.2$ Hz for both rigid (Fig. 3.3a) and flexible canopy models (Fig. 3.3b) and also for experiments without plants, decreasing afterwards for $F \geq 1.2$ Hz. This result for U_w was also predicted by linear wave theory (Fig. 3.3a and 3.3b), where U_w increased with the frequency for $F \leq 1.2$ Hz. For frequencies $F \geq 1.2$ Hz, the linear wave theory also suggests that the wave attenuation increases with the wave frequency (Hansen and Reidenbach, 2012; Wiberg and Sherwood, 2008). The theoretical model for U_w at $z = 5$ cm was calculated from equation 3.4. a in equation 3.4 was calculated by fitting the linear wave theory solution to the measurements obtained at the highest measurement location ($z/h_v = 1.6$).

For rigid plants, the wave attenuation ratio, defined as the proportion of the wave velocity with plants and the velocity without plants was in the range from 0.91 to 0.75 for SPF between 1% and 10%, respectively. For the flexible vegetation, the wave attenuation was lower than for the rigid vegetation and it was in the range from 0.96 to 0.85 for SPF between 1% and 10%, respectively. Despite this wave attenuation, results show that the wave penetrated into the canopy for all the cases studied.

Wave orbital excursion lengths $A_w (= U_w/2\pi F)$, calculated at $z/h_v = 1.1$ were between 0.24 and 1.10 cm. An estimate of the wave penetration could be inferred from the parameter A_w/S , where S is the edge-to-edge distance (Lowe et al., 2005a). Values of this parameter are shown in Table 3.1. $A_w/S < 1$ for all the experiments indicated that the penetration of the wave in the

canopy corresponded to the inertial force dominated regime, as described by Lowe et al. (2005a).

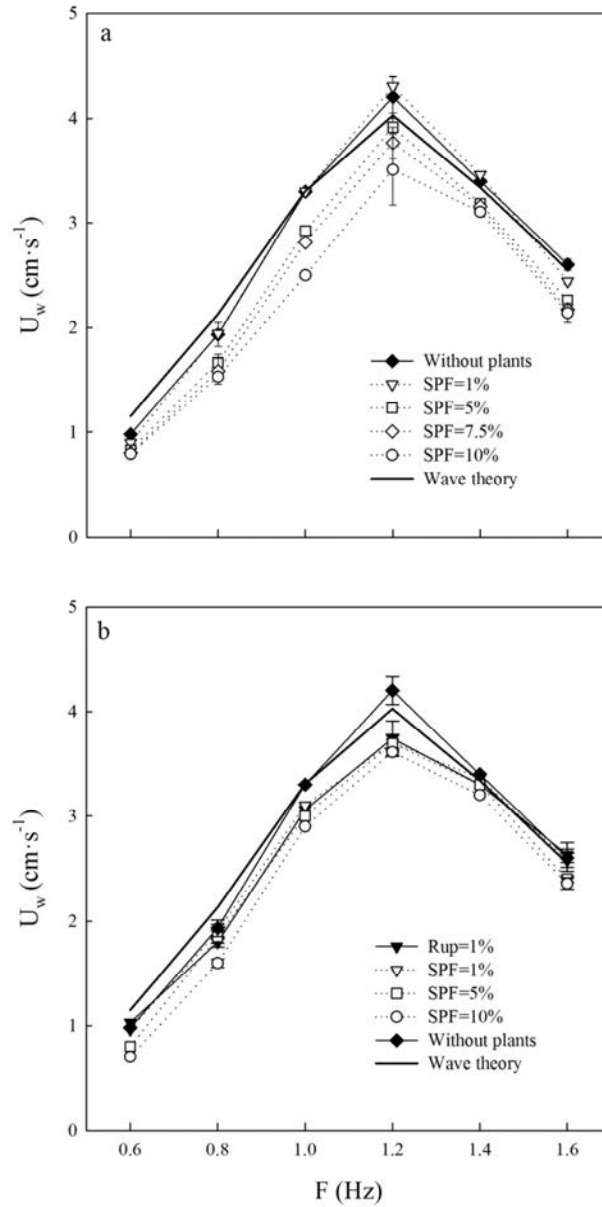


Fig. 3.3. Wave velocities at $z/h_v = 0.4$ for the different SPF studied and for rigid (a) and flexible (b) canopies. The solid line represents the theoretical value predicted for the no canopy case by the linear wave theory and calculated from equation 3.4 for the range of the wave frequencies studied.

Table 3.1. Wave and vegetation parameters for the experiments carried out: solid plant fraction (SPF), number of stems per square meter, wave frequency, the corresponding wavelengths calculated from the dispersion equation (Dean and Dalrymple, 1991) and the A_w/S parameter measured at $z/h_v = 1.1$, where $A_w = U_w/(2\pi F)$ and S is the plant-to-plant distance.

Run canopy model	SPF (%)	n_s (stems·m ⁻²)	F (Hz)	λ (m)	A_w/S ($z/h_v=1.1$)
Without vegetation					
WP1			0.6	2.65	
WP2			0.8	1.86	
WP3			1.0	1.37	
WP4			1.2	1.03	
WP5			1.4	0.78	
WP6			1.6	0.61	
Submerged rigid vegetation model					
SRV1	1	128	0.6	2.65	0.04
SRV2	5	640	0.6	2.65	0.09
SRV3	7.5	960	0.6	2.65	0.18
SRV4	10	1280	0.6	2.65	0.18
SRV5	1	128	0.8	1.86	0.05
SRV6	5	640	0.8	1.86	0.23
SRV7	7.5	960	0.8	1.86	0.19
SRV8	10	1280	0.8	1.86	0.32
SRV9	1	128	1.0	1.37	0.11
SRV10	5	640	1.0	1.37	0.17
SRV11	7.5	960	1.0	1.37	0.35
SRV12	10	1280	1.0	1.37	0.46
SRV13	1	128	1.2	1.03	0.07
SRV14	5	640	1.2	1.03	0.19
SRV15	7.5	960	1.2	1.03	0.30
SRV16	10	1280	1.2	1.03	0.45
SRV17	1	128	1.4	0.78	0.08
SRV18	5	640	1.4	0.78	0.23
SRV19	7.5	960	1.4	0.78	0.31
SRV20	10	1280	1.4	0.78	0.41
SRV21	1	128	1.6	0.61	0.06
SRV22	5	640	1.6	0.61	0.18
SRV23	7.5	960	1.6	0.61	0.24
SRV24	10	1280	1.6	0.61	0.34
Submerged flexible vegetation model					
SFV1	1	128	0.6	2.65	0.03
SFV2	5	640	0.6	2.65	0.08
SFV3	10	1280	0.6	2.65	0.20
SFV4	1	128	0.8	1.86	0.07
SFV5	5	640	0.8	1.86	0.38
SFV6	10	1280	0.8	1.86	0.36
SFV7	1	128	1.0	1.37	0.07
SFV8	5	640	1.0	1.37	0.32
SFV9	10	1280	1.0	1.37	0.66
SFV10	1	128	1.2	1.03	0.10
SFV11	5	640	1.2	1.03	0.32
SFV12	10	1280	1.2	1.03	0.48
SFV13	1	128	1.4	0.78	0.09

Run canopy model	SPF (%)	n_s (stems·m ⁻²)	F (Hz)	λ (m)	A_w/S ($z/h_v=1.1$)
SFV14	5	640	1.4	0.78	0.25
SFV15	10	1280	1.4	0.78	0.44
SFV16	1	128	1.6	0.61	0.07
SFV17	5	640	1.6	0.61	0.19
SFV18	10	1280	1.6	0.61	0.34
Submerged real vegetation model					
SREV1	1	128	0.6	2.65	0.03
SREV2	1	128	0.8	1.86	0.07
SREV3	1	128	1.0	1.37	0.07
SREV4	1	128	1.2	1.03	0.10
SREV5	1	128	1.4	0.78	0.10
SREV6	1	128	1.6	0.61	0.08

Fig. 3.4 shows the vertical distribution of ΔTKE at $z/h_v = 1.6, 1.1$ and 0.4 , for comparison between runs of rigid (Fig. 3.4a, 3.4c, and 3.4e), and flexible models (Fig. 3.4b, 3.4d and 3.4f), respectively, as well as the results for the ‘natural’ case of *R. maritima* (thick black line in all figures). For measurements carried out above the submerged rigid vegetation, the percentage difference of TKE with and without plants (ΔTKE) was always found to be positive for all the frequencies studied (Fig. 3.4a and 3.4c); also, ΔTKE was found to increase with the frequency. For a canopy density of 1%, ΔTKE was the lowest, indicating that turbulent kinetic energy was similar to that without plants, especially for frequencies below 1.2 Hz, with $\Delta TKE \sim 0$ (Fig. 3.4a). Larger canopy densities produced a larger ΔTKE , especially for larger frequencies ($F \geq 1.2$ Hz). However, for densities of 1% and 10%, ΔTKE for larger frequencies was 2 to 3 times lower than those found for the densities of 5% and 7.5% (Fig. 3.4a).

Above the submerged flexible canopy (Fig. 3.4b and 3.4d), ΔTKE was found to be slightly positive for the density of 1%. It varied from ~ 0 for the lowest frequency and increased to 35% for the largest frequency. When the canopy density increased, ΔTKE followed the same pattern, that is, ΔTKE increased with frequency. Above the submerged flexible canopy, at both depths studied (Fig. 3.4b and 3.4d), ΔTKE increased with the wave frequency and decreased with increasing the canopy density. Positive ΔTKE (Fig. 3.4d) was found only for the canopy density of 1% (all frequencies) and for high wave frequencies ($F \geq 1.2$ Hz) for the experiments with SPF= 5%. For SPF=5% and frequencies below 1.2 Hz, ΔTKE was always

negative. For the largest canopy density of 10%, ΔTKE was always negative for all frequencies.

Well inside the rigid canopy model (5 cm above the bottom), ΔTKE was found to be positive for frequencies up to 1.2 Hz (Fig. 3.4e). For the lowest canopy density of 1%, ΔTKE was constant and positive for all the frequencies. However, larger canopy densities resulted in negative ΔTKE for frequencies above 1.2 Hz. For low canopy densities (1% and 5%) and low frequencies (below 1.2 Hz), ΔTKE was nearly constant with frequency with percentages below 25%. For higher canopy densities (7.5% and 10%) ΔTKE increased with frequencies up to 1.0 Hz, to ΔTKE of $\sim 50\%$ up to 100% . For higher frequencies of 1.4 and 1.6 Hz, ΔTKE was negative, reaching a value of -25% for canopy densities of 5% and 7.5%, and reaching a value of -50% for canopy densities of 10% (Fig. 3.4e).

Well inside the flexible canopy model (Fig. 3.4f), ΔTKE was negative for all the frequencies and plant densities, with percentages below -25% . Larger negative ΔTKE was attained for the largest canopy density. Contrary to that found above and close to the canopy top (Fig. 3.4b and 3.4d), ΔTKE slightly decreased with frequency.

To make comparisons, the experiments with the *R. maritima* canopy were represented in both schemes: submerged rigid vegetation (Fig. 3.4a, 3.4c and 3.4e) and submerged flexible vegetation (Fig. 3.4b, 3.4d, and 3.4f). Well above the *R. maritima* canopy (Fig. 3.4a and 3.4b) ΔTKE was low and positive for frequencies up to 1.2 Hz. For higher frequencies (1.4 and 1.6 Hz), ΔTKE increased considerably, reaching percentages of 80%. Just above the real plant canopy, ΔTKE increased with frequency (Fig. 3.4c and 3.4d), but at a lower rate than that found well above the canopy (Fig. 3.4a). The percentage of ΔTKE attained at the highest frequency was lower, $\sim 50\%$, than that found well above the canopy, $\sim 100\%$ (Fig. 3.4a). Well inside the *R. maritima* canopy, ΔTKE was negative for all the frequencies (Fig. 3.4f). As the frequency increased, ΔTKE decreased slightly with percentages below -25% . Well inside the *R. maritima* canopy, the dependence of ΔTKE on frequency, was found to be similar to that of the flexible canopy, for the same canopy density of $\text{SPF} = 1\%$.

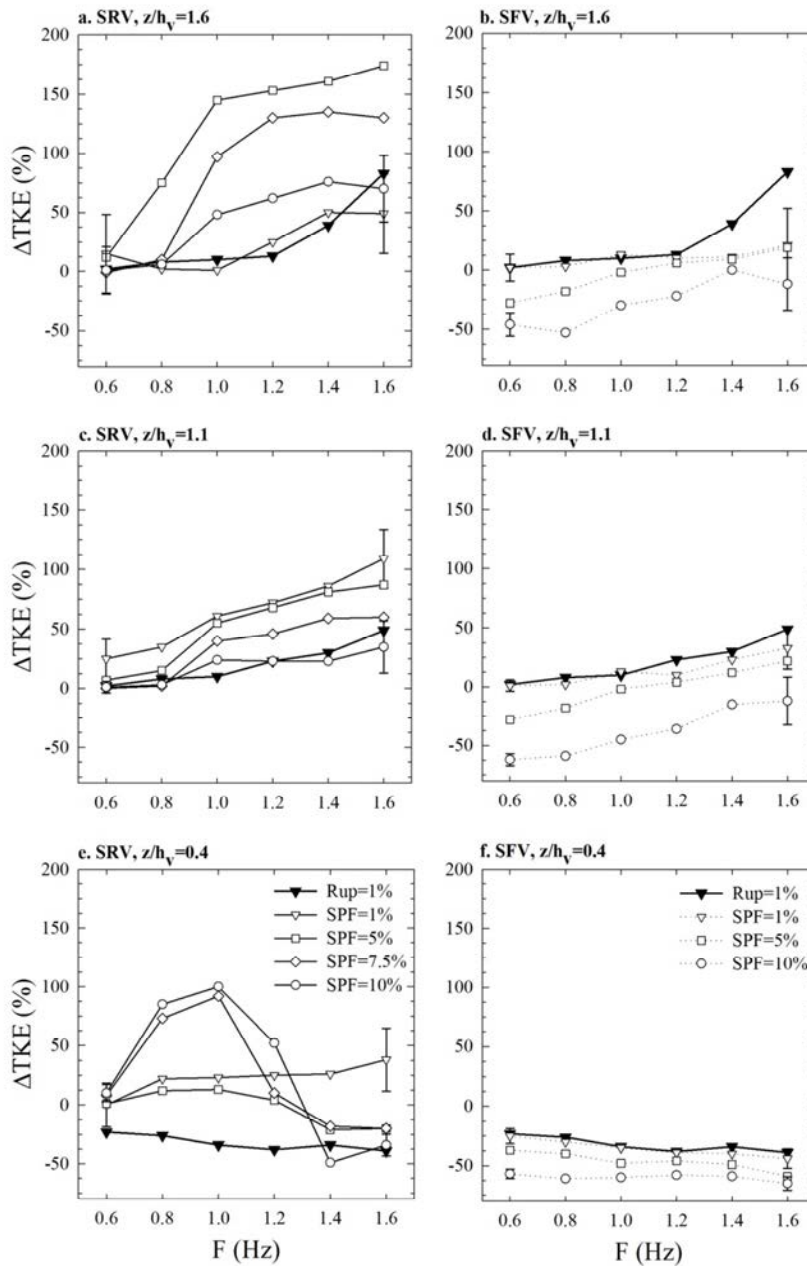


Fig. 3.4. Relation between ΔTKE (%), calculated using equation 3.6, with the wave frequency for different canopy densities (SPF). Results for submerged rigid canopy models (SRV) are presented in the left hand panels (a, c and e), while results for submerged flexible canopy models (SFV) are presented in the right hand panels (b, d and f). Top panels (a and b) correspond to the results for $z/h_v = 1.6$, middle panels (c and d) correspond to the results for $z/h_v = 1.1$ and bottom panels correspond to the results for $z/h_v = 0.4$. Results for *R. maritima* (Rup) were included in all the plots. Vertical error bars are presented for the lowest and largest frequencies and for 1% and 10% canopy densities.

3.3.2. Sediment resuspension within canopy models

Different regimes of turbulent flow inside and outside the vegetation area change the TKE and the transport rate of suspended sediment (Houwing, 1999; López and García, 1998). The bottom shear stress plays an important role in fine sediment movement and the morphology of bed form (Venier et al., 2012). It has been reported that plants can cause the increase of the shear stress of the bottom of the tidal flat or the reduction of vertical shear (Leonard et al., 2002) and the resuspension of bottom sediment (Widdows et al., 2008). The parameter ΔC was chosen to compare the concentration of the vegetated case to the concentration of the non-vegetated case and calculated according to:

$$\Delta C(z) = \left(\frac{C_c(z) - C_{wc}(z)}{C_{wc}(z)} \right) \cdot 100 \quad (3.7)$$

where C_c is the particle volume concentration at the steady state in the canopy experiments and C_{wc} is the equivalent in the non-canopy experiments.

Fig. 3.5 shows the vertical distribution of ΔC , for the range of small particles (2.5 to 6.0 μm), at the vertical heights $z/h_v = 1.6$, 1.1 and 0.4, for comparison between runs of rigid (Fig. 3.5a, 3.5c, and 3.5e), and flexible models (Fig. 3.5b, 3.5d and 3.5f), respectively, as well as the results for the ‘natural’ case of *R. maritima* (thick black line in all figures). The vertical distribution of ΔC above the rigid canopy was found to be positive, except for canopy densities of 7.5% and 10%, which at very high frequencies presented negative ΔC . The lower the canopy density, the higher the resuspension of particles, at both $z/h_v = 1.6$ (Fig. 3.5a) and $z/h_v = 1.1$ (Fig. 3.5c). In addition, ΔC exhibited a tendency to decrease as frequencies increased. Inside the canopy the results presented the same tendency (Fig. 3.5e), with ΔC increasing with decreasing canopy density but declining at increasing wave frequencies. On the contrary, and as shown in Fig. 3.5b, 3.5d and 3.5f, for the flexible canopy experiments, ΔC above and within the canopy was always negative, and with a slight decrease of ΔC at increasing frequencies, for frequencies above 1 Hz. ΔC for the real plant model (*R. maritima*), was closer to ΔC obtained for the flexible canopy than to ΔC obtained for the rigid canopy, at the same 1% density of flexible vegetation.

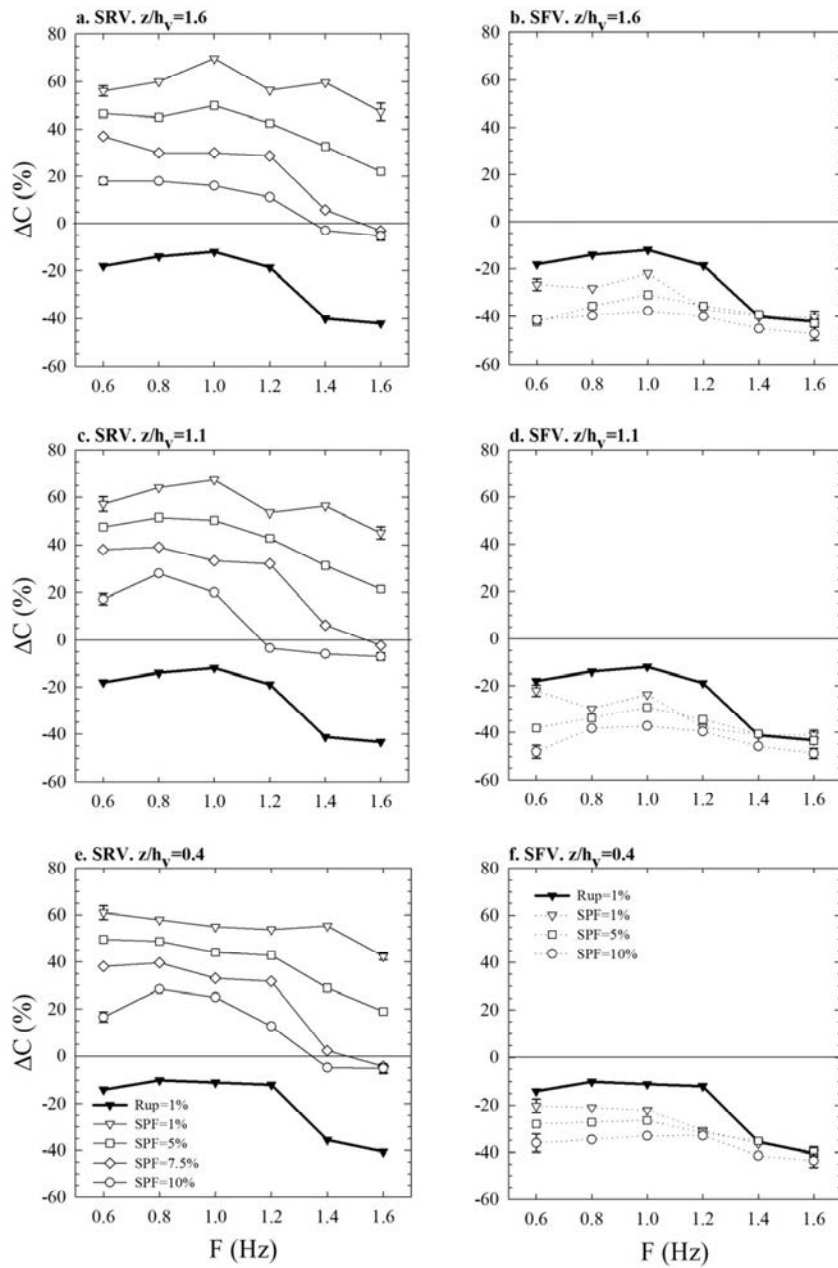


Fig. 3.5. Relationship between ΔC (%), calculated using equation 3.7, for the particle range of diameters from 2.5 to 6.0 μm with the frequency for the different canopy densities (SPF). The representation of the results was the same like that used in Fig. 3.4.

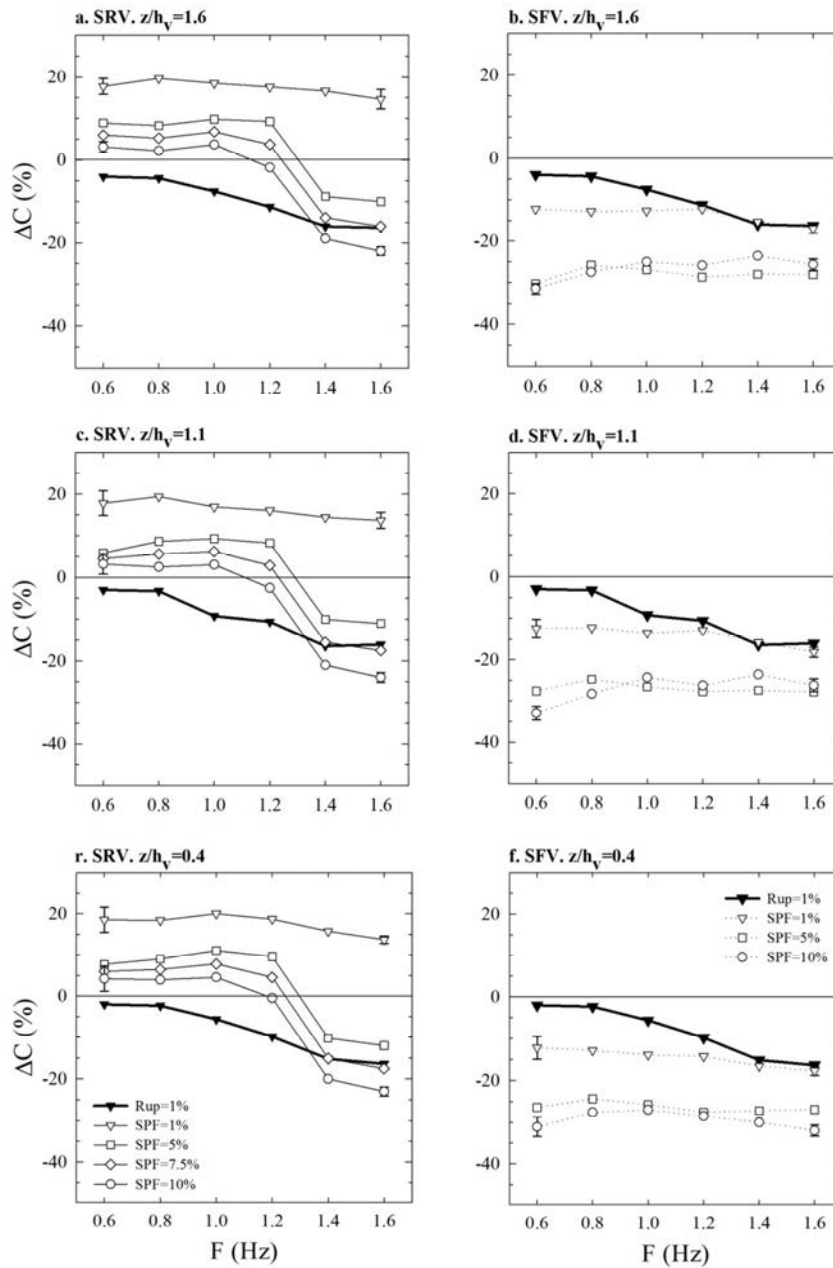


Fig. 3.6. Relationship between ΔC (%), calculated using equation 3.7, for the particle range of diameters from 6.0 to 100 μm with the frequency for the different canopy densities (SPF). The representation of the results was the same like that used in Fig. 3.4.

Fig. 3.6 shows the same results as Fig. 3.5, but for large particles in the range between 6.0 and 100 μm . The resuspension of the 6.0 to 100 μm particles was found to be larger for the rigid vegetated experiments with the lowest density of 1% (Fig. 3.6a) and also, for the experiments with densities of 5%, 7.5% and 10% for wave frequencies ≤ 1.2 Hz, at all depths. In contrast, for the higher canopy densities, ΔC was found to be negative for the highest frequencies of 1.4 and 1.6 Hz, i.e., the higher the density, the higher the ΔC . Fig. 3.6a, 3.6c and 3.6e show that these results were found both above and inside the canopy bed. For the flexible canopies, the largest negative values of ΔC were found for the largest SPF 5% and 10%. As was also found for the small particles (Fig. 3.5b, 3.5d and 3.5f), ΔC was found to be largely negative when increasing the density of the canopy bed. No significant differences of ΔC were found with depths, indicating a homogeneous vertical distribution of particles. ΔC for the real canopy (*R. maritima*) also mimicked the results obtained in the flexible canopy, at the same canopy density of flexible vegetation of 1%.

ΔC for the 2.5 to 6.0 μm particles (Fig. 3.7a) and for the 6.0 to 100 μm particles (Fig. 3.7b), was then compared to the ratio between the Reynolds stress ($u'w'$) with the presence of a canopy, and the Reynolds stress ($u'w'_{wc}$) for experiments without a canopy at $z/h_v = 0.4$ for all the experiments carried out. For both particle size ranges, $u'w'/u'w'_{wc}$ below 1 resulted in negative ΔC (Fig. 3.7a and 3.7b), showing that a low concentration of particles in suspension was found compared to the vegetation-free canopy experiments. In contrast, for the case with $u'w'/u'w'_{wc}$ above 1, ΔC was positive. A larger ΔC (up to 60%) was found for the smaller particle range (Fig. 3.7a), compared to the ΔC for the largest particle range, up to 20% (Fig. 3.7b), for the same $u'w'/u'w'_{wc}$. In general, experiments with flexible and natural canopies presented $\Delta C < 0$, i.e. a lower resuspension in the vegetated experiments than with the vegetation-free experiments. In contrast, the rigid vegetation was the only one with $\Delta C > 0$ for the majority of experiments.

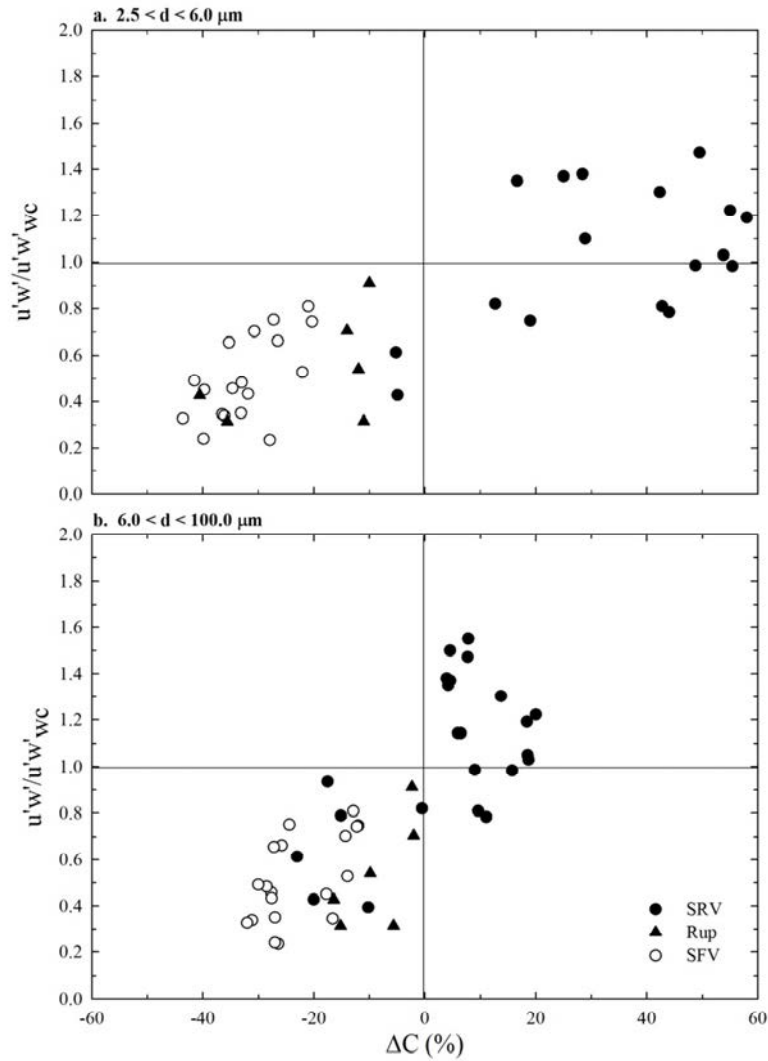


Fig. 3.7. Ratio between $u'w'$ for vegetated experiments and $u'w'$ for the vegetation-free experiments against ΔC , for experiments carried out with the three canopy models. (a) 2.5 to 6.0 μm particles and (b) 6.0 to 100 μm particles.

3.4. Discussion

3.4.1. Canopy scale turbulence distribution

Developing models to predict flows inside natural canopies is challenging due to the difficulties in incorporating the complexity of the canopy geometry and the broad range of length scales. While some models approximate vegetation with higher bottom friction factors (Möller et al., 1999), the majority implement an empirical drag coefficient to estimate drag forces along the plant (Mendez and Losada, 2004). Taking into account that Lowe et al. (2005a, 2005b) showed that A_w/S was the most relevant parameter affecting the attenuation of the flow inside the canopy, we hypothesize that the TKE inside the canopy can be written in the following form:

$$\frac{TKE}{U_w^2} = k \left(\frac{A_w}{S} \right)^a \quad (3.8)$$

Fig. 3.8 shows the best fit of the data with $k = 0.016$, $a = -0.0519$ ($R^2 = 0.6114$, 99% confidence), where it can also be seen that highest values of the TKE correspond to the rigid plants. Here the TKE at $z = 5$ cm was considered representative for the behavior of the TKE within the canopy.

Although several studies have pointed out that canopies provide sheltering, showing a decrease in the TKE compared to canopy-free environments, these results show that sheltering was attained for all cases in the flexible canopy, while the net effect on rigid cylinders was dependent on both canopy density and wave frequency. Inside the rigid canopy the TKE was larger compared to the equivalent experiments without vegetation, for the cases of $SPF = 1\%$ (i.e., $128 \text{ shoots} \cdot \text{m}^{-2}$) for all frequencies, and for the higher densities (5%, 7.5% and 10%) and the lower frequencies from 0.6 to 1.2 Hz (Fig. 3.4). The increase in TKE was attributed to the generation of stem-wake turbulence, in accordance with the results obtained by Pujol et al. (2013b). Fig. 3.9 shows the plant Reynolds number calculated as $Re_p = DU_w/\nu$, where D is a stem parameter scale (the diameter of the cylinders for the rigid canopy or the blade width for the flexible canopy) and ν is the kinematic viscosity. Experiments with

$Re_p > 250$ and $\Delta TKE > 0$ corresponded to the rigid canopy environments with low wave frequencies and high SPF canopies.

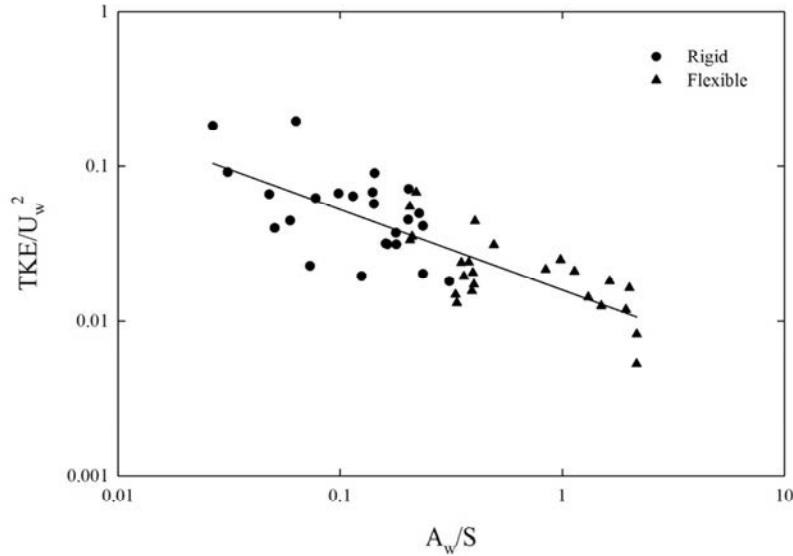


Fig. 3.8. TKE/U_w^2 vs. A_w/S , calculated at $z/h_v = 0.4$ for both rigid and flexible vegetation.

For the rigid canopy there were also cases where $\Delta TKE < 0$ (Fig. 3.4) indicating that these canopy configurations might provide sheltering depending on both the wave velocity and the SPF. These cases correspond to the highest plant densities (SPF = 5%, 7.5% and 10%, i.e. 640, 960 and 1280 shoots·m⁻²) and highest wave frequencies ($F = 1.4$ and 1.6 Hz). In these cases maximum values of ΔTKE were found at the top of the canopy corresponding to a zone characterized by maximum shear as described by Pujol et al. (2013b). As pointed out by Hendriks et al. (2008), in the region of the canopy-water interface, turbulent vertical transport of momentum is enhanced due to augmented turbulent shear stresses. Koftis et al. (2013) found that for a *P. oceanica* meadow of 360 stems·m⁻², at the positions above the top of the seagrass ($z/h_v = 1.09$ and 1.45), the energy at the peak frequencies of the spectrum were amplified, revealing the effects attributed to the movement of the plant leaves.

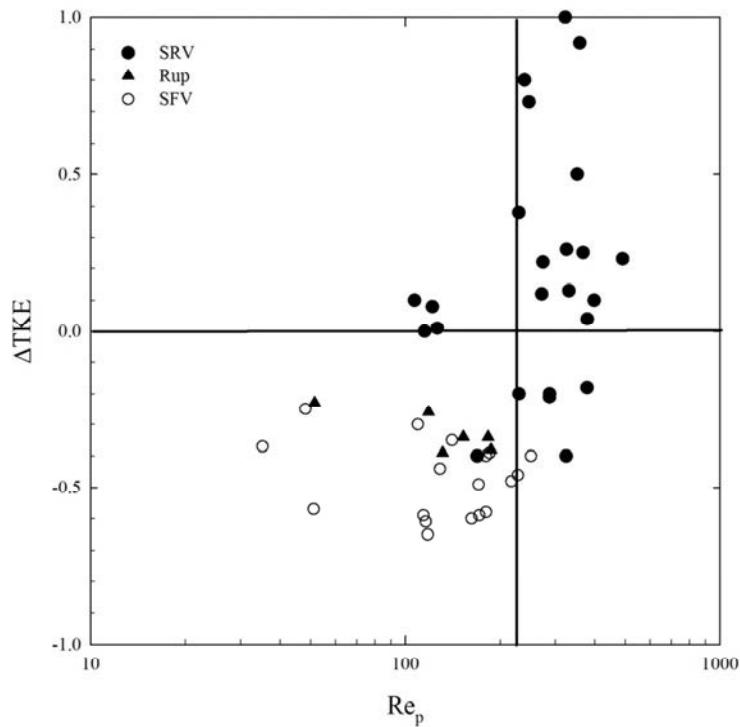


Fig. 3.9. Relationship between ΔTKE and the stem Reynolds number (Re_p) for the different canopy models used at $z/h_v = 0.4$.

For the flexible canopies $Re_p < 250$, and no TKE production was observed. Therefore, all the energy in the mean flow was dissipated without turbulence production. Indeed, results showed that inside the flexible vegetation canopy, ΔTKE decreased with canopy density, with no minimum threshold required to initiate wave velocity attenuation through a reduction in the TKE compared with the non-vegetated case, in accordance with other studies that found that the canopy density enhanced wave height reduction and therefore wave attenuation (Bouma et al., 2005; Fonseca and Cahalan, 1992; Gambi et al., 1990; Granata et al., 2001; Koftis et al., 2013; Manca et al., 2012; Neumeier and Ciavola, 2004).

3.4.2. Sediment resuspension within canopies

Studies show that resuspension is controlled by the bottom shear stress, that can be computed by estimates of $\langle u'w' \rangle$ within the constant stress region of the bottom boundary layer and extrapolated to the bed, which is normally well correlated with the TKE (Hansen and Reidenbach, 2012, 2013). Computation of the current shear stress within vegetation is not well described, especially in the presence of wave activity, but under unidirectional currents, a useful parameterization is through estimates of the near-bottom TKE (Widdows et al., 2008). In the present study, a linear correlation $\langle u'w' \rangle = -0.033\text{TKE}$ with $R^2 = 0.5676$ (99% confidence) was found.

The results showed that rigid canopies were not always effective in promoting the protection against resuspension. Cases with $\Delta C > 0$ corresponded to rigid canopies where resuspension was enhanced. Only a few cases for rigid canopies had $\Delta C < 0$ (higher frequencies and higher SPF). On the contrary, for all the flexible canopies and for the *R. maritima* $\Delta C < 0$, showing that flexible plants were able to reduce the sediment resuspension.

In the cases with $\Delta C > 0$, the energy from the main flow is dissipated via the production of the TKE; however for flexible canopies energy from the main flow dissipates without producing TKE.

Observations made by Mac Vean and Lacy (2014) indicate that wave shear stresses at the bed led to high resuspension and sediment-induced stratification, and the Stokes drift velocity as well as wind stress at the water surface increased mean shear within the water column. The correlation between wave attenuation and resuspension of particles was also reported by Gruber and Kemp (2010). These authors linked an amount of wave attenuation, 37% in a submerged bed of *Stuckenia pectinata*, with a 60% reduction of total suspended solids, during a period of peak plant biomass. In the present study, the mean wave attenuation through the range of frequencies studied was 20% for the densest rigid vegetation model and 15% for the densest flexible vegetation model.

3.5. Conclusions

In summary, this study showed that the resuspension of sediments in submerged canopies under progressive waves was reduced for both the flexible and *R. maritima* vegetation canopies (encompassing both sparse and dense canopies) at all the wave frequencies studied. This reduction also coincided with a reduction in TKE and bottom shear stress well inside the canopy.

In contrast, the net effect on resuspension due to rigid cylinders depends on the SPF. Rigid cylinders enhanced sediment resuspension for all wave conditions within sparse vegetation (1% SPF) via an increase of TKE. For denser cases (SPF = 5, 7.5 and 10%), enhancement in resuspension occurred for wave frequencies lower than 1.2 Hz, while resuspension was damped at higher frequencies. Such a difference is attributed to the turbulent wake generation at $Re_p > 250$. Flexible canopies along with the densest rigid canopies at high frequencies, showed the ability to diminish sediment resuspension and therefore, their ability to diminish the erosion of the sediment at the bottom of the bed. In these cases the energy from the main flow dissipates without producing TKE. The physical mechanisms involved in the way that flexible plants dissipate the energy from the main flow is still not understood.

Chapter 4: Sediment resuspension within submerged vegetation model canopies in an oscillating grid chamber

Aquatic plants, hydrodynamic turbulence and sediment fluxes interact with each other in a complex, non-linear fashion. Most studies of these interactions have considered the turbulence to be generated primarily by mean flow. However, there are many situations where turbulence is otherwise generated. In this chapter, turbulent interactions with vegetation are studied, and their effects on sediment suspension, in the absence of mean flow. In a water tank, turbulence was generated by oscillating a grid above simulated canopies of rigid or flexible vegetation, which had a base layer of sediment. Measurements of turbulent kinetic energy (TKE) and suspended sediment concentration were made. Both the rigid and flexible canopies reduced TKE compared to without-plant cases, the reduction being greater in denser canopies. In denser canopies, flexible plants reduced TKE more effectively, but in sparser canopies, they increased TKE, whereas rigid plants reduced it. I infer that this is due to the greater freedom for turbulence generation by leaf-flapping in low-density, flexible canopies. The concentration of suspended sediment was a linear function of the TKE for all canopies. Thus, both sediment mobilization at low canopy densities and sediment stabilization at high canopy densities were less in rigid canopies than in flexible canopies. Assuming that stable substrates are a strong control on plant survival, this suggests that sparse, rigid vegetation may be more resilient than sparse, flexible vegetation, but dense, flexible vegetation may be more resilient than dense, rigid vegetation.

4.1. Background

One of the most important effects of aquatic vegetation on hydrodynamics is its reduction of turbulence, which leads to a reduction in sediment resuspension, and thus increases water clarity (Vermaat et al. 2000; Madsen et al. 2001; Pujol et al. 2010). Increases in water clarity enhance light penetration and therefore aquatic plant productivity, thus creating a positive

feedback (Ward et al. 1984; Koch 2001). This effect is likely to be strongest in periods when plant growth peaks, at the end of spring and during summer. Plants with different morphologies may alter the hydrodynamics differently (Vermaat et al. 2000; Pujol et al. 2010; Pujol et al. 2013a; Pujol et al. 2013b). Studies using emergent plants have shown that the turbulence inside their canopies decreases linearly with increasing stem density, and that even low densities of plants can cause substantial reduction of turbulence (Horppila et al. 2013). However, Bouma et al. (2009) found that sparse canopies of rigid plants increased the unidirectional flow velocity and thus scouring and resuspension of sediment, counteracting the water-clarifying effects of turbulence reduction. These increases in the flow velocity may redistribute seeds and nutrients, particularly during periods of plant senescence in winter, fall and early spring, when canopy densities are relatively sparse (Hansen and Reidenbach, 2013). In shallow vegetated coastal areas, sediments are often disturbed by wind stirring, and resuspension occurs frequently and is governed by the intensity of the external forcing event (Black et al. 2002) and canopy properties (Ondiviela et al. 2014).

Much research has been carried out in laboratory flumes and in the field to determine the effects of emergent and submerged vegetation canopies on hydrodynamics, for both unidirectional and waves regimes, (e.g. Mendez et al. 1999; Nepf 1999; Nepf and Vivoni 2000; Poggi et al. 2003; Pujol et al. 2013a; Pujol et al. 2013b). In all of these studies, the conversion of mean flow kinetic energy to turbulent kinetic energy results from the interaction of the mean flow with the vegetation. The turbulence is generated in the wakes of individual stems and the canopy as a whole, and by shear due to velocity gradients in the mean flow field (Neumeier, 2007).

The oscillating grid is a device that produces nearly isotropic zero-mean flow turbulence (Desilva and Fernando 1994; Colomer et al. 2005; Serra et al. 2008). Oscillating grids have been used since 1950s to study isotropic turbulence in the absence of the mean shear associated with flowing water. The properties of the turbulence are determined by the geometry of the grid, the frequency and amplitude of the oscillations, and the distance from the grid (Holzner et al., 2006; Nokes, 1988). Close to the grid, distinct jets and wakes are formed, but these merge with each other to produce a zero-mean flow, isotropic turbulence field beyond a threshold distance away from the grid (Desilva and Fernando, 1994).

OGT can be used as an analogue to open-channel flow systems by setting operational parameters of the grid (stroke, frequency, etc.) such that the total kinetic energy of the turbulence matches that expected either at the bed or free surface for an open channel flow. Due to the predictable and reproducible nature of the turbulence generated by the oscillating grid, replicate tests of sediment resuspension and chemical fluxes can be readily accomplished (Orlins and Gulliver, 2003). Oscillating grids have also been used to study the resuspension of both cohesive (Tsai and Lick 1986) and non-cohesive (Huppert et al. 1995) sediments. Tsai and Lick (1986) found that the concentration of resuspended cohesive sediment was proportional to the oscillation frequency of the grid. Huppert et al (1995) found that above a critical oscillating frequency, a given mass of non-cohesive sediment particles can be kept in suspension indefinitely. The critical frequency depends on the diameter of the sediment particles. Orlins and Gulliver (2003) used OGT to study sediment resuspension from beds with different times of consolidation. They presented a detailed mapping of TKE produced by the grid and showed that steady-state suspended sediment concentrations were achieved within 10-30 min for a range of turbulence levels, and that the suspended sediment concentration was proportional to the TKE generated by the grid. They also found that, for the same level of TKE, less-consolidated sediment beds are subject to greater amounts of resuspension.

In canopies of aquatic vegetation, the turbulence induced by the wind affects the bottom boundary layer of the flow field in a manner that depends on the canopies' properties. The interaction between wind-generated turbulence and plant canopies has been simulated in the laboratory using an oscillating grid chamber (Pujol et al. 2010). In these experiments, two zones were identified: one at the top of the canopy, which was characterized by a reduction in TKE, and the other at the bottom of the canopy, where the TKE progressively decayed as the stems dissipated the turbulence, with the dissipation proportional to $(TKE)^{3/2}$ (Casamitjana et al. 2012).

The aim of the current study was to use an OGT set-up to investigate the relationship between the resuspension of natural, cohesive sediments in vegetated environments and the amount of isotropic, shear-free turbulence, with the aims of gaining understanding of this relationship by studying it in isolation from other phenomena such as mean flow, and mimicking field

situations dominated by turbulence. This study has been completed with the analysis of some scales that are an estimate of the size of the different eddies generated by the grid movement.

4.2. Procedure

4.2.1. Experimental setup

The study was conducted in an oscillating grid turbulence chamber (Fig. 4.1) consisting of a Plexiglas box with interior dimensions of $0.28 \text{ m} \times 0.28 \text{ m} \times 0.33 \text{ m}$. This was filled with water to a depth, h_w , of 0.315 m . A Plexiglas grid was suspended from above the chamber such that its center was $z_0 = 0.065 \text{ m}$ below the water surface (0.25 m above the bottom of the chamber). The square, 0.01 m -deep grid was composed of 5×5 bars, with a spacing (or ‘mesh size’) between the bars of $M = 0.05 \text{ m}$, giving a solidity of 31% (defined as the fractional solid area occupied by bars). It was oriented horizontally and oscillated vertically, by a variable-speed motor located outside the tank, with a fixed stroke of $s = 0.05 \text{ m}$, and frequencies of $F = 2.8, 3.8$ and 4.8 Hz . A clearance of 2 mm was maintained between the sidewalls and the grid. The vertical direction is defined as z (positive downwards), and $z = 0$ as the mean vertical position of the oscillating grid.

4.2.2. Vegetation models

Simulated canopies of either rigid or flexible vegetation were placed in the tank prior to each experimental run. The rigid canopy models consisted of PVC cylinders of diameter $d = 6 \text{ mm}$ and length $h_s = 0.10 \text{ m}$ (Fig. 4.2a). The flexible canopy models were constructed by attaching flexible polyethylene blades to rigid PVC dowels 0.02 m long and 6 mm in diameter, with tape (Fig. 4.2b). Each simulated plant had eight plastic blades 4 mm in width, 0.10 m in length and 0.07 mm in thick. These flexible plant simulants were dynamically and geometrically similar to typical seagrasses, as described by Ghisalberti and Nepf (2002), Folkard (2005), Pujol et al. (2013a) and El Allaoui et al. (2015). The similarity was evaluated in terms of the lambda parameters (λ_1 and λ_2) defined by Ghisalberti and Nepf (2002).

$$\lambda_1 = \frac{(\rho_w - \rho_v)h_s^3}{Eb^2} \quad (4.1)$$

$$\lambda_2 = \frac{Eb^2}{h_s^3 U_c^2} \quad (4.2)$$

Where ρ_w ($=1000 \text{ kg}\cdot\text{m}^{-3}$) is the water density, ρ_v ($=908.5 \text{ kg}\cdot\text{m}^{-3}$) is the plant density, E ($2.5 \times 10^8 \text{ Pa}$) is the modulus of elasticity, b is the plant width and U_c is the mean flow velocity. Like Pujol et al (2013a) and Folkard (2005), in the present study, λ_2 was not considered due to its strong dependence on the mean flow velocity, and λ_1 was calculated to be $0.065 \text{ s}^2\cdot\text{m}^{-1}$, close to the value found by Pujol et al (2013a) of $0.07 \text{ s}^2\cdot\text{m}^{-1}$. The blades' density was less than that of water (as in the case for real seagrasses) so that, at rest, the flexible canopy height was the same as that of the rigid canopy.

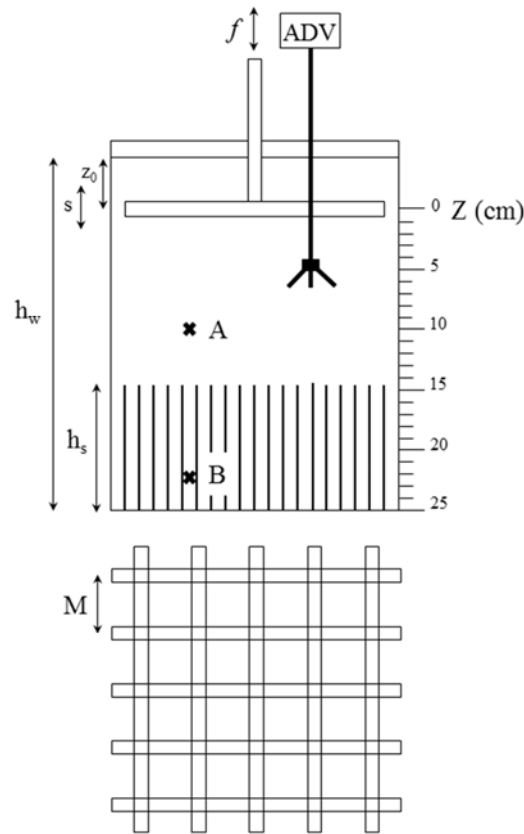


Fig. 4.1. Scheme of the experimental set-up. A and B represents the position of the water velocity measurements.

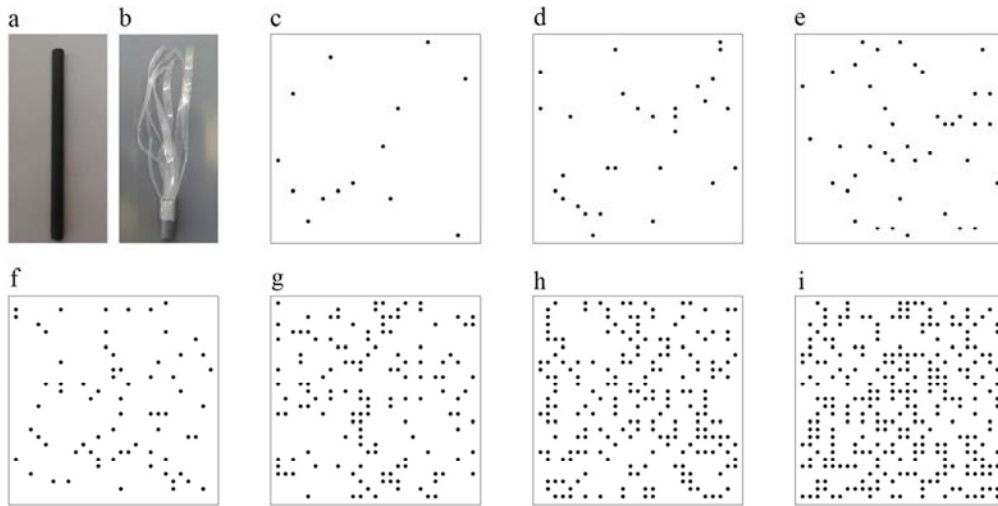


Fig. 4.2. Illustration of the submerged aquatic vegetation models: (a) submerged rigid vegetation; (b) submerged flexible vegetation; and plots of plants distributions: (c) SPF = 0.5 %; (d) SPF = 1 %; (e) SPF = 1.5 %; (f) SPF = 2.5 %; (g) SPF = 5 %; (h) SPF = 7.5 %; (i) SPF=10 %.

The canopy density was varied between runs and was quantified, following Pujol et al. (2010), using the solid plant fraction $SPF = 100n\pi(d/2)^2/A$, where n is the number of plant stems, and A is the total bed surface area covered by the canopy. For the flexible canopies, d was taken as the diameter of their rigid sections (6 mm). SPF of 0.5, 1, 1.5, 2.5, 5, 7.5 and 10% were used for both rigid and flexible canopy runs (Table 4.1, Fig. 4.2c-i). These SPFs corresponded to densities of 177, 354, 531, 884, 1768, 2652 and 3536 plants·m⁻². To create each canopy, the plants were secured in 6 mm-diameter holes, which were configured in a regular grid with 0.01 m center-to-center spacing in a plastic base board. The position of each plant within this grid was identified using a random number generator (“Flow structure in canopy models dominated by progressive waves,” n.d.; Serra et al., 2004). Holes left unfilled once all of the plants had been placed were filled with small dowels positioned flush with the board’s surface.

In addition, the vertical variation in canopy density varied from rigid to flexible canopies. Following Neumeier and Amos (2006), the vertical variation in the canopy density was assessed from the lateral obstruction of the canopy by taking a lateral picture of a 2.5 cm thick

canopy in front of a white background. Flexible blades were painted black to increase the image contrast. Images of the lateral obstruction were digitized and image analysis techniques were applied to differentiate the vegetation from the background. Finally, the lateral obstruction percentage was calculated (Fig. 4.3). While rigid canopies had a lateral obstruction that remained constant with height, the lateral obstruction of flexible plants varied with height with maximum percentages from $z=17$ cm to $z=23$ cm (Fig. 4.3).

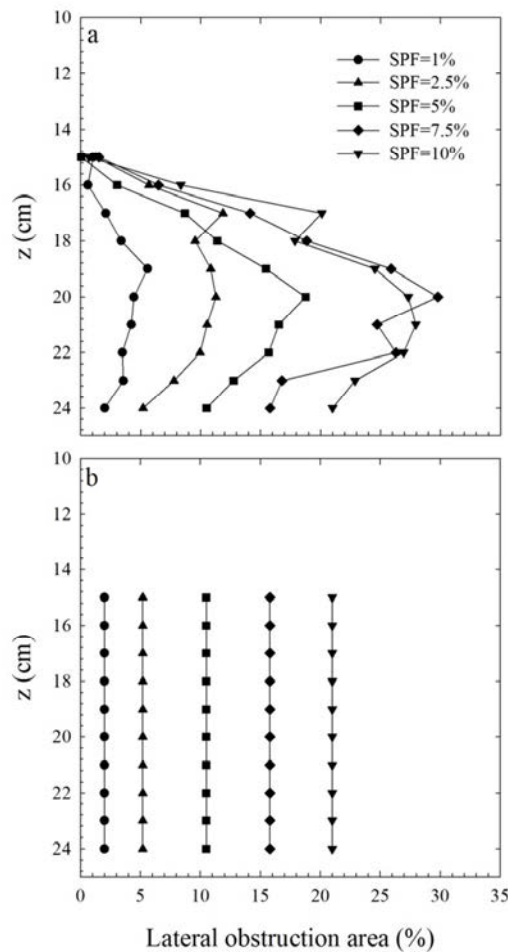


Fig. 4.3. Plot of the lateral obstruction percentage: (a) Submerged flexible vegetation, (b) Submerged rigid vegetation.

Table 4.1. Vegetation parameters for the experiments carried out: solid plant fraction, number of stems per square meter, oscillating grid frequency.

Run canopy model	SPF (%)	n_s (stems·m ⁻²)	F (Hz)
Without vegetation			
WP1			2.8
WP2			3.8
WP3			4.8
Submerged rigid vegetation model			
SRV1	1	354	2.8
SRV2	2.5	884	2.8
SRV3	5	1768	2.8
SRV4	7.5	2652	2.8
SRV5	10	3536	2.8
SRV6	1	354	3.8
SRV7	2.5	884	3.8
SRV8	5	1768	3.8
SRV9	7.5	2652	3.8
SRV10	10	3536	3.8
SRV11	1	354	4.8
SRV12	2.5	884	4.8
SRV13	5	1768	4.8
SRV14	7.5	2652	4.8
SRV15	10	3536	4.8
Submerged flexible vegetation model			
SFV1	0.5	177	2.8
SFV2	1	354	2.8
SFV3	1.5	531	2.8
SFV4	2.5	884	2.8
SFV5	5	1768	2.8
SFV6	7.5	2652	2.8
SFV7	10	3536	2.8
SFV8	0.5	177	3.8
SFV9	1	354	3.8
SFV10	1.5	531	3.8
SFV11	2.5	884	3.8
SFV12	5	1768	3.8
SFV13	7.5	2652	3.8
SFV14	10	3536	3.8
SFV15	0.5	177	4.8
SFV16	1	354	4.8
SFV17	1.5	531	4.8
SFV18	2.5	884	4.8
SFV19	5	1768	4.8
SFV20	7.5	2652	4.8
SFV21	10	3536	4.8

4.2.3. Sediment bed emplacement

Once the simulated canopy had been secured at the base of the experimental tank, and the tank filled with water, the bottom of the tank was covered with sediment collected from a natural salt marsh in the Baix Ter Natural Park, a wetland area situated in the North-East of Catalonia (NE Spain). This sediment was cleaned to remove traces of organic matter such as leaves and roots and then sieved to remove particles larger than 500 μm .

The sediment particle size distribution was analyzed by means of a laser particle size analyzer (LISST-100, Sequoia Scientific, Inc., WA, USA). Based on the classification by Rijn (2007) and Blott and Pye (2012), the sediment was divided into three ranges of particle diameter (Fig. 4.4). The first range (2.5-6.0 μm) corresponds to clays and very fine silts (strongly cohesive), the second range (6.0-170 μm) corresponds to fine to coarse silts and small sand particles (weakly cohesive), and the third range (>170 μm) corresponds to small and medium sand particles (non-cohesive). Fig. 4.4 shows that $\approx 99\%$ of the particles fell into the first range. Particles in the second and third ranges accounted for the remaining 1% of particle numbers, but 58.8% of the total particle volume concentration (Fig. 4.4). Moreover, the particle volume distribution for particles in these two ranges was approximately constant throughout all the experiments, indicating that they were not re-suspended in any of the experiments. For this reason, these larger particles were not considered in the analysis, and only particles in the smallest size range were analyzed.

The bottom of the tank was covered with homogeneous sediment to a uniform depth of 5 mm. This seeding was performed by manually moving a tube, which was connected to a container holding the sediment mixture, around the bottom of the chamber through the vegetation. The seeding resulted in a cloud of particles of ≈ 0.05 m in height, which was left to settle for 2 days after the seeding, following Ros et al. (2014). Since scouring was not observed in any of the experiments, thicker sediment beds were not considered.

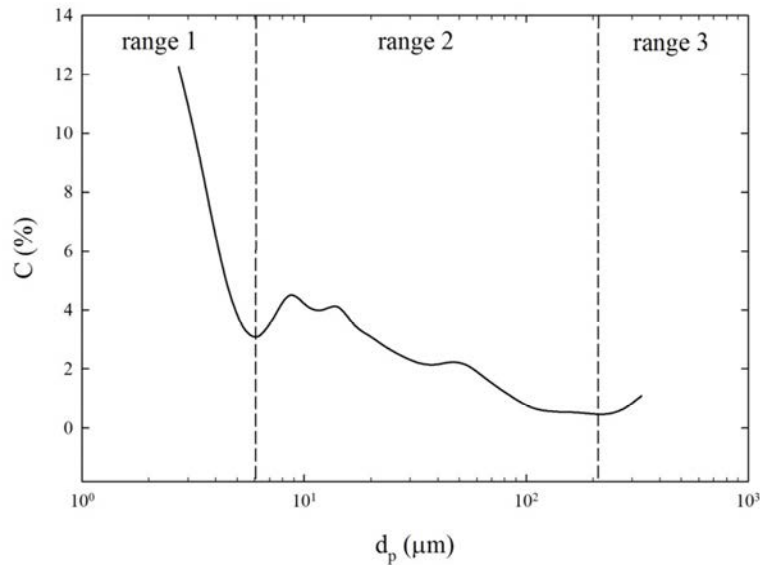


Fig. 4.4. Particle size distribution for the salt marsh sediment used in the experiments. Vertical dash line represent the classification by Rijn (2007). The smaller particles ($d_p < 6 \mu\text{m}$) correspond to the particle range of clay and very fine silts (very cohesive sediment). Vertical dashed lines represent the limits between different particle size ranges.

4.2.4. Turbulence measurements

The three-dimensional turbulent velocity field (u , v , w) inside the tank was measured with a three-component Acoustic Doppler Velocimeter (ADV) (Sontek/YSI16-MHzMicroADV). The ADV had an acoustic frequency of 16 MHz, a sampling volume of 0.09 cm^3 , a sampling frequency of 50 Hz and measured in the range $0\text{-}30 \text{ cm}\cdot\text{s}^{-1}$. The distance between the head of the ADV and the sampling volume was 0.05 m. The ADV was mounted on a movable vertical frame that allowed it to be manually situated at working depths between $z = 0.10 \text{ m}$ and $z = 0.24 \text{ m}$. For all experiments, the ADV was placed horizontally 0.07 m ($1.4\times$ the mesh size) from one side wall and 0.12 m ($2.4\times$ the mesh size) from the other side wall, as suggested by Orlins and Gulliver (2003), in order to avoid side-wall effects. In addition, following Desilva and Fernando (1994), the mesh endings were designed to reduce mean secondary circulation. To avoid any spikes in the data that were artifacts of instrument operation, rather than representative of the flow, ADV measurements with beam correlations

below 70% or with instantaneous velocities outside of two standards deviations from the mean were discarded for the analysis (“Flow structure in canopy models dominated by progressive waves,” n.d.). The use of single point ADV measurements for characterizing OGT turbulence can be justified by noting that several authors (e.g. Desilva and Fernando 1992, Hopfinger and Toly 1976 and Matsunaga et al 1999) found that at a certain distance from the grid, turbulence is isotropic and the velocity fluctuations u' , v' and w' are proportional to $1/z$. It seems therefore plausible to use single-point ADV measurements in this context, at least at $|z| > 2M$, where M is the spacing between bars see (Atkinson et al 1987). In the present study, $M = 5$ cm, therefore for $|z| > 10$ cm, the turbulence is expected to be isotropic.

To obtain valid data acquisition within the canopy for the densest canopies of flexible plants, a few stems were removed (a maximum of 3 stems for the $SPF = 10\%$ canopy density) to avoid blocking the pathway of the ADV beams, following Neumeier and Ciavola (2004), Pujol et al. (2010) and Pujol et al. (2013a). To minimize the effect of this ‘hole’, its shape was specifically designed to allow the ADV acoustic receivers and the acoustic transmitter to perform properly, whilst removing as few stems as possible.

For each experiment, a vertical velocity profile was taken from $z = 0.10$ m to $z = 0.24$ m depth (see Fig. 4.1) at 0.01 m intervals to reveal the structure of the turbulence field. Therefore, the vertical profiles covered measurements inside and above the canopy. At each depth the instantaneous water velocity (U_i , V_i , W_i), was measured for 10 minutes (thus giving 30000 measurements for each velocity component) and then decomposed as $U_i = U + u'$, where U is the time-averaged velocity component in one horizontal direction (x) and u' is the turbulent component in this direction. The velocity components v (speed in the y -direction – the horizontal direction orthogonal to the x -direction) and w (speed in the vertical direction) were similarly decomposed into $V + v'$ and $W + w'$ respectively. The turbulent kinetic energy per unit mass (TKE) was then calculated from the root mean square values of the three turbulent components:

$$TKE = \frac{1}{2}(\overline{u'^2} + \overline{v'^2} + \overline{w'^2}) \quad (4.3)$$

4.2.5. Sediment entrainment measurements

Sediment samples of 100 mL were obtained by means of a pipette that was introduced through the opening of the lid situated at the top of the OGT. Samples were collected at two different depths ($z=0.1$ m, i.e. 0.05 m above the canopy, and at $z=0.20$ m, i.e. 0.05 m below the top of the canopy). For all the experimental runs, the particle volume distribution of suspended sediment was measured using the LISST-100 laser particle size analyzer, which has been used extensively and has been found to be appropriate for measuring either organic particles (Serra et al. 2003) or mineral particles (Granata et al., 2001; Serra et al., 2005). From these measurements, the particle volume concentration in each range (Fig. 4.4) was obtained by summing the particle volume concentration of all the particle sizes within the range. The total density of suspended sediment (TSS, $\text{g}\cdot\text{L}^{-1}$) was calculated by multiplying the particle volume concentration by the sediment density (which was measured to be $2.52 \text{ g}\cdot\text{cm}^{-3}$).

Given that the smaller particles in the size spectra can remain in suspension quasi-indefinitely, suspended sediment concentration (C) was calculated relatively, as the value measured at a time t (C_t) subtracted from the value measured prior to the start of the oscillations at $t = 0$ (C_0), i.e. $C = C_t - C_0$. Each experimental run started at the lowest oscillation frequency of the grid, 2.8 Hz. A steady state was reached after 30 minutes, and after 30 minutes more (60 minutes from the beginig) the oscillation frequency was increased to 3.8 Hz. When a new steady state was reached after a further 30 minutes, after 30 minutes more of oscillation (120 minutes from the beginig), the frequency was increased to its highest value of 4.8 Hz. Thus, each run lasted a total of 180 minutes.

4.3. Results and discussion

4.3.1. Turbulent field in the presence of a bottom canopy

For experiments without plants, the TKE decreased with vertical distance from the grid (Fig. 4.5). This result was also described by Pujol et al. (2010). For experiments with rigid or flexible canopies, two layers were distinguished: an above-canopy layer and a within-canopy layer (Fig. 4.5). In the above canopy layer, the TKE for both rigid and flexible canopies

(SPF = 5 %) was close to that measured without plants. Within the canopy layer, the TKE for both the rigid and flexible canopy (SPF = 5 %) cases was below that for the run without plants.

The TKE at $z = 22$ cm was chosen to represent the TKE within the canopy for the purpose of comparing between experimental runs (Fig. 4.1b). In Fig. 4.6, TKE is plotted for both rigid (left panel) and flexible (right panel) plants for all the canopy densities studied, and also for the without-plants case. In all cases, the TKE was found to increase with grid oscillation frequency. In all of the rigid canopy cases, the TKE was lower than in the without-plants case (SPF = 0 %) for all the frequencies tested, and reached a minimum at an intermediate value within the range of SPF values studied.

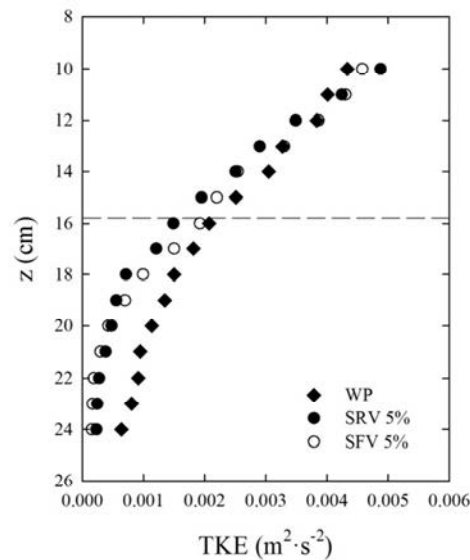


Fig. 4.5. TKE profiles for experiments carried without plants, and flexible and rigid vegetation with SPF = 5 %, and $F = 4.8$ Hz.

The TKE measured inside the flexible canopy peaked towards the sparser end of the range of canopy densities used, at SPF = 1%, decreasing with increasing density at SPF values above

that. This is – at first glance – unexpected, since flexible canopies are expected to reduce TKE (Ros et al. 2014). For sparse canopies ($SPF \leq 1.5\%$), in-canopy TKE was higher for the flexible canopies than for the rigid canopies, while the opposite was the case for the densest canopies ($SPF \geq 5\%$). The differences observed between the TKE for flexible and for rigid canopies might be attributed to the different distribution of the plant area with height, i.e. the lateral obstruction area (Fig. 4.3). Rigid plants presented a constant lateral obstruction area with height while the lateral obstruction area for flexible plants was variable. This variability was greatest for the densest flexible canopies with $SPF = 7.5\%$ and 10% , in which the lateral obstruction area reached maximum values of 28% , representing an obstruction area 43% (for $SPF=7.5\%$) and 25% (for $SPF=10\%$) higher than for the rigid plants.

The peak in TKE values at $SPF \leq 1.5\%$ in the flexible canopy data may be due to greater movement of the flexible plants at smaller SPF values. SPF was calculated using the diameter of the solid stalk at the base of each plant, in the same way as for the rigid canopies. However, whereas the rigid canopies remain this size throughout, in the flexible plant cases, the leaves spread out increasingly with height. In the sparser canopies, the plants are widely spaced enough that the leaves can move relatively freely and create significantly increased amounts of turbulence. As the SPF increases, however, the leaves constrain each other's movement more, and this effect is reduced.

Fig. 4.7 shows the spectrum of the TKE measured at two vertical depths, $z = 0.11\text{ m}$ (0.05 m above the canopy) and $z = 0.20\text{ m}$ (0.05 m below the top of the canopy). For the non-canopy case (Fig. 4.7a) the spectra are similar, and the formation of the inertial subrange (represented by the straight lines of slope $-5/3$) is observed. However for the cases with vegetation (Figs. 4.7b and 4.7c) the spectrum from within the canopy differs from the spectrum from outside it. Inside the canopy, peaks at the grid frequency ($F = 4.8\text{ Hz}$) or multiples of it (e.g. $F=14.4\text{ Hz}$) are observed for both rigid and flexible cases, probably due to the confinement of the turbulence motions to the spaces between the plants; this is not observed in the non-canopy case. These peaks are even clearer in the spectra of the vertical turbulent component of the velocity (w' , not shown here), the dominant frequency of which matches that of the oscillating grid. This is to be expected, since the grid oscillates in a vertical direction. Also, it can be seen than at higher frequencies (above 5 Hz) there is a flattening of the spectra, which

can be attributed to the white noise that is found in ADV data when measuring sampling volumes within 1 cm of an obstruction (Dombroski and Crimaldi, 2007). A smaller difference in power density between the inside and outside of the canopy is observed in Fig. 4.7d: as noted previously, inside the sparser canopies, TKE increased due to the freer movement of the leaves.

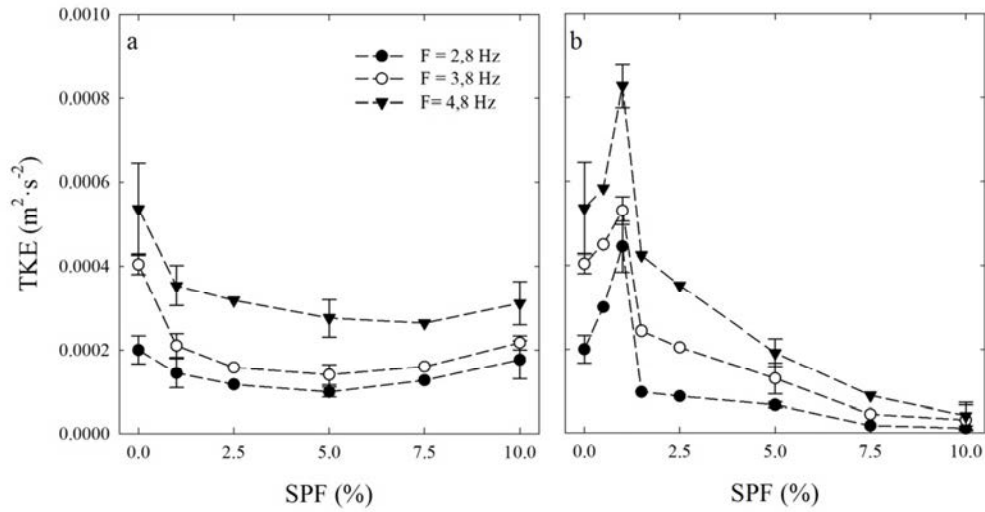


Fig. 4.6. Relationship between the TKE the SPF for different oscillating frequencies for both rigid (a) and flexible (b) canopies.

Table 4.2 shows the values of the dissipation rate (ϵ), Kolmogorov length scale $\eta = (v^3/\epsilon)^{1/4}$, Taylor micro-scale $\lambda_T = (10vTKE/\epsilon)^{1/2}$ and integral length scale $l = (TKE)^{3/2}/\epsilon$. The dissipation was calculated by using a $k-\epsilon$ model following the method described by Casamitjana et al. (2012). Briefly, the $k-\epsilon$ model simulates the profiles of TKE (k) and dissipation (ϵ). As boundary conditions, the measured value of the TKE (k_0) and the estimated value of the dissipation (ϵ_0) at a certain distance from the grid were used for all the simulated cases. As I do not know the values of ϵ_0 , they were estimated by trial and error until the experimental data for the TKE profiles fit the theoretical curve. The plot of k_0 with ϵ_0 showed

a very good correlation ($R^2 = 0.99$) with a relationship $\epsilon_o \sim k_o^{1.6}$. This correlation is similar to the one found by Matsunaga et al (1999) who reported a value of 1.7 for the exponent of k_o .

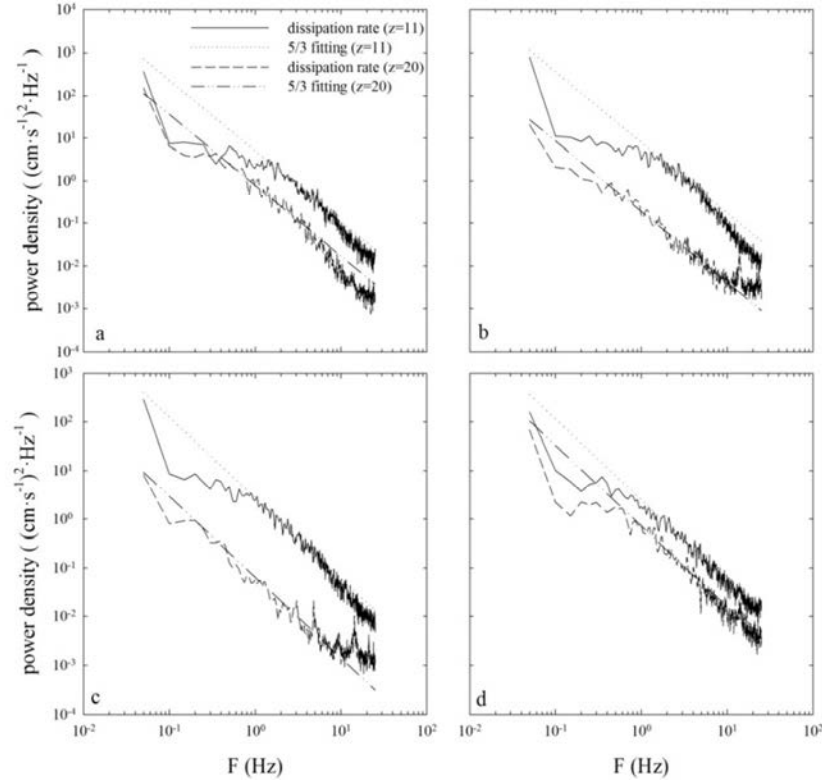


Fig. 4.7. Turbulent kinetic energy spectra above the canopy ($z = 11$ cm) and within the canopy ($z = 22$ cm) for the experiments: (a) without plants; (b) submerged rigid vegetation (SPF = 7.5 %); (c) submerged flexible vegetation (SPF = 7.5 %); (d) submerged flexible vegetation (SPF = 1 %).

Table 4.2. Summary of TKE, dissipation (ϵ), Kolmogorov scale (η), Taylor scale (λ_T) and integral length scale (l).

Canopy model	SPF (%)	z (cm)	TKE ($m^2 \cdot s^{-2}$)	ϵ ($m^2 \cdot s^{-3}$)	η (mm)	λ_T (mm)	l (mm)
WP	0	10	$4.3 \times 10^{-03} \pm 0.7 \times 10^{-03}$	$1.7 \times 10^{-03} \pm 0.4 \times 10^{-03}$	0.20 ± 0.01	5.1 ± 1.1	168 ± 93
WP	0	22	$6.0 \times 10^{-04} \pm 1.0 \times 10^{-04}$	$1.4 \times 10^{-04} \pm 0.4 \times 10^{-04}$	0.30 ± 0.02	6.5 ± 1.5	104 ± 58
SRV	5	10	$4.8 \times 10^{-03} \pm 0.4 \times 10^{-03}$	$2.0 \times 10^{-03} \pm 0.3 \times 10^{-03}$	0.20 ± 0.01	4.9 ± 0.6	169 ± 53
SRV	5	22	$4.4 \times 10^{-04} \pm 0.4 \times 10^{-04}$	$7.8 \times 10^{-05} \pm 1.3 \times 10^{-05}$	0.30 ± 0.01	7.5 ± 0.9	117 ± 36
SFV	5	10	$4.5 \times 10^{-03} \pm 0.9 \times 10^{-03}$	$1.8 \times 10^{-03} \pm 0.6 \times 10^{-03}$	0.20 ± 0.01	4.9 ± 1.3	163 ± 104
SFV	5	22	$2.8 \times 10^{-04} \pm 0.5 \times 10^{-04}$	$6.6 \times 10^{-05} \pm 2.2 \times 10^{-05}$	0.40 ± 0.03	6.5 ± 1.7	71 ± 45

The Kolmogorov length scale, which is an estimate of the size of the smallest eddies present in the flow, was typically one order of magnitude smaller than the Taylor micro-scale, which is a measure of the size of the eddies in the inertial subrange and three orders of magnitude smaller than the integral length scale, which is a measure of the large-scale eddies in the production range.

It can be seen that the smallest eddies (Kolmogorov length scale) and the inertial sub-range eddies (Taylor micro-scale) increased in size with distance from the grid. However, while the largest eddies (integral length scale) decreased the estimated error is too high to determine a clear trend of the size of the largest eddies with distance from the grid. Nokes (1988) and Desilva and Fernando (1992) found the integral length scale to be proportional to the distance from the grid, but in this case, probably due to the anisotropy of the larger eddies, only the smaller eddies' sizes were proportional to depth.

In Fig. 4.7, it is surprising that the $-5/3$ slope distribution of power density can be seen even inside the canopy. In all the experiments, the mean plant-to-plant distance was greater than 14 mm, which is larger than the Taylor micro-scale (Table 4.2). Because of this, eddies inside the canopy are able to follow the universal spectrum. However the flattening of the spectra at higher frequencies inside the canopy indicates that the ADV data are overwhelmed by acoustic noise at these frequencies. A similar flattening of the spectra within stands of the seagrass *Thalassia testudinum* was found by Koch and Gust (1999).

4.3.2. Sediment resuspension in the presence of a bottom canopy

The evolution of the resuspended sediment concentration C_t with time is shown in Fig. 4.8, for the experiments carried out with both flexible and rigid canopies with SPFs of 5%. The dashed line in the plot represents the time evolution of the grid oscillation frequency. The concentration of particles in the smallest size range (Fig. 4.4) increased rapidly during the first 15 minutes of grid oscillation, and more slowly during the remaining 45 minutes, for all the frequencies studied. Similarly, Oguz et al. (2013) found that 15 minutes were required for sediment resuspension to reach a steady state in a wave-dominated environment. Again, there was a relatively rapid increase in sediment concentration in the first 15 minutes, and a slower

increase thereafter up to 30 min, when an approximate steady state was achieved. C_t is smaller in the flexible vegetation case than in the rigid vegetation case at all times (Fig. 4.8).

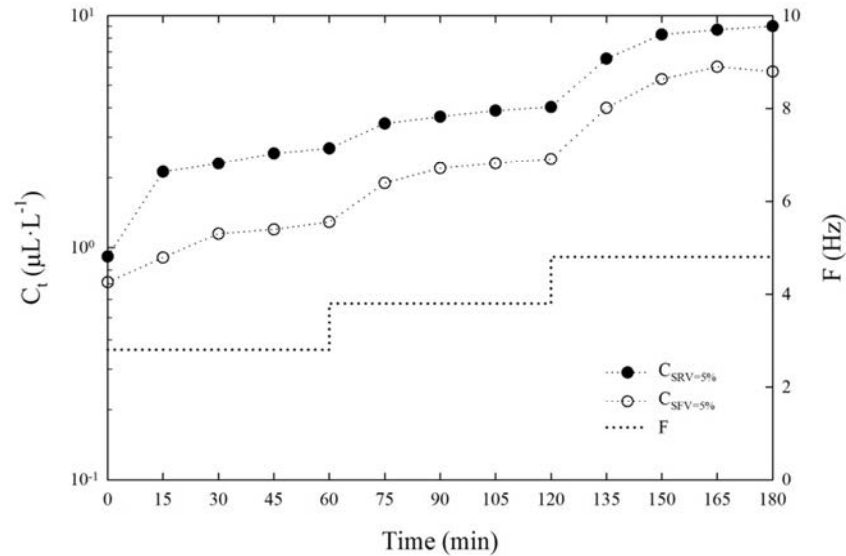


Fig. 4.8. Time evolution in the sediment concentration for experiments carried out for both rigid and flexible canopies for SPF = 5 %. The dashed line shows the evolution of the oscillating frequency in a set of experiments.

Fig. 4.9 shows the mean suspended sediment concentration during the stage of relatively steady concentration (30 to 60 minutes of grid oscillation at the given frequency), C_{ss} , for the smallest range of particle sizes (2.5 to 6.0 μm , Fig. 4.4) measured at $z = 0.22$ m, for the rigid vegetation (Fig. 4.9a) and the flexible vegetation (Fig. 4.9b). For comparison, this data for the no-canopy case (SPF = 0%) is also plotted in these figures. Suspended sediment concentrations measured at $z = 0.10$ m (results not shown) were found to be similar to those at $z = 0.22$ m shown here, indicating that the vertical distribution of particles in the system was homogeneous. In all the experimental runs, the sediment concentration increased with grid oscillation frequency. This was also found by Tsai and Lick (1986) who measured the sediment resuspension in an oscillating grid chamber in the absence of vegetation simulants working in the range of frequencies 5.5-12.5 Hz. For the rigid vegetation case (Fig. 4.9a), the

concentration of suspended sediment was similar to the concentration of the without-plants case, and remained near-constant over the full range of SPFs studied. However, for the flexible vegetation case (Fig. 4.9b), the suspended sediment concentration varied strongly with SPF. For low SPFs ($\leq 1.5\%$), C_{ss} showed a peak coinciding with the peak found in the TKE for the same experimental runs. The magnitude of the peak increased to a greater-than-linear extent with the frequency of oscillation. For canopies with SPFs $> 1.5\%$, the sediment concentration decreased as the plant density increased, reaching levels smaller than those found for the corresponding rigid vegetation cases at SPFs $\geq 5\%$.

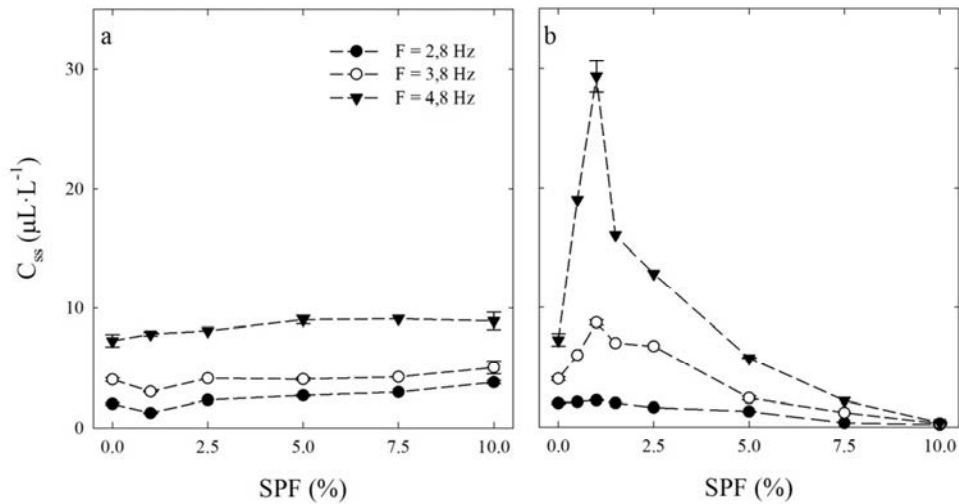


Fig. 4.9. Relationship between the suspended sediment concentration at the steady state (C_{ss}) and the SPF for different oscillating frequencies for both rigid (a) and flexible (b) canopies.

The relationship between TSS and TKE is presented in Fig. 4.10, which also shows results obtained by Orlins and Gulliver (2003). In the absence of simulated vegetation, Orlins and Gulliver (2003) reported sediment resuspension from a bed consolidated for two days (as in these experiments) at oscillating grid frequencies between 3.0 and 7.0 Hz and for a grid stroke of 0.03 m. In the study reported here, the TSS was found to increase with the TKE following a linear trend with a gradient of 1.05 ($p < 0.01$), which is smaller than the gradient obtained

by Orlins and Gulliver (2003) of 2.64. This difference may be due to the higher cohesiveness of the bed sediment in this study, which is due to the amount of clay particles. Of the sediment used by Orlins and Gulliver (2003) 14% was clays, therefore this was less cohesive than the sediment used in the present study, of which 41% was clays. Also note that the TKE values from the flexible vegetation cases cover a wider range than both the rigid vegetation and without-plants cases, and the results of Orlins and Gulliver (2003). This indicates that the flexible canopies are capable of producing lower TKE and therefore lower sediment resuspension when the canopy is dense (Figs 4.6 and 4.10), but are also capable of producing higher TKE when the canopy density is low and causing increased sediment resuspension.

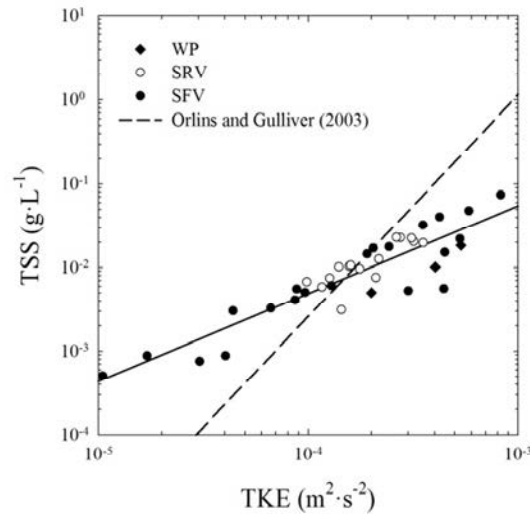


Fig. 4.10. Relationship between the total suspended sediment (TSS) and Turbulent Kinetic Energy (TKE) for either rigid, flexible and the without plants experiments. The dashed line shows the results for this relationship found by Orlins and Gulliver (2003). The thick black line shows the results of the experiments of this thesis.

Wu and Hua (2014) used a racetrack flume with a set of rotating plates situated at the water surface which was intended to simulate wind driven turbulence in a shallow lake. They studied sediment resuspension within a canopy of natural emergent plants with a density of 334 shoots·m⁻² and in a canopy of submerged plants with a density of 167 shoots·m⁻². They

found that the rigid plants reduced sediment resuspension more than the flexible plants. In their study, the canopy densities were similar to those in the $SPF = 1\%$ cases used in the present study, which had $354 \text{ shoots} \cdot \text{m}^{-2}$. In the experiments of this thesis, at this low density, the flexible canopy was found to generate more TKE than the rigid canopies, producing more sediment resuspension, in accordance with the results found by Wu and Hua (2014).

4.4. Conclusions

Simulations of rigid and flexible plant canopies have been found to reduce TKE in shear-free conditions compared to the without-plant cases. The reduction of the TKE is greater for denser canopies. At the higher values of canopy density studied here ($SPF \geq 5\%$), flexible canopies were able to reduce TKE more than rigid canopies. In contrast, at lower canopy densities ($SPF \leq 1.5\%$) flexible canopies increased TKE compared to the without-plants case, whereas rigid canopies reduced it. Observations suggest that this is due to the greater freedom for the leaves of the flexible canopies to flap in the low-density cases, enabling them to create turbulent energy that is added to that provided by the oscillating grid.

The analysis of the Kolmogorov length scale and the Taylor micro-scale showed that the size of the medium and smallest eddies is still smaller than the plant-to-plant distance at the bed, and then eddies can penetrate deep into the canopy and resuspend sediment from the bed. However, there is a difference between rigid and flexible plants at the top of the canopy, the plant-to-plant distance for flexible plants at the top is smaller due to the merging of the leaves, greater for denser canopies. This fact might bring differences between rigid and flexible plants in terms of the penetration of the eddies within the vegetation.

The concentration of sediment resuspended from the bed in these experiments was a linear function of the TKE, with similar trends for both rigid and flexible canopies. Therefore, since dense flexible canopies result in lower levels of TKE, I can infer that they will provide greater sediment stabilization. However, sparse flexible canopies increase the TKE and thus the suspended sediment concentration, thus enhancing the exchanges of mass between the bed and water column (and, by extrapolation, enabling greater mobility of sediments). The effects

of both sediment mobilization at low canopy densities and sediment stabilization at high canopy densities are less in rigid canopies compared to flexible canopies. Assuming that stable substrates are a strong control on plant survival, this suggests a mechanism that may lead to sparse distributions of rigid vegetation being better able to survive than sparse flexible vegetation, but dense distributions of flexible vegetation being better able to survive than dense rigid vegetation.

Chapter 5: Influence of extreme flooding events on wetlands

In a water channel, extreme flooding events were simulated by discharging particle-laden water into free particles water. The effect of the presence of rigid emergent vegetation was studied. The experiments were made with models of emergent rigid vegetation because most of the wetlands are dominated by the presence of many aquatic plants with rigid structure, like *Arthrocnemum macrostachyum* or *Juncus maritimus*. Measurements of the velocity of the main flow (the barotropic current) and the progression of the leading-edge that followed the flow (the baroclinic current) were made, as well as measurements of the sedimentation rate through the channel. Aquatic plants reduced the maximum velocity of the flow through the channel. Denser canopies reduced more the velocity but generated more TKE than sparser canopies. The velocity is reduced by dissipating the energy by generating turbulence. The increase in the TKE was attributed to the increase in the canopy density, which was analyzed through a parameter called bed roughness that was found to be proportional to the plant density. The progression of the front undertook two regimes. A first inertial regime and a second regime dominated by the drag of the return current. The transition from one regime to the other was found to depend on the discharge volume. While in absence of plants the progression was from inertial to drag dominated regime, in the presence of a high canopy density the inertial regime was not observed. Therefore, aquatic plants exerted a drag on the front before it reached the vegetation. The presence of aquatic vegetation enhanced the sediment deposition from the gravity current.

5.1. Background

As a result of both the predicted sea level rise or the increase on the strength of storms associated with the climatic change, there is growing concern over the increased flood risk and erosion of mudflats and salt marshes. However, there is a lack of adequate understanding

of the interactions between hydrodynamics (tidal currents and waves), plants and sediment. This lack of knowledge is especially more accentuated when storms and other extreme events flood the wetlands.

Particle-laden gravity-driven flows occur in a large variety of natural and industrial situations. Typical examples include turbidity currents, volcanic eruptions, and sand storms (see Simpson, 1997, for a review). On mountain slopes, debris flows and snow avalanches provide particular instances of vigorous dense flows, which have special features that make them different from usual gravity currents. Tidal waters that flood coastal wetlands are typically turbid (Adam, 1990) and flow velocity of tides is reduced as they move over mangrove and salt marsh vegetation, enabling sediments and organic material to settle on the marsh surface (Adam, 1990; Saenger, 2002). The sediment contribution in coastal wetlands has been found to derive from tidal incursions rather than terrigenous processes, and vertical accretion is typically proportional to the volume of water inundating the marsh surface (Rogers et al., 2013). Vertical accretion is well recognized as an important factor in wetland stability and also in the wetland resilience in front of the sea-level rise (Kirwan and Guntenspergen, 2010).

Short-term perturbations, such as storms and droughts, may influence the relationship between the tidal flow, vertical accretion and marsh elevation (Rogers and Saintilan, 2008). Rogers et al. (2013) state that elevation dynamics in salt marshes appear to be regulated by vertical accretion over long time periods and modulated by hydrology at short time periods. Storms redistribute sediments through scouring and settling and therefore can cause significant geomorphic changes in coastal wetlands (Smith et al., 2009). Climate change and sea-level rise will add pressure on coastal wetlands, including an increase in the frequency and intensity of short-term perturbations (Webster et al., 2005), compromising the future resilience of wetlands.

Sediment gravity flows are represented by four different mechanisms of keeping grains within the flow in suspension. In grain flow, sediments are kept in suspension by grain-to-grain interactions, with the fluid acting only as a lubricant. In fluidized flow, the pressure on the interstitial pore fluid increases and suspends the grains in the upper part of the flow. Debris flow are composed of a slurry-like mass of liquefied mud that move downhill under the force

of gravity and in turbidity currents grains are suspended by fluid turbulence within the flow (Postma, 1986).

The capture of suspended particles by submerged structures is important to biological cycles and chemical fates (Elliott, 2000; Paterson and Black, 1999; Raudkivi, 1998). Biologically, suspension feeders utilize hydrosol filtration for food capture (Belinsky et al., 2006). In addition, the transport of suspended particles is important in the life cycle of many species. For example, settlement of planktonic larvae is dictated, at least in part by the physics of particle motion and substrate encounter (Butman, 1987).

In lock-release gravity currents three phases can be distinguished, as observed by several investigators (Adduce et al., 2012). In the first phase, the front position varies as t^1 , i.e. the front velocity is constant with time. In the second phase, the front's position varies with $t^{1/2}$. Finally, gravity currents may transition to a third phase in which the dominant force balance is between viscous and buoyancy forces and the front's position varies with $t^{2/3}$. Gravity currents may become drag-dominated where they propagate into partially or fully vegetated channels, which have been simulated in laboratory experiments by arrays of rigid cylindrical obstacles (Hatcher et al., 2000). Under such cases the position of the front evolved as $t^{1/2}$.

Bonnecaze et al. (1993) studied a particle-laden gravity current spreading over a horizontal surface. In such case, the position of the front depended on $t^{2/3}$. Soler et al. (2016) found that the front of a particle-driven gravity current spreading over a horizontal surface with the presence of an array of obstacles follow a law of $t^{2/3}$ until it decelerates and transitions to a drag-dominated regime, following $t^{1/2}$.

This chapter aims to fill the knowledge gaps about the geomorphic influence of extreme flooding storms on wetlands by investigating how the canopies of emergent plants modify a barotropic current, and how the sediment deposition from a barotropic current is altered by the presence of plants. A particle laden gravity flow is created by opening a sluice gate. This opening creates an injection of water with particles that circulates through a flume with different canopy densities. The effect of different flooding event intensities has been studied with different volumes of the water inundating the salt marsh, i.e. different water discharges.

The gravity current will be driven by the initial height of the inflow of water and also by the difference in the sediment concentration between the gravity current and the ambient flow.

5.2. Procedure

5.2.1. Experimental set up

Laboratory experiments were conducted in a 5.46 m long by 0.4 m wide flume (Fig. 5.1). A sluice gate was placed at a distance of 1.57 m of one of the ends of the channel. It separated the channel in two different sections with different water depths. On the long section the water depth, $h_w = 0.07$ m was ensured by the height of an overflow situated at the end of the channel. On the short section the water depth was variable, always higher than h_w , and the difference between them was named H (Fig. 5.1). The lock gate was opened to a height of 0.03 m above the channel bed, for all the experiments, to allow the water flow from one of the sections to the other, and thus simulate the flood. To simulate floods of different intensities, four values of H were considered (H=2.5, 5, 10 and 15 cm) corresponding to discharges of $V = 15.7$ L, 31.4 L, 62.8 L and 94.2 L.

The longitudinal direction was defined as x , and $x=0$ was the longitudinal position at the gate. y was defined as the transversal direction, and $y=0$ at the centerline of the tank. The vertical direction was defined as z , and $z=0$ corresponded to the depth at the channel bed.

5.2.2. Vegetation models

The rigid emergent canopy was simulated with rigid PVC cylinders 0.6 cm wide and 14 cm long. Different canopy densities were used for the different experiments. According to Pujol et al. (2010) and Serra et al. (2004), the Solid Plant Fraction can be defined as $SPF = 100n\pi(d/2)^2/A$, where n is the number of plant stems, and A is the total bed surface area covered by the canopy. The SPF considered in the experiments was 1, 2.5 and 5% (Table 5.1). Runs without canopy were also considered. The plants were secured in 6 mm-diameter holes, which were positioned using a random number generator (Serra et al., 2004).

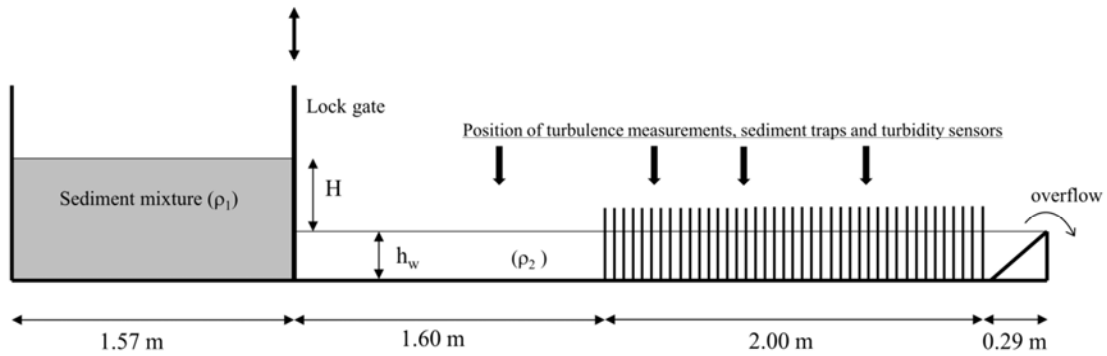


Fig. 5.1. Scheme of the experimental set-up.

Table 5.1. Vegetation parameters for the experiments carried out: solid plant fraction, number of stems per square meter and H .

Run Canopy model	SPF (%)	n_s (stems·m ⁻²)	H (cm)
Without vegetation			
WP1			2.5
WP2			5
WP3			10
WP4			15
Emergent Rigid vegetation			
ERV1	1	354	2.5
ERV2	2.5	884	2.5
ERV3	5	1768	2.5
ERV4	1	354	5
ERV5	2.5	884	5
ERV6	5	1768	5
ERV7	1	354	10
ERV8	2.5	884	10
ERV9	5	1768	10
ERV10	1	354	15
ERV11	2.5	884	15
ERV12	5	1768	15

5.2.3. Theory

The momentum equation for unidirectional gravity currents propagating through an array of obstacles, following Hatcher et al. (2000), can be decomposed as:

$$\frac{\partial u}{\partial t} + u \frac{\partial u}{\partial x} = -\Lambda u^2 + g \frac{dH}{dx} \quad (5.1)$$

where:

$$\Lambda = \frac{c_D \phi}{d} \quad (5.2)$$

Where d is the obstacle width, in this case the diameter of the plant. ϕ is the volume fraction ($\phi \ll 1$). C_D is the discharge coefficient. At the steady state:

$$u \frac{\partial u}{\partial x} + \Lambda u^2 \sim g \frac{dH}{dx} \quad (5.3)$$

Scaling analysis gives:

$$\frac{u^2}{x} + \Lambda u^2 = \frac{\alpha g H}{x} \quad (5.4)$$

Where α is a scaling constant ($\alpha = 0.19$). Therefore:

$$u^2 [1 + \Lambda x] = \alpha g H \quad (5.5)$$

$$u = \sqrt{\frac{gH}{1 + \alpha \Lambda x}} \quad (5.6)$$

which describes the reduction in the flow velocity as the front penetrates inside the canopy.

5.2.4. Turbulence measurements

The three components of the velocity were recorded with downwards looking Acoustic Doppler Velocimeter (Sontek/YSI16-MHzMicroADV), already described in section 2.2. The ADV measured at $z = 1$ cm above the channel bed. Four measurements of velocity were taken for each experiment, at $x = 120, 185, 240$ and 305 cm. The measurements lasted 5 minutes since the sluice gate was opened, and were repeated 5 times in order to perform the statistics that will be described later on this chapter, section 5.2.7.

5.2.5. Sediment characteristics

The short compartment of the channel was filled with a homogeneous mixture of water and sediment. The sediment was collected from a natural salt marsh in the Baix Ter Natural Park, a wetland area situated in the North-East of Catalonia (NE Spain). This sediment was cleaned to remove traces of organic matter such as leaves and roots and then sieved to remove particles larger than $500 \mu\text{m}$. A constant sediment concentration of $0.5 \text{ g}\cdot\text{L}^{-1}$ was used for all the experiments. The mixture of sediment and water was stirred for 10 minutes at the same velocity for all the experiments carried out. The stirring was performed just before the beginning of each experiment to avoid the settling of some sediment particles. After stirring, it was introduced in the compartment of the flume and mixed gently during 10 seconds to obtain a uniform distribution. After this, the system was left during 20 seconds before opening the gate at the start of the experiment.

The sediment used in the experiments of this chapter was the same as in the Chapter 4 experiments was used (Fig.4.4.), with the same particle size distribution.

5.2.6. Sediment measurements

Once the sluice gate was opened, the sediment edge advanced through the channel. Four turbidity sensors (Seapoint Turbidity Meter, Seapoint Sensors Inc., NH, USA) were collocated at $x = 120, 185, 240$ and 305 cm. They measured the time reached for the sediment edge to attain each point. The velocity measurements were completed with the video recorded for each experiment. Four sediment traps were located below the turbidity sensors, to collect all the settled sediment. The traps were covered at the time the sediment front arrived at the

end of the channel ($x = 305$ cm). The content of the traps was analyzed with the Laser in Situ Scattering and Transmissometry probe, LISST-100.

5.2.7. Calculation of the mean flow and the turbulent kinetic energy

The mean flow velocity and the turbulence were estimated using an ensemble averaging technique, described by Rapp and Melville (1990). The instantaneous velocity was decomposed into the sum of the ensemble mean velocity, $\langle u \rangle$, and the deviation from the ensemble, u' .

$$u = \langle u \rangle + u' \quad (5.7)$$

The deviation from the ensemble mean reflects three different sources:

$$u' = u'_t + u'_{rw} + u'_{mn} \quad (5.8)$$

where u'_t represents the turbulent component of the velocity, u'_{rw} is the motion associated to random waves, which is not the case of the present work, and u'_{mn} is the measurement noise.

The instrument noise of the ADV can be evaluated from the standard deviation of the time series before the passage of the front, at which time there are neither turbulent motions. The measurement noise was $0.0056 \text{ m}\cdot\text{s}^{-1}$ for the horizontal component. This noise level was so much smaller than the velocity rms measured after the arrival of the front, indicating that turbulence was measurable above the instrument noise. The TKE was estimated as the root mean square of u' considering the 5 replicas of each experiment undertaken (Pujol and Nepf, 2012). The velocity of the front, u , was calculated as the mean velocity among the 5 replicas carried out for each case.

5.3. Results and discussion

5.3.1. Turbulent field in the presence of a canopy

The maximum velocity of each water discharge was taken in account as it was found to be representative of the hydrodynamics for each experiment. The maximum velocity in the x direction, u_{\max} , at $z = 1$ cm, increased with H (Fig. 5.2). For all the experiments carried with the same H, the maximum velocity at $x = 120$ cm (before the canopy) was similar for the different SPF considered. The higher velocity was $\sim 40 \text{ cm}\cdot\text{s}^{-1}$ for $H = 15$ cm, and the lower velocity was $\sim 12 \text{ cm}\cdot\text{s}^{-1}$ for $H = 2.5$ cm. For the unimpeded case (Fig. 5.2a), for $H = 2.5$ and 5 cm u_{\max} was constant along the flume, and decreased slightly along the flume for the experiments carried out with $H=10$ and 15 cm. For the experiments with emergent canopies (Figs. 5.2b, 5.2c and 5.2d), u_{\max} decreased along the channel.

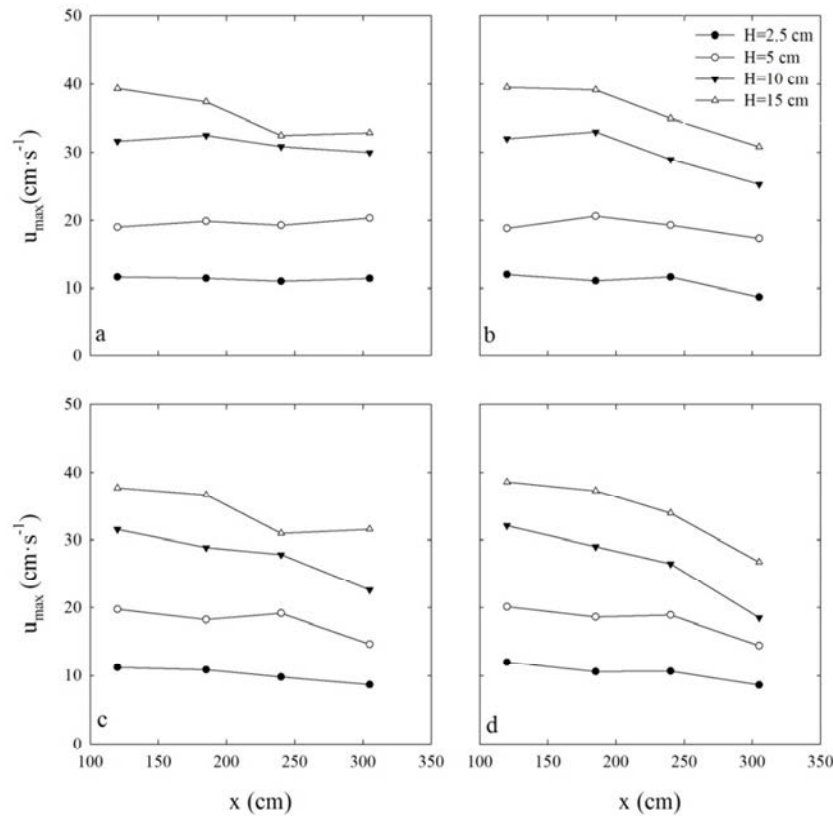


Fig. 5.2. u_{\max} profiles along the channel for the different discharge heights (H). (a) without plants. (b) SPF = 1%. (c) SPF=2.5%. (d) SPF=5%.

Fig. 5.3 shows the mean TKE for the first second immediately after the arrival of the flow at every measuring position in the channel. The unimpeded experiment (Fig. 5.3a) had lower TKE (under $10 \text{ cm}^2 \cdot \text{s}^{-2}$) than experiments with the presence of vegetation, except at $x = 120 \text{ cm}$, where the vegetation is not present in any of the experiments. Therefore, for all the experiments carried out, the TKE at $x = 120 \text{ cm}$ is similar to the TKE found for the unimpeded case. In the experiments with $\text{SPF} = 1\%$ and $\text{SPF} = 2.5\%$, the TKE presented a similar behavior between experiments carried at the same H . For the lower H cases ($H = 2.5$ and 5 cm), TKE increases gradually with x for all the x values. However, for experiments carried out with high H ($H = 10$ and $H = 15 \text{ cm}$), the TKE was high, increasing up to $x=240 \text{ cm}$, and decreasing afterwards to the end of the channel (Figs. 5.3b and 5.3c). The experiments with the highest $\text{SPF}=5\%$ presented a maximum of TKE at $x = 185 \text{ cm}$, around $35 \text{ cm}^2 \cdot \text{s}^{-2}$ for the experiments with high H ($H = 10$ and $H = 15 \text{ cm}$) and $19 \text{ cm}^2 \cdot \text{s}^{-2}$ and $5 \text{ cm}^2 \cdot \text{s}^{-2}$ for $H = 5 \text{ cm}$ and $H = 2.5 \text{ cm}$, respectively (Fig. 5.3d). After this position in x , the TKE decreased gradually to the end of the flume.

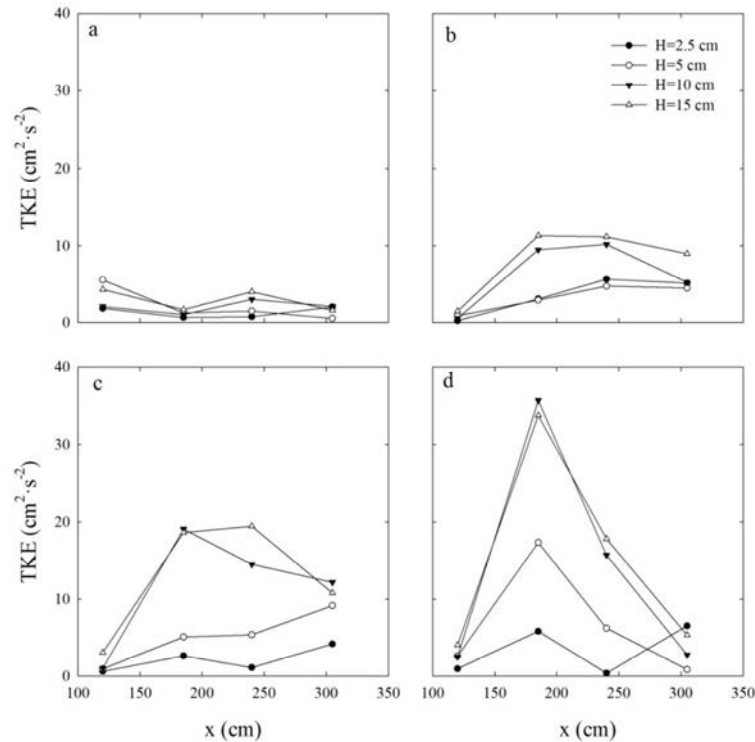


Fig. 5.3. TKE profiles along the channel for the different discharge heights (H). (a) without plants. (b) $\text{SPF} = 1\%$. (c) $\text{SPF}=2.5\%$. (d) $\text{SPF}=5\%$.

The model explained in the theory of this chapter (section 5.2.3) was used to predict the velocity in the channel. In Fig. 5.4 it can be seen the predicted velocity from equation 5.6 compared to the experimental values for the different SPF's. In each figure the experimental value of the velocity at $x = 120$ cm has been taken as the initial value of the velocity in equation (5.6). The parameter α was estimated to minimize the difference between the predicted and the experimental values for all the studied cases (Fig. 5.4 a, b and c) by using the SOLVER function from the Excel software (Microsoft Office). The obtained parameter that minimized these differences was $\alpha = 0.19$.

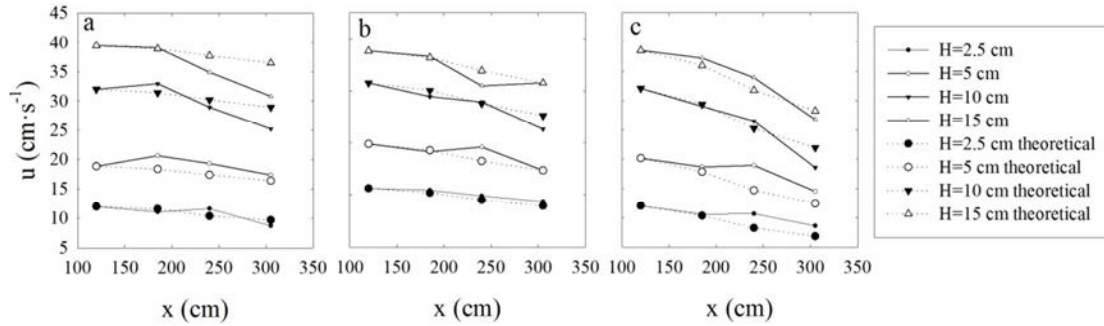


Fig. 5.4. Theoretical velocity compared to maximum velocity, at $x = 120$ cm. (a) SPF = 1 %. (b) SPF = 2.5 %. (c) SPF = 5 %.

Notice that u_{\max} differs from $\sqrt{2gH}$ as at a first glance it would be expected to hold. From the experiments, $u^* = u_{\max} / \sqrt{2gH}$ are comprised between 0.1 and 0.25 (see Fig. 5.5). This is because the discharge orifice occurs at the boundary layer where the velocity is significantly reduced. Therefore $u_{\max} = f \sqrt{2gH}$ where f is $\sim 0.1-0.2$.

Also it has to be noted that for a given SPF there are differences in the values of u^* between the different heights (Fig. 5.5). This happens because velocity at the orifice depends not only on the height. When fluid discharges through an orifice, the velocity increases and the fluid

pressure decreases. A little downstream of the orifice the flow reaches its point of maximum convergence, the *vena contracta* where the velocity reaches its maximum and the pressure reaches its minimum (Çengel and Cimbala, 2006). The discharge coefficient, C_d is a dimensionless number used to characterize the velocity loss behavior of orifices in fluid systems.

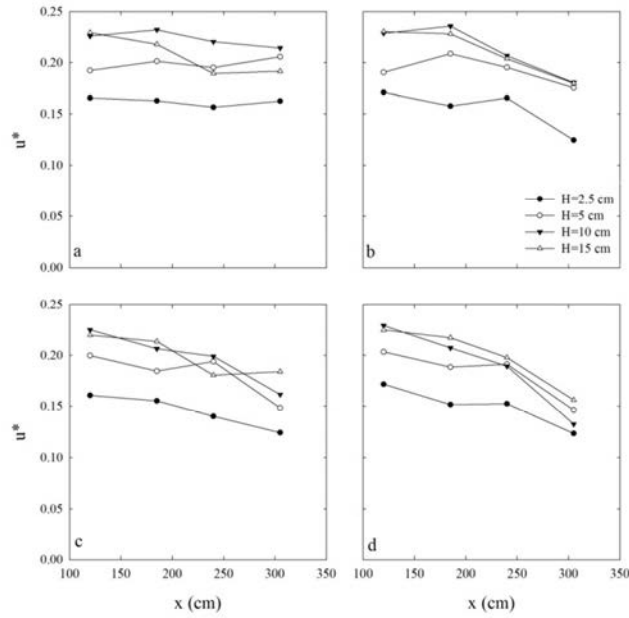


Fig. 5.5. u^* profiles along the channel for the different discharge heights (H). (a) without plants. (b) SPF = 1 %. (c) SPF = 2.5 %. (d) SPF = 5 %.

In general C_d is a function of the Reynolds number ($Re = \rho v D / \mu$), where $D = 0.03\text{m}$ is the height of the lock opening, and μ is the viscosity, and follows $C_d = a - (b/Re^{0.5})$ (Çengel and Cimbala, 2006). Therefore it was expected that the velocity u_{\max} would be:

$$u_{\max} = C_d f \sqrt{2gH} = \left[af - \frac{bf}{Re^{0.5}} \right] \sqrt{2gH} \quad (5.9)$$

and the values of af and bf were calculated to obtain the best fit (Fig. 5.6). Where $af = 0.29$ and $bf = 3.57$.

It has been seen that the $f < 1$, therefore the velocity u_{\max} was measured inside the boundary layer. An estimation of the thickness of the boundary layer can be obtained from $\delta = 5\nu/u^*$ (Kundu et al., 1990), where $\nu = 0.01 \text{ cm}^2 \cdot \text{s}^{-1}$ is the water kinematic viscosity and $u^* = (\text{TKE})^{1/2}$. In all the studied cases $\delta = 0.01\text{-}0.1 \text{ cm}$, which are smaller than the depth of the measuring point (1 cm), it indicates that the measurements were not in the laminar sub-layer and occurred at the logarithmic layer. The velocity on the logarithmic layer has the form:

$$u_{\max} = \frac{u^*}{k} \ln \left[\frac{y}{y_o} \right] \quad (5.10)$$

where $k = 0.4$ is the von Karman constant and y_o the soil roughness. Values of y_o can be obtained by equation 5.10 by fitting the experimental u_{\max} values with the u^* values, taking into account that $y = 5\text{cm}$.

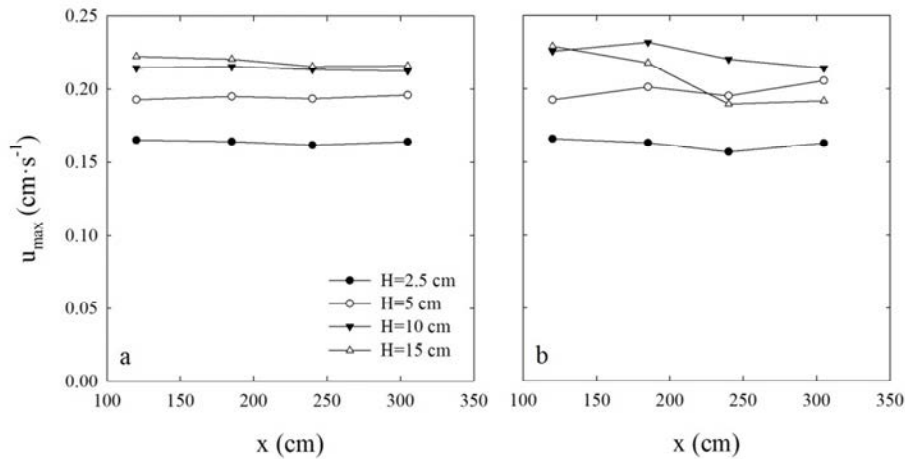


Fig. 5.6. u_{\max} profiles along the channel for the different discharge heights (H) and for the without plants experiments. (a) u_{\max} calculated following (Çengel and Cimbala, 2006). (b) u^* .

In table 5.2 and Fig. 5.7 it can be clearly seen as the roughness is an increasing function of the SPF as it would be expected. The obtained correlation is $y_o = 8.8 \text{ SPF} + 0.0017$ with $R = 0.9985$. Also in table 5.2 the equivalent roughness for a sand bed of grain diameter d_p has been estimated following the results of Nikuradse (Kundu et al., 1990), who established that $d_p = 30y_o$ when $u^* d_p / \nu > 70-100$, which is this case.

Table 5.2. Soil roughness (y_o) and grain diameter (d_p)

SPF (%)	y_o (cm)	d_p (cm)
0	0.009	0.29
1	0.084	2.55
2.5	0.214	6.42
5	0.446	13.41

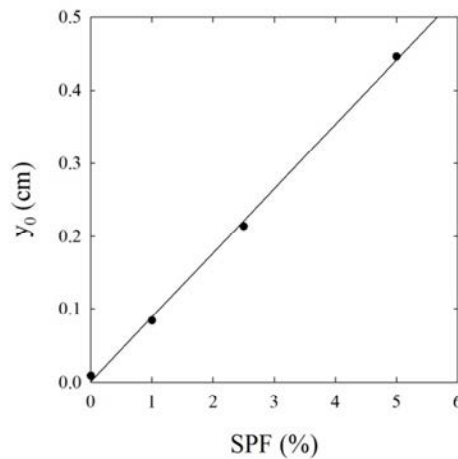


Fig. 5.7. Soil roughness (y_o) vs. SPF.

5.3.2. Sediment transport

The progression of the leading edge was analyzed for both situations the experiments without plants and the experiments with the higher plant density (SPF = 5%). For the experiments with $H = 15$ cm, the leading edge progression was too fast to make accurate measurements, so the results of these experiments were discarded for the sediment analysis. In Fig. 5.8 it

can be seen the progression of the leading edge. The non-dimensional relation x/H is shown in y-axis. x-axis shows the relation t/t^* , where $t^* = H / \sqrt{2g'H}$ and $g' = g \cdot \Delta\rho/\rho_2$, $\Delta\rho$ is the difference of densities between both fluids (ρ_1 and ρ_2 , see Figure 5.1). The inertial adjustment phase can be observed for the without plants case at the beginning of the flume and it is represented by a straight line with slope 1, the drag adjustment phase by a straight line with slope 0.3 and the viscous phase by a straight line with slope 0.2, as found by Rottman and Simpson (1983). For the case without plants (Fig 5.8b) the slope changes from inertial (slope 1) to viscous dominated (slope 0.2) whereas for the case with plants it changes from drag (slope 0.3) to viscous dominated (slope 0.2). Also, the slope change takes place at the same x/H position for all the experiments, so it can be deduced that the longitudinal position (x) where the phase change takes place is proportional to the water discharge (H).

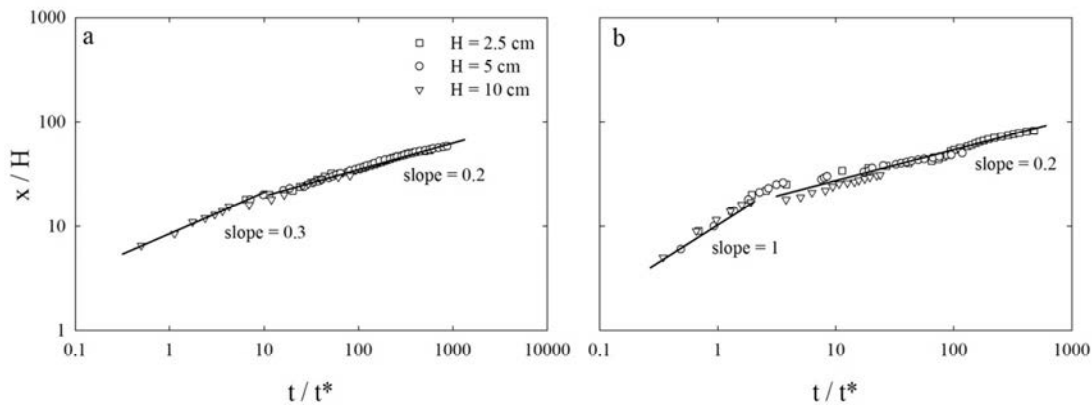


Fig. 5.8. Relationship between x/H and t/t^* . (a) SPF=5%. (b) Without plants.

The sediment settled on the bed and collected by the sediment traps was also analyzed. Fig. 5.9 shows the settling rate c^* , calculated following $c^* = m/(A_T \cdot t_{sed})$, where m is the sediment mass, A_T is the trap area and t_{sed} is the time between the arrival of the front at the given trap and the arrival of the front at the end of the channel. This time changed from one trap to the other since the time elapsed from the arrival of the front until the front reached the

end of the flume was different due to the different positions of the traps along the channel (see Figure 5.1). The sediment concentration increased as H increased, and for all the experiments with plants was higher than for the experiments without plants. The unimpeded experiments had a decreasing sediment concentration along the channel, while the experiments with plants presented lower sediment concentration at the central position in the channel ($x = 180$ cm) than in the channel edges ($x = 120$ cm and $x = 240$ cm). Furthermore, for the experiments with vegetation, the sediment trap situated before the vegetation presented different settling rates than the experiments without plants. This result indicates that the vegetation was capable of modifying the deposition of sediment on the bare soil but in regions situated nearby the vegetated zone. Therefore, the vegetation generated a drag on the gravity current that delayed the velocity of the front and enhanced the depositional rate of sediment.

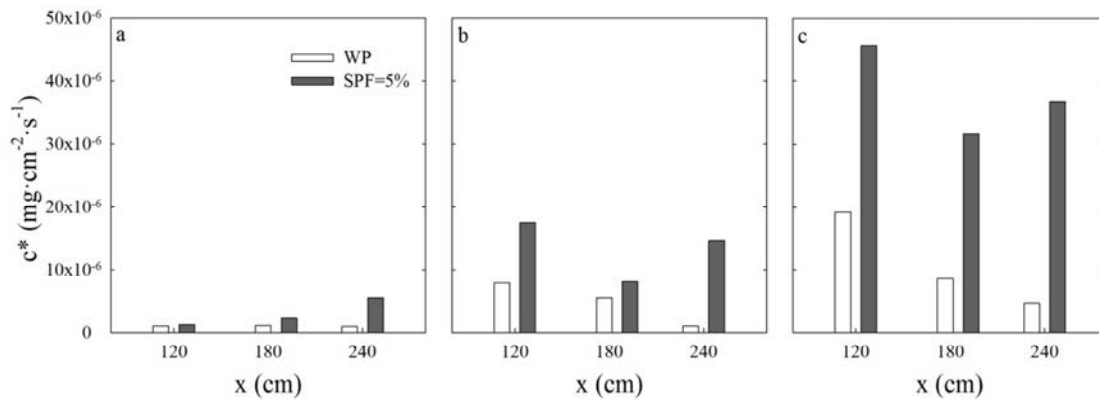


Fig. 5.9. Sediment rate deposited in the traps ($x = 120, 180$ and 240 cm) for both experiments without plants and with plants (SPF = 5 %). (a) $H = 5$ cm. (b) $H = 10$ cm. (c) $H = 15$ cm.

5.4. Conclusions

When an extreme flooding event with particles occurs, two different phenomena take place at a different time scales.

At a time scale $t_1 = L/C_d f \sqrt{2gH}$, where L is the length of the flume, a water wave propagates due to barotropic forces acting on the flow. In this case t_1 is 3-5 s. However at a time scales $t_2 = L/\sqrt{2g'H}$ a baroclinic current of particles replaces the barotropic current. In this case t_2 is 3-180 s. For these cases a transition between inertial to viscous dominated regime was found for the non-plants case whereas a transition between drag dominated to viscous regime was found for the plants case.

Emergent plant canopies have been found to reduce the maximum velocity of particle-laden water discharges simulating extremes flooding events, producing turbulent kinetic energy. The extent of the velocity reduction and the TKE production depended on the discharge and on the presence of aquatic plants in the flume.

The progression of a gravity current follows the flow generated by the discharge. For both the without plants and the plants experiments, the progression of the front has two phases, and the position where the phase change takes place is proportional to the height of the water discharge. For the unimpeded experiment, the progression is inertial then viscous dominated. For the experiments with plants the progression is drag then viscous dominated. The presence of plants enhances the sediment deposition from the gravity current within and in the nearby region of the vegetated zone.

Chapter 6: General discussion

This thesis has focused on the sediment transport through vegetated areas by three different processes (waves, pure turbulence and extreme flooding events). Each chapter of this thesis includes its own results and discussion section. Therefore, this Chapter aims to produce a more general discussion comparing the results of this thesis with those from others and also setting all the results together with the idea of providing an overview of the findings of this thesis.

Some hydrodynamics parameters, characteristics of these processes, have been taken in account, such as the wave frequency, the oscillating grid frequency and the water discharge height. Parameters of the environmental conditions of wetlands (plant density and plant flexibility) have also been considered. The analysis of the role of each of these parameters has shown how they modify the hydrodynamics, and also how they modify the sediment transport, promoting sediment settling or resuspension. Finally, ecological implications of these processes and future perspectives have been established.

6.1. Hydrodynamics

6.1.1. Plant density effects

The TKE and the flow velocity were found to depend on the canopy density. In all the cases studied, the mean flow was reduced within a vegetated region. In Chapter 3 and in Chapter 4 the TKE was reduced by the presence of the vegetation, except for sparse flexible canopies in the OGT. Experiments with waves have demonstrated that ΔTKE (TKE compared to the experiments without plants) decreases with an increase of the plant density for the flexible canopies, whereas for the dense canopies of rigid plants, when the oscillating frequencies are low, the behavior is the opposite. For the extreme flooding events, an increase in plant density implies an increase in TKE production but especially at the edge of the vegetation, whereas well inside the meadow the TKE decreases again providing shelter to the organisms and

stabilizing the sediment. This might explain the differences between the edge of a meadow and the region within a meadow. The edge is usually a region with a low biomass of vegetation. This might be due to the great mixing and sediment resuspension, which will coincide with a decrease in the water clarity. Carr et al. (2010) and Boer (2007) stated the negative effects of an increase in the water turbidity in seagrasses, resulting in their collapse due to the decrease in the light availability.

The OGT experiments allow understanding a process of turbulence without a main current associated. The results showed that, for SPF above 1.5%, the TKE was reduced for all the oscillating frequencies. TKE behavior, for the sparsest canopies, depended on the plant flexibility that will be discussed later on this chapter.

6.1.2. Plant flexibility effects

Flexible plants were only taken into account in Chapter 3 and Chapter 4 (waves and OGT). Experiments of extreme flooding events have been done with rigid canopy models.

In wave environments, ΔTKE is always higher for runs with rigid plants than for flexible ones, so the flexible plants generate less TKE than rigid ones. All the flexible canopies and the rigid dense canopies (only for high frequencies) reduce TKE compared to the unimpeded experiments, where sheltering prevails. These cases correspond to plant Reynolds number below 250, which indicates that all the energy of the mean flow is dissipated without production of TKE. Unlike this, TKE production (no sheltering) is associated to rigid sparse canopies (low frequencies) which generate stem-wake turbulence (Pujol et al., 2013b).

The role of plant flexibility is important to understand hydrodynamics in the sparse canopies on the OGT experiments. Only sparse canopies ($SPF \leq 1.5\%$) generate more TKE than the experiments without plants. This is due to the free movement of the blades, in contrast to denser canopies where the blades have a limited movement.

6.2. Sediment transport

The process of sediment transport has different phases: resuspension of particles from the bed, displacement of particles through the water column, and deposition of the particles. Experiments of Chapter 3 and Chapter 4 (waves and OGT) begun with a consolidated bed of sediments. The experiments aimed to understand the processes of resuspension of these particles. Experiments of Chapter 5 start with a mixture of suspended particles on the fluid, and the progression of gravity current and the deposition of sediment have been analyzed.

6.2.1. Plant density effects

The resuspension in wave environments is controlled by the bottom shear stress, $\langle u'w' \rangle$, which has a good correlation with the TKE. ΔC , defined as the suspended sediment concentration difference between the canopy and the free canopy cases, has been found to depend on the plant density. An inverse correlation has been found between ΔC and SPF: ΔC decreases when SPF increases, i.e. plant density has a reduction effect on sediment resuspension.

In OGT experiments, sediment resuspension was found to be a linear function with TKE. For some plant densities of the flexible canopy, sediment resuspension was enhanced, compared to the unimpeded case. For a given frequency, the concentration of resuspended sediment with rigid plants is similar for all the SPF. That means that rigid plants have little effect on sediment resuspension.

Finally, extreme flooding events experiments show that the front of the propagating gravity current follows an inertial regime that expands a distance that depends on the discharge. The presence of vegetation modifies its behavior evolving from a drag to a viscous dominated regime. Therefore, the presence of plants delays the progression of the front and as a consequence of the velocity flow reduction, sediment deposition is enhanced along the channel.

6.2.2. Plant flexibility effects

Flexible plants under oscillatory flows (flexible models and real plants of *R. maritima*) reduce sediment resuspension compared to the experiments without plants. Dense rigid canopies, for high wave frequencies, also reduce sediment resuspension. All these cases that reduced sediment resuspension coincided with a reduction in the TKE, and therefore the TKE was found to explain the sediment resuspension.

OGT experiments show a linear trend between sediment resuspension and TKE, as found by Orlins and Gulliver (2003). TKE generation was found for sparse flexible canopies, and, as it was expected, sediment resuspension was enhanced under these conditions. Dense flexible canopies, which is found that produce sheltering, also reduce the sediment resuspension.

In the third experiment carried out (Chapter 5) the edge of a vegetated region was found to experience more TKE than the inner part of the canopy. This could produce scouring of sediment in this region and also an increase in the turbidity that could produce negative feedbacks on the vegetation. More work should be done in order to address whether a flexible canopy would generate the same behavior at the edge like the one observed for a rigid canopy.

6.3. Ecological implications

Canopies of aquatic vegetation (seagrasses and salt marshes) are ecosystems that must be taken in account for the management plants for its important ecological function and its role in coastal protection. From an ecological point of view, macrophytes (both submerged and emerged) create a habitat for many other species by providing shelter from predation (Hemminga and Duarte, 2000). Moreover, they are feeding areas and nursery grounds (Short and Neckles, 1999; Unsworth et al., 2008).

The results of this thesis show that canopies under certain morphological conditions have the ability to diminish the amount of sediment resuspension (under waves and turbulence conditions) and to enhance sedimentation (under flooding conditions). Both of the processes imply a reduction in suspended sediment in the water, and therefore an increase in water

clarity. Clearer water provides greater light penetration and therefore an increase in aquatic plant productivity, thus creating a positive feedback (Koch, 2001; Ward et al., 1984) for the canopy. A reduction in sediment resuspension (or erosion), and a favored sedimentation, may result in stable substrates, which in turn provide a strong control in plant survival. The difference found between edge of vegetated zones and the inner part of vegetated zones might explain why seagrasses have a lower biomass at the edge than at the center of the patch of vegetation. Tanner (2005) found that the total seagrass biomass tended to vary smoothly with distance from the patch edge, rather than abruptly increasing from zero to a maximum density. Also, Bologna and Heck (2002) found that while shoot density and plant biomass were greater in the interior of a meadow of *Thalassia testudinum* bed than at the edges, mean faunal density was significantly greater at edges than in interior sites. Bologna and Heck (1999) also found more abundance of bay scallops at edges of grass beds than in the interior. They pointed that scallops appear to trade off higher predation risk for increased growth rates due to an increase in the food availability at edges.

From the point of view of coastal protection, a main issue for many governments, canopies of aquatic vegetation plays an important role by attenuating waves and currents in flooding events and coastal erosion (Ondiviela et al., 2014). Duarte et al. (2013) considered that coastal flooding and erosion are becoming a major threat to coastal areas, and found that vegetated coastal habitats provided mechanisms to contribute to the protection of coasts by decreasing the intensity of incoming energy. The results obtained in this thesis show that, in most of the studied conditions, aquatic canopies help at sediment stabilization by increasing sedimentation rates and decreasing sediment resuspension (compared to the non-vegetated areas), which in turn contributes at plants stabilization allowing for greater coastal protection.

6.4. Future perspectives

The results of this thesis help at understanding the role played by aquatic canopies in sediment transport, under three different hydrodynamic conditions (waves, pure turbulence and extreme flooding events). All the results were obtained by experimental observation in laboratory, where the experimental conditions are very controlled (e.g. constant sediment

composition and plant density). This thesis opens up a range of possibilities for further research in sediment dynamics in aquatic canopies. From my point of view, the next step in this research should be the investigation of the same processes in field conditions. It would be also interesting to investigate the sediment exchange at the edge of the canopy.

Chapter 7: Conclusions

This thesis has focused on the hydrodynamics and sediment transport through aquatic vegetation in wetlands under different processes. It has been found that submerged aquatic vegetation (rigid and flexible models as well as real plants) and emergent aquatic vegetation modify the hydrodynamics (waves, turbulence and floods), and therefore determine the rate of sediment resuspension or deposition through the vegetated areas. The most important conclusions of this thesis are:

- a. Under progressive waves, sediment resuspension is related to the ability of canopies to modify TKE. Compared to the experiments without plants, the flexible canopies (flexible models and real vegetation), as well as the rigid canopies (higher plant density and higher waves frequencies), reduce TKE, and thus reduce the amount of sediment resuspension. In contrast, sparser canopies of rigid vegetation models, at lower wave frequencies, increase TKE, by generating turbulent wakes at $Re_p > 250$, therefore increasing the sediment resuspension.
- b. Under pure and nearly isotropic turbulence, the concentration of resuspended sediment is a linear function of the TKE, with similar trends for both rigid and flexible canopies except for the sparse flexible canopies. Dense canopies of submerged flexible vegetation reduced more TKE than canopies of submerged rigid vegetation. The sediment resuspension decreased in both rigid and flexible canopies following the decrease in TKE. The freely movement of blades in sparse flexible canopies increased the TKE compared to the without-plants case and thus the suspended sediment concentration.
- c. Under extreme flooding events, emergent rigid plant canopies reduce the maximum velocity of the particle-laden water discharges producing an increase in the TKE. The flooding flow is followed by a particle-laden gravity current, whose progression velocity is modified by the presence of plants from an inertial-dominated regime to a

viscous-dominated regime. In addition, canopies of emergent plants increase the sediment deposition, not only within the canopy but also before it due to the delay caused by the drag exerted by the vegetation.

In summary, high densities of submerged aquatic vegetation (both rigid and flexible models) have the ability to stabilize the sediment bed by reducing the amount of resuspended sediment due to a reduction in TKE, under waves and turbulence conditions. In contrast, under flooding events, emergent aquatic vegetation generates TKE as a consequence of the energy dissipation of the flow, whose velocity is reduced, and under these conditions sediment deposition is enhanced.

More efforts should be done to understand sediment transport in wetlands by investigating with different sediment compositions (with organic matter) and other experimental conditions (different plant models and different mean water depths). It could also be interesting to investigate the sediment transport in the field conditions to compare with the experimental results obtained in the laboratory.

Chapter 8: References

- Adam, P., 1990. Salt marsh ecology. Cambridge University Press, Cambridge.
- Adduce, C., Sciortino, G., Proietti, S., 2012. Gravity currents produced by lock exchanges: experiments and simulations with a two-layer shallow-water model with entrainment. *J. Hydraul. Eng.* 138, 111–121.
- Alcamo, J., Floerke, M., Maerker, M., 2007. Future long-term changes in global water resources driven by socio-economic and climatic changes. *Hydrol. Sci. J.* 52, 247–275.
- Atkinson, J.F., Damiani, L., Harleman, D.R.F., 1987. A comparison of velocity-measurements using a laser anemometer and a hot-film probe, with application to grid-stirring entrainment experiments. *Phys. Fluids* 30, 3290–3292.
- Belinsky, M., Rubin, H., Agnon, Y., Kit, E., Atkinson, J.F., 2006. Characteristics of Resuspension, Settling and Diffusion of Particulate Matter in a Water Column. *Environ. Fluid Mech.* 5, 415–441.
- Black, K., Tolhurst, T., Paterson, D., Hagerthey, S., 2002. Working with natural cohesive sediments. *J. Hydraul. Eng.* 128, 2–8.
- Blott, S.J., Pye, K., 2012. Particle size scales and classification of sediment types based on particle size distributions: Review and recommended procedures. *Sedimentology* 59, 2071–2096.
- Boer, W.F., 2007. Seagrass–sediment interactions, positive feedbacks and critical thresholds for occurrence: a review. *Hydrobiologia* 591, 5–24.
- Bologna, P. a X., Heck, K.L., 1999. Differential predation and growth rates of bay scallops within a seagrass habitat. *J. Exp. Mar. Bio. Ecol.* 239, 299–314.
- Bologna, P., Heck, K., 2002. Impact of habitat edges on density and secondary production of seagrass-associated fauna. *Estuaries* 25, 1033–1044.
- Bonnecaze, R., Huppert, H., Lister, J., 1993. Particle-driven gravity currents. *J. Fluid Mech.* 250.
- Bouma, T., Friedrichs, M., Klaassen, P., van Wesenbeeck, B., Brun, F., Temmerman, S., van Katwijk, M., Graf, G., Herman, P., 2009. Effects of shoot stiffness, shoot size and current velocity on scouring sediment from around seedlings and propagules. *Mar. Ecol. Prog. Ser.* 388, 293–297.

- Bouma, T.J., De Vries, M.B., Low, E., Peralta, G., Táncoz, I.C., van de Koppel, J., Herman, P.M.J., 2005. Trade-Offs Related To Ecosystem Engineering: a Case Study on Stiffness of Emerging Macrophytes. *Ecology* 86, 2187–2199.
- Butman, C., 1987. Larval settlement of soft-sediment invertebrates. The spatial scales of pattern explained by active habitat selection and the emerging role of hydrodynamic processes. *Oceanogr. Mar. Biol. - An Annu. Rev.* 25, 113–165.
- Carr, J., D’Odorico, P., McGlathery, K., Wiberg, P., 2010. Stability and bistability of seagrass ecosystems in shallow coastal lagoons: Role of feedbacks with sediment resuspension and light attenuation. *J. Geophys. Res. - biogeosciences* 115.
- Casamitjana, X., Pujol, D., Colomer, J., Serra, T., 2012. Application of a $k-\epsilon$ formulation to model the effect of submerged aquatic vegetation on turbulence induced by an oscillating grid. *Cont. Shelf Res.* 34, 1–6.
- Çengel, Y., Cimbala, J., 2006. *Fluid mechanics*. McGraw-Hill.
- Colomer, J., Peters, F., Marrasé, C., 2005. Experimental analysis of coagulation of particles under low-shear flow. *Water Res.* 39, 2994–3000.
- Coulombier, T., Neumeier, U., Bernatchez, P., 2012. Sediment transport in a cold climate salt marsh (St. Lawrence Estuary, Canada), the importance of vegetation and waves. *Estuar. Coast. Shelf Sci.* 101, 64–75.
- Dean, R.G., Dalrymple, R.A., 1991. *Water Wave Mechanics for Engineers and Scientists*, 1st ed. WorldScientific Publishing, Singapore.
- Desilva, I., Fernando, H., 1994. Oscillating grids as a source of nearly isotropic turbulence. *Phys. Fluids* 6, 2455–2464.
- Desilva, I., Fernando, H., 1992. Some aspects of mixing in a stratified turbulent patch. *J. Fluid Mech.* 240, 601–625.
- Dombroski, D.E., Crimaldi, J.P., 2007. The accuracy of acoustic Doppler velocimetry (ADV) measurements in turbulent boundary layer flows over a smooth bed. *Limnol. Oceanogr. Methods* 5, 23–33.
- Duarte, C.M., Losada, I.J., Hendriks, I.E., Mazarrasa, I., Marbà, N., 2013. The role of coastal plant communities for climate change mitigation and adaptation. *Nat. Clim. Chang.* 3, 961–968.
- El Allaoui, N., Serra, T., Soler, M., Colomer, J., Pujol, D., Oldham, C., 2015. Modified hydrodynamics in canopies with longitudinal gaps exposed to oscillatory flows. *J. Hydrol.* 531, 840–849.

- Elliott, A., 2000. Settling of fine sediment in a channel with emergent vegetation. *J. Hydraul. Eng.* 126, 570–577.
- Folkard, A.M., 2005. Hydrodynamics of model *Posidonia oceanica* patches in shallow water. *Limnol. Oceanogr.* 50, 1592–1600.
- Fonseca, M.S., Cahalan, J. a., 1992. A preliminary evaluation of wave attenuation by four species of seagrass. *Estuar. Coast. Shelf Sci.* 35, 565–576.
- Gambi, M.C., Nowell, A.R.M., Jumars, P.A., 1990. Flume observations on flow dynamics in *Zostera Marina* (eelgrass) beds. *Mar. Ecol. Prog. Ser.* 61, 159–169.
- Ghisalberti, M., Nepf, H.M., 2002. Mixing layers and coherent structures in vegetated aquatic flows 107, 3011.
- Granata, T., Serra, T., Colomer, J., Casamitjana, X., Duarte, C., Gacia, E., 2001. Flow and particle distributions in a nearshore seagrass meadow before and after a storm. *Mar. Ecol. Prog. Ser.* 218, 95–106.
- Gruber, R.K., Kemp, W.M., 2010. Feedback effects in a coastal canopy-forming submersed plant bed. *Limnol. Oceanogr.* 55, 2285–2298.
- Halpern, B.S., McLeod, K.L., Rosenberg, A. a., Crowder, L.B., 2008. Managing for cumulative impacts in ecosystem-based management through ocean zoning. *Ocean Coast. Manag.* 51, 203–211.
- Hansen, J., Reidenbach, M., 2012. Wave and tidally driven flows in eelgrass beds and their effect on sediment suspension. *Mar. Ecol. Prog. Ser.* 448, 271–287.
- Hansen, J.C.R., Reidenbach, M.A., 2013. Seasonal growth and senescence of a *Zostera marina* seagrass meadow alters wave-dominated flow and sediment suspension within a coastal bay. *Estuaries and Coasts* 36, 1099–1114.
- Hatcher, L., Hogg, A., Woods, A., 2000. The effects of drag on turbulent gravity currents. *J. Fluid Mech.* 416, 297–314.
- Hayter, E.J., Mehta, A.J., 1982. Modelling of estuarial fine sediment transport for tracking pollutant movement. Final report No. UFL/COEL-8L/009.
- Hemminga, M., Duarte, C.M., 2000. *Seagrass ecology*. Cambridge University Press, Cambridge.
- Hendriks, I.E., Sintes, T., Bouma, T.J., Duarte, C.M., 2008. Experimental assessment and modeling evaluation of the effects of the seagrass *Posidonia oceanica* on flow and particle trapping. *Mar. Ecol. Prog. Ser.* 356, 163–173.

- Holzner, M., Liberzon, A., Guala, M., Tsinober, A., Kinzelbach, W., 2006. Generalized detection of a turbulent front generated by an oscillating grid. *Exp. Fluids* 41, 711–719.
- Hopfinger, E., Toly, J., 1976. Spatially decaying turbulence and its relation to mixing across density interfaces. *J. Fluid Mech.* 78, 155–175.
- Horppila, J., Kaitaranta, J., Joensuu, L., Nurminen, L., 2013. Influence of emergent macrophyte (*Phragmites australis*) density on water turbulence and erosion of organic-rich sediment. *J. Hydrodyn. Ser. B* 25, 288–293.
- Houwing, E.-J.J., 1999. Determination of the critical erosion threshold of cohesive sediments on intertidal mudflats along the Dutch Wadden Sea coast. *Estuarine, Coast. Shelf Sci.* 49, 545–555.
- Huppert, H., Simpson, J., 1980. The slumping of gravity currents. *J. Fluid Mech.* 99, 785–799.
- Huppert, H.E., Turner, J.S., Hallworth, M.A., 1995. Sedimentation and entrainment in dense layers of suspended particles stirred by an oscillating grid. *J. Fluid Mech.* 289, 263–293.
- Infantes, E., Orfila, A., Simarro, G., Terrados, J., Luhar, M., Nepf, H., 2012. Effect of a seagrass (*Posidonia oceanica*) meadow on wave propagation. *Mar. Ecol. Prog. Ser.* 456, 63–72.
- Keulegan, G.H., 1957. An experimental study of the motion of saline water from locks into fresh water channels.
- Kirwan, M., Guntenspergen, G., 2010. Influence of tidal range on the stability of coastal marshland. *J. Geophys. Res.* 115.
- Koch, E., 2001. Beyond Light: Physical, Geological, and Geochemical Parameters as Possible Submersed Aquatic Vegetation Habitat Requirements. *Estuaries* 24, 1–17.
- Koch, E., Gust, G., 1999. Water flow in tide- and wave-dominated beds of the seagrass *Thalassia testudinum*. *Mar. Ecol. Prog. Ser.* 184, 63–72.
- Koftis, T., Prinos, P., Stratigaki, V., 2013. Wave damping over artificial *Posidonia oceanica* meadow: A large-scale experimental study. *Coast. Eng.* 73, 71–83.
- Kundu, P., Cohen, I., Dowling, D., 1990. *Fluid mechanics*. Elsevier.
- Leonard, L., Wren, P., Beavers, R., 2002. Flow dynamics and sedimentation in *Spartina alterniflora* and *Phragmites australis* marshes of the Chesapeake Bay. *Wetlands* 22, 415–424.
- López, F., García, M., 1998. Open-channel flow through simulated vegetation: Suspended sediment transport modeling. *Water Resour. Res.* 34, 2341–2352.

- Lotze, H.K., Lenihan, H.S., Bourque, B.J., Bradbury, R.H., Cooke, R.G., Kay, M.C., Kidwell, S.M., Kirby, M.X., Peterson, C.H., Jackson, J.B.C., Bay, M., 2006. and Coastal Seas. *Science* (80-.). 312, 1806–1809.
- Lowe, R.J., Koseff, J.R., Monismith, S.G., 2005a. Oscillatory flow through submerged canopies: 1. Velocity structure. *J. Geophys. Res. - Ocean.* 110, 1–17.
- Lowe, R.J., Koseff, J.R., Monismith, S.G., Falter, J.L., 2005b. Oscillatory flow through submerged canopies: 2. Canopy mass transfer. *J. Geophys. Res. - Ocean.* 110, 1–14.
- Luhar, M., Coutu, S., Infantes, E., Fox, S., Nepf, H., 2010. Wave-induced velocities inside a model seagrass bed. *J. Geophys. Res.* 115, C12005.
- Mac Vean, L.J., Lacy, J.R., 2014. Interactions between waves, sediment, and turbulence on a shallow estuarine mudflat. *J. Geophys. Res. - Ocean.* 119, 1534–1553.
- Madsen, J.D., Chambers, P.A., James, W.F., Koch, E.W., Westlake, D.F., 2001. The interaction between water movement, sediment dynamics and submersed macrophytes. *Hydrobiologia* 444, 71–84.
- Manca, E., Cáceres, I., Alsina, J.M., Stratigaki, V., Townend, I., Amos, C.L., 2012. Wave energy and wave-induced flow reduction by full-scale model *Posidonia oceanica* seagrass. *Cont. Shelf Res.* 50-51, 100–116.
- Matsunaga, N., Sugihara, Y., Komatsu, T., Masuda, A., 1999. Quantitative properties of oscillating-grid turbulence in a homogeneous fluid. *Fluid Dyn. Res.* 25, 147–165.
- Mendez, F., Losada, I., Losada, M., 1999. Hydrodynamics induced by wind waves in a vegetation field. *J. Geophys. Res. - Ocean.* 104, 18383–18396.
- Mendez, F.J., Losada, I.J., 2004. An empirical model to estimate the propagation of random breaking and nonbreaking waves over vegetation fields. *Coast. Eng.* 51, 103–118.
- Mikkelsen, O. a., Hill, P.S., Milligan, T.G., Chant, R.J., 2005. In situ particle size distributions and volume concentrations from a LISST-100 laser particle sizer and a digital floc camera. *Cont. Shelf Res.* 25, 1959–1978.
- Möller, I., Spencer, T., French, J.R., Leggett, D.J., Dixon, M., 1999. *Wave Transformation Over Salt Marshes: A Field and Numerical Modelling Study from North Norfolk, England.* *Estuar. Coast. Shelf Sci.* 49, 411–426.
- Monismith, S.G., 2007. Hydrodynamics of coral reefs. *Annu. Rev. Fluid Mech.* 39, 37–55.
- Nepf, H., 1999. Drag, turbulence, and diffusion in flow through emergent vegetation. *Water Resour. Res.* 35, 479–489.

- Nepf, H., Ghisalberti, M., White, B., Murphy, E., 2007. Retention time and dispersion associated with submerged aquatic canopies. *Water Resour. Res.* 43, n/a–n/a.
- Nepf, H.M., Vivoni, E., 2000. Flow structure in depth-limited, vegetated flow. *J. Geophys. Res.* 105, 28547–28557.
- Neumeier, U., 2007. Velocity and turbulence variations at the edge of salt marshes. *Cont. Shelf Res.* 27, 1046–1059.
- Neumeier, U., Amos, C., 2006. Turbulence reduction by the canopy of coastal *Spartina* salt-marshes. *J. Coast. Res. I*, 433–439.
- Neumeier, U., Ciavola, P., 2004. Flow resistance and associated sedimentary processes in a *Spartina maritima* salt-marsh. *J. Coast. Res.* 20, 435–447.
- Nokes, R., 1988. On the entrainment rate across a density interface. *J. Fluid Mech.* 188, 185–204.
- O'Brien, M.P., Cherni, J., 1934. Model law for motion of salt water through fresh. *Trans. Am. Soc. Civ. Eng.* 99, 576–94.
- Oguz, E., Elginöz, N., Koroglu, A., Kabdasli, M., 2013. The effect of reed beds on wave attenuation and suspended sediment concentration. *J. Coast. Res.* 65, 356–361.
- Ondiviela, B., Losada, I.J., Lara, J.L., Maza, M., Galván, C., Bouma, T.J., van Belzen, J., 2014. The role of seagrasses in coastal protection in a changing climate. *Coast. Eng.* 87, 158–168.
- Orlins, J.J., Gulliver, J.S., 2003. Turbulence quantification and sediment resuspension in an oscillating grid chamber. *Exp. Fluids* 34, 662–677.
- Paterson, D., Black, K., 1999. Water flow, sediment dynamics and benthic biology. *Adv. Ecol. Res.* 29, 155–193.
- Paul, M., Bouma, T.J., Amos, C.L., 2012. Wave attenuation by submerged vegetation: combining the effect of organism traits and tidal current. *Mar. Ecol. Prog. Ser.* 444, 31–41.
- Poggi, D., Porporato, A., Ridolfi, L., Albertson, J.D., Katul, G.G., 2003. The effect of vegetation density on canopy sub-layer turbulence. *Boundary-Layer Meteorology* 111, 565–587.
- Postma, G., 1986. Classification for sediment gravity-flow deposits based on flow conditions during sedimentation. *Geology* 14, 291–294.
- Pujol, D., Casamitjana, X., Serra, T., Colomer, J., 2013a. Canopy-scale turbulence under oscillatory flow. *Cont. Shelf Res.* 66, 9–18.

- Pujol, D., Colomer, J., Serra, T., Casamitjana, X., 2010. Effect of submerged aquatic vegetation on turbulence induced by an oscillating grid. *Cont. Shelf Res.* 30, 1019–1029.
- Pujol, D., Nepf, H., 2012. Breaker-generated turbulence in and above a seagrass meadow. *Cont. Shelf Res.* 49, 1–9.
- Pujol, D., Serra, T., Colomer, J., Casamitjana, X., 2013b. Flow structure in canopy models dominated by progressive waves. *J. Hydrol.* 486, 281–292.
- Rapp, R.J., Melville, W.K., 1990. Laboratory measurements of deep-water breaking waves. *Philos. Trans. R. Soc. London Ser. A-mathematical Phys. Eng. Sci.* 331, 735–&.
- Raudkivi, A., 1998. *Loose Boundary Hydraulics*. CRC Press.
- Reed, D.J., 1995. The response of coastal marshes to sea-level rise - Survival or submergence. *Earth Surf. Process. Landforms* 20, 39–48.
- Rogers, K., Saintilan, N., 2008. Relationships between surface elevation and groundwater in mangrove forests of southeast Australia. *J. Coast. Res.* 24, 63–69.
- Rogers, K., Saintilan, N., Howe, A.J., Rodríguez, J.F., 2013. Sedimentation, elevation and marsh evolution in a southeastern Australian estuary during changing climatic conditions. *Estuar. Coast. Shelf Sci.* 133, 172–181.
- Ros, À., Colomer, J., Serra, T., Pujol, D., Soler, M., Casamitjana, X., 2014. Experimental observations on sediment resuspension within submerged model canopies under oscillatory flow. *Cont. Shelf Res.* 91, 220–231.
- Rottman, J., Simpson, J., 1983. Gravity currents produced by instantaneous releases of a heavy fluid in a rectangular channel. *J. Fluid Mech.* 135, 95–110.
- Saenger, P., 2002. *Mangrove ecology, silviculture and conservation*. Kluwer Academic Press, Dordrecht, Netherlands.
- Serra, T., Casamitjana, X., Colomer, J., Granata, T.C., 2002. Observations of the particle size distribution and concentration in a coastal system using an in situ laser analyzer. *Mar. Technol. Soc. J.* 36, 59–69.
- Serra, T., Colomer, J., Logan, B.E., 2008. Efficiency of different shear devices on flocculation. *Water Res.* 42, 1113–21.
- Serra, T., Fernando, H.J.S., Rodríguez, R. V., 2004. Effects of emergent vegetation on lateral diffusion in wetlands. *Water Res.* 38, 139–47.
- Serra, T., Granata, T., Colomer, J., Stips, A., Møhlenberg, F., Casamitjana, X., 2003. The role of advection and turbulent mixing in the vertical distribution of phytoplankton. *Estuar. Coast. Shelf Sci.* 56, 53–62.

- Serra, T., Soler, M., Julia, R., Casamitjana, X., Colomer, J., 2005. Behaviour and dynamics of a hydrothermal plume in Lake Banyoles, Catalonia, NE Spain. *Sedimentology* 52, 795–808.
- Short, F.T., Neckles, H.A., 1999. Review. The effects of global climate change on seagrasses. *Aquat. Bot.* 63, 169–196.
- Simpson, J., 1997. *Gravity Currents: In the Environment and the Laboratory*. Cambridge.
- Simpson, J., Britter, R., 1979. Dynamics of the head of a gravity current advancing over a horizontal surface. *J. Fluid Mech.* 94, 477–&.
- Smith, T.J., Anderson, G.H., Balentine, K., Tiling, G., Ward, G. a., Whelan, K.R.T., 2009. Cumulative impacts of hurricanes on Florida mangrove ecosystems: sediment deposition, storm surges and vegetation. *Wetlands* 29, 24–34.
- Soler, M., Colomer, J., Serra, T., Casamitjana, X., Folkard, A.M., 2016. Sediment deposition from turbidity currents in simulated aquatic vegetation canopies. *under Rev.*
- Tanner, J.E., 2005. Edge effects on fauna in fragmented seagrass meadows. *Austral Ecol.* 30, 210–218.
- Terrados, J., Duarte, C.M., 2000. Experimental evidence of reduced particle resuspension within a seagrass (*Posidonia oceanica* L.) meadow. *J. Exp. Mar. Bio. Ecol.* 243, 45–53.
- Tsai, C.-H., Lick, W., 1986. A Portable Device for Measuring Sediment Resuspension. *J. Great Lakes Res.* 12, 314–321.
- Türker, U., Yagci, O., Kabdaşlı, M.S., 2006. Analysis of coastal damage of a beach profile under the protection of emergent vegetation. *Ocean Eng.* 33, 810–828.
- Unsworth, R.K.F., De Leon, P.S., Garrard, S.L., Jompa, J., Smith, D.J., Bell, J.J., 2008. High connectivity of Indo-Pacific seagrass fish assemblages with mangrove and coral reef habitats. *Mar. Ecol. Prog. Ser.* 353, 213–224.
- Van Katwijk, M.M., Bos, A.R., Hermus, D.C.R., Suykerbuyk, W., 2010. Sediment modification by seagrass beds: Muddification and sandification induced by plant cover and environmental conditions. *Estuar. Coast. Shelf Sci.* 89, 175–181.
- Van Rijn, L.C., 2007. Unified view of sediment transport by currents and waves. I: Initiation of motion, bed roughness, and bed-load transport. *J. Hydraul. Eng.* 133, 649–667.
- Venier, C., Figueiredo da Silva, J., McLelland, S.J., Duck, R.W., Lanzoni, S., 2012. Experimental investigation of the impact of macroalgal mats on flow dynamics and sediment stability in shallow tidal areas. *Estuar. Coast. Shelf Sci.* 112, 52–60.

- Vermaat, J., Santamaria, L., Roos, P., 2000. Water flow across and sediment trapping in submerged macrophyte beds of contrasting growth form. *Arch. fur Hydrobiol.* 148, 549–562.
- Ward, L., Kemp, W., Boynton, W., 1984. The influence of waves and seagrass communities on suspended particulates in an estuarine embayment. *Mar. Geol.* 59, 85–103.
- Webster, P., Holland, G., Curry, J., Chang, H., 2005. Changes in tropical cyclone number, duration, and intensity in a warming environment. *Science* (80-.). 309, 1844–1846.
- Whitehouse, R., Soulsby, R., Roberts, W., Mitcgener, H., 2000. *Dynamics of estuarine muds*, 1st ed. HR Wallingford.
- Wiberg, P.L., Sherwood, C.R., 2008. Calculating wave-generated bottom orbital velocities from surface-wave parameters. *Comput. Geosci.* 34, 1243–1262.
- Widdows, J., Pope, N.D., Brinsley, M.D., Asmus, H., Asmus, R.H., 2008. Effects of seagrass beds (*Zostera noltii* and *Z-marina*) on near-bed hydrodynamics and sediment resuspension. *Mar. Ecol. Prog. Ser.* 358, 125–136.
- Wu, D., Hua, Z., 2014. The effect of vegetation on sediment resuspension and phosphorus release under hydrodynamic disturbance in shallow lakes. *Ecol. Eng.* 69, 55–62.
- Yih, C.S., 1947. *A study of the characteristics of gravity waves at a liquid interface*. State University of Iowa.

Appendix

Continental Shelf Research 91 (2014) 220–231



Contents lists available at ScienceDirect

Continental Shelf Research

journal homepage: www.elsevier.com/locate/csr



Research papers

Experimental observations on sediment resuspension within submerged model canopies under oscillatory flow



Àlex Ros^{*}, Jordi Colomer, Teresa Serra, Dolors Pujol, Marianna Soler, Xavier Casamitjana

Department of Physics, Campus Montilivi, Escola Politècnica Superior II, University of Girona, 17071 Girona, Spain

ARTICLE INFO

Article history:
Received 27 November 2013
Received in revised form
2 October 2014
Accepted 14 October 2014
Available online 23 October 2014

Keywords:
Progressive waves
Submerged aquatic vegetation
Sediment dynamics
Resuspension
Sediment distribution

ABSTRACT

A set of laboratory experiments were conducted to study the effect of submerged aquatic vegetation in sediment resuspension under progressive waves. Three vegetation models (rigid, flexible and real plants of *Ruppia maritima*), six wave frequencies (in the range $F=0.6\text{--}1.6$ Hz) and four plant densities (Solid Plant Fractions, SPF in the range of 1–10%) were used. The sediment bed properties corresponded to a salt marsh wetland with a bimodal particle size distribution with two particle populations (population 1: particle diameters in the range of 2.5 to 6.0 μm , and population 2: particle diameters in the range of 6.0 to 100 μm).

Within the canopy, wave velocities were attenuated for all the canopies studied and for all the frequencies analyzed. The change in the TKE (ΔTKE) compared with the case without plants was studied. For the rigid canopy model, in comparison to the unimpeded experiment, an increase in ΔTKE inside the canopy for smaller frequencies ($F=0.6\text{--}1.2$ Hz) was observed together with stem Reynolds numbers Re_p above 250. As a result, sediment resuspension for both sediment populations was higher than that of the unimpeded experiment. However, at higher frequencies ($F=1.4$ and 1.6 Hz) and higher plant densities (SPF=5%, 7.5% and 10%), the ΔTKE inside the canopy decreased, coinciding with stem Reynolds number Re_p below 250. As a result, sediment resuspension for larger canopy densities and larger frequencies was reduced.

For the flexible vegetation model, in comparison with the unimpeded experiment, a reduction in the ΔTKE inside the canopy was nearly always found. Resuspended sediment concentrations were found to decrease as flexible canopy densities increased. For the flexible vegetation the stem Reynolds number was $Re_p < 250$ and no production of ΔTKE was observed. The real case of a canopy of *R. maritima* behaved similarly to the flexible model canopy.

© 2014 Elsevier Ltd. All rights reserved.

1. Introduction

Seagrasses and salt marshes are ecosystem engineers with the well-known function of reducing the action of waves and storm surges (Granata et al., 2001; Türker et al., 2006). Sheltering is characteristic of dense canopies, where turbulence cannot penetrate deep into the canopy, and flushing is controlled by the stem-scale turbulence (Nepf et al., 2007). Under wave-dominated flows, near-bed turbulence levels within seagrass canopies are lower than those on bare soils (Granata et al., 2001; Hendriks et al., 2008; Pujol et al., 2013). As a consequence, wave energy and sediment resuspension are reduced by seagrasses (Terrados and Duarte, 2000; Bouma et al., 2005; Infantes et al., 2012; Paul et al., 2012). In addition, the reduction in sediment resuspension improves water clarity, which in turn, provides greater light

penetration and consequently an increase in productivity, thus creating a positive feedback for the sea and wetland grasses growth (Ward et al., 1984; Koch, 2001).

The reduction of sediment resuspension within the canopy is directly linked to the modification of currents, wave velocity and turbulence (Neumeier, 2007; Pujol et al., 2013) as well as to the intrinsic properties of the canopy itself, canopy density and flexibility of plants. As pointed out by van Katwijk et al. (2010) at the relatively wave-exposed, sandy sites, dense vegetation cause mudification (increase in fine sediments and organic content) of the sediments. In contrast, in sheltered sites with muddy sediments, dense vegetation has no effect on the sediment composition. In sparse sheltered vegetation, contrary to non-sheltered canopies, with muddy sediments, sandification (decrease in fine sediments and organic content) prevails. In events where the flow level is above the vegetation, sedimentation decreases with distance, from the seaward marsh edge and from the creeks, in parallel with a grain-size fining or mudification (Neumeier and Amos, 2006). Coastal zones present a large variety of clay, silt and

^{*} Corresponding author. Tel.: +34 972 418372; fax: +34 972 418098.
E-mail address: alex.ros@udg.edu (À. Ros).

sand composition. Different particle sizes compose the sediment bed in view of their density and settling velocity and are prone to differential resuspension when facing an external physical forcing. Therefore, sediment resuspension will highly depend on the characteristics of plants as well as on the intensity of reduction of wave velocity by the canopies and the generation of turbulent kinetic energy through the interaction between waves and the canopy.

The attenuation of the flows inside canopies has been studied by Lowe et al. (2005a, 2005b). The authors conducted laboratory experiments and developed an analytical model to investigate the flow structure inside a submerged canopy, such as a coral reef. Their model was developed by considering the momentum balance around individual canopy elements within a larger canopy. They demonstrated that the flow inside a canopy was always lower than above the canopy, and that the degree of flow attenuation varied as a function of canopy geometry parameters, such as the height and spacing of the elements, as well as coefficients that parameterize the effects of various forces exerted by the canopy element. The canopy flow attenuation was found to depend on the non-dimensional parameter A_w/S where A_w is the wave orbital excursion length and S is defined as the edge-to-edge average distance between closest elements in any direction. This ratio has been called the Keulegan–Carpenter number (Monismith, 2007), although for Mendez and Losada (2004) the definition of this number is slightly different (S was defined as the plant area per unit height of each vegetation stand normal to the wave velocity). The two definitions of S are proportional and give account of the density of the canopy. When A_w/S is large, the flow is drag dominated and velocities inside the canopy are much lower than in the free stream. In contrast, when A_w/S is small, the interstitial flow is inertia dominated and interior velocities more nearly match exterior ones, and total mass transfer is enhanced over that of steady flows. This paper aims at understanding the relationship between the turbulent kinetic energy, the shear stress and sediment resuspension in terms of the canopy density and depending on whether the stem is flexible or rigid. The environmental flow under study is a field of monochromatic waves. The wave frequency is also a key parameter that will be analyzed in the present work.

2. Materials and methods

2.1. Experimental setup

The study was conducted in a 6 m × 0.5 m × 0.5 m wave flume. A scheme of the setup is shown in Fig. 1. The mean water depth, h , was 0.3 m. A plywood beach, with a slope of 1:3 and covered with a 7 cm layer of foam rubber, was located at the end of the flume. A vertical paddle, called a flap type wavemaker, was placed at the front of the flume and was driven by a variable-speed motor with a constant stroke of 5 cm and a variable frequency F in the range from 0.6 to 1.6 Hz (Table 1). Since $\lambda/2$ was always larger (Table 1) than the water depth (of 30 cm), the generated waves always reached the bottom of the flume (where λ is the wave length). Furthermore, since $\lambda/20 < h < \lambda/2$, these waves corresponded to waves in transitional waters, i.e. intermediate to shallow waves, which are in accordance with the typical waves in vegetated coastal regions. We defined the longitudinal direction as x , and $x=0$ was the longitudinal position at the wavemaker, $y=0$ at the centerline of the tank and z is the vertical direction, $z=0$ corresponded to the depth at the flume bed. Wave conditions in the present study corresponded to the laminar regime, i.e. to wave Reynolds number, $Re_w = U_{w\infty} A_w / \nu < 10000$, where $U_{w\infty}$ represents the orbital wave velocity unaffected by the canopy

(i.e. the wave velocity far above the canopy, here considered at $z=22$ cm above the bottom), called free-stream velocity, and A_w is the wave orbital excursion length of the free-stream potential flow. The submergence ratio, defined as h_v/h (where h_v is the plant height), was 0.47, which falls in the upper limit of those used in other studies (Manca et al., 2012).

2.2. Vegetation models

The rigid canopy model consisted of rigid PVC cylinders 1 cm in diameter and 14 cm long. Different canopy densities were also considered in the experiments. According to Pujol et al. (2010), the canopy density can be defined as the solid plant fraction at the bottom occupied by stems, $SPF = 100 \cdot n\pi(d/2)^2/A$, where n is the number of plants, d is the diameter of the model plant, and A is the planform area. $SPFs$ of 1%, 5%, 7.5% and 10% were used for experiments with submerged rigid vegetation, $SPFs$ of 1%, 5% and 10% were used for those experiments with submerged flexible vegetation and 1% for those with real plants (Table 1). The vegetation pattern for each SPF was made at random by means of a computer function (Pujol et al., 2013). A plastic board was regularly perforated with holes of 1 cm with a distance of 1.5 cm between the centers of two neighbor holes. The random pattern of vegetation was made filling the corresponding holes with the cylinders and leaving some holes at the bottom that were afterwards filled with small dowels with the length equal to the bottom board thickness. The same procedure was repeated for each SPF .

The flexible canopy model was constructed with implants of polyethylene (high density) blades attached with a plastic band to a PVC dowel 2 cm long and 1 cm in diameter. Each plant had eight plastic blades of 4 mm width. The model plants were dynamically and geometrically similar to typical seagrasses, as described by Ghisalberti and Nepf (2002), Folkard (2005) and Pujol et al. (2013). The canopy density for flexible plants was calculated based on the area occupied by the dowels that fixed the plants at the bed.

The real plant model consisted of *Ruppia maritima*, which is a typical plant found in salt marshes and especially abundant in the Mediterranean coastal areas. It produces long, narrow, straight leaves and is characterized by seasonally contrasting growth of tall flowering reproductive shoots in mid-summer and shorter vegetative roots during the remainder of the growing season. The plants for the model were cut to a height of $h_v = 14$ cm, so that results could be compared with those obtained for the rigid and flexible canopy models. The real plant blades were attached to the same PVC dowels used for the flexible canopy model.

2.3. Measuring technique

The Eulerian velocity field was defined as (u, v, w) in the (x, y, z) directions, respectively. The three components of the velocity were recorded with a downwards looking Acoustic Doppler Velocimeter (Sontek/YSI16-MHzMicroADV). The acoustic frequency was 16 MHz, the sampling volume was 0.09 cm³ and the distance to the sampling volume was 5 cm. The ADV sampled at 50 Hz, limiting the velocity spectra to 25 Hz due to Nyquist frequency. The ADV was mounted on a movable vertical frame that allowed it to be manually situated at working depths of $z=5$ cm (i.e. $z/h_v=0.4$), well inside the canopy model, $z=15$ cm (i.e. $z/h_v=1.1$) and $z=22$ cm (i.e. $z/h_v=1.6$), these two last depths corresponding to the layer above the canopy models. It measured during 20 min at each depth. After measuring at one depth it was moved vertically and left for 15 min before measuring again. Each experiment lasted 120 min. To avoid spikes due to poor correlations, ADV measurements with beam correlations below 80% along and

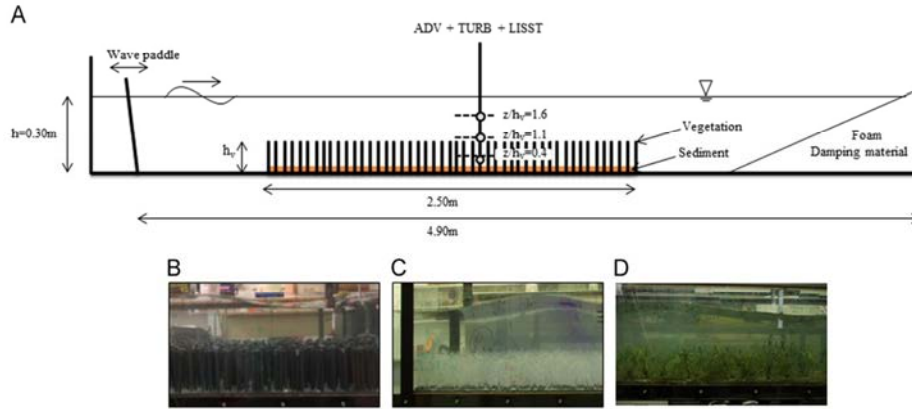


Fig. 1. (a) Scheme of the experimental set-up. Experiments were conducted in a 6 m long flume. The streamwise coordinate is denoted by x , with x positive in the downstream direction, and $x=0$ at the mean position of the wave maker. The vertical coordinate is z , with $z=0$ at the bed. The mean water depth, h_w , is 30 cm. The plant height in still water is $h_p=14$ cm. The model meadow was 250 cm long. The horizontal dashed lines indicate the position of the velocity (ADV) and sediment concentration measurements, both turbidity and particle sediment concentration (TURB+LISST). The beach slope at the end of the tank is not scaled. (b) Picture of the submerged rigid canopy. (c) Picture of the submerged flexible canopy. (d) Picture of the submerged real canopy (*R. maritima*).

outlier instantaneous velocities higher than two standard deviations were discarded for the analysis.

The longitudinal measurements of the velocity were taken at an antinode, in order to eliminate the lower-order spatially periodic variation in wave and velocity amplitude associated with a maximum of 10% of reflection measured in the flume (Luhar et al., 2010; Pujol et al., 2013). Then, the model bed was shifted longitudinally along the flume to measure at 150 cm from the vegetation edge. To obtain valid data acquisition within the canopy, some stems were removed to avoid blocking the pathway of the ADV beams, as was done by Neumeier and Ciavola (2004), Pujol et al. (2010, 2013). To minimize the effect of this 'hole', its shape was specifically designed to allow the ADV acoustic receivers and the acoustic transmitter to perform properly.

2.4. Methods of analysis

For general wave flows, the instantaneous velocity e.g. U_i , can be decomposed as

$$U_i = U_c + U_w + u' \quad (1)$$

where U_c is the steady velocity associated with the current, U_w is the unsteady wave motion which represents spatial variations in the phase averaged velocity field, and u' is the turbulent velocity, that is the instantaneous velocity fluctuation in the x direction. As in Lowe et al. (2005a) and Luhar et al. (2010), U_c is the space and phase-averaged velocity found as:

$$U_c = \frac{1}{2\pi} \int_0^{2\pi} U_i(\varphi) d\varphi \quad (2)$$

where $U_i(\varphi)$ is the instantaneous velocity, according to the phase. Wave velocity, U_w , was obtained by using a phase averaging technique. The Hilbert transform was used to average oscillatory flow velocities with a common phase (Pujol et al., 2013). The root mean square (rms) of $U_i(\varphi)$ was considered as the characteristic value of the orbital velocity U_w at each depth and was calculated

according to the following operation:

$$U_w = \sqrt{\frac{1}{2\pi} \int_0^{2\pi} (U_i(\varphi) - U_c)^2 d\varphi} \quad (3)$$

In absence of vegetation, the linear wave model leads to the following equation for the horizontal wave velocity component,

$$U_w = a\omega \frac{\cosh kz}{\sinh kh} \cos(kx - \omega t) \quad (4)$$

where a is the wave amplitude, k is the wave number and ω is the wave radian frequency.

Then, the turbulent kinetic energy (TKE) was calculated as

$$TKE = \frac{1}{2} (\langle u'^2 \rangle + \langle v'^2 \rangle + \langle w'^2 \rangle) \quad (5)$$

where $\langle \rangle$ denotes the time average. The TKE difference between measurements with and without plants, expressed as a percentage, was calculated according to:

$$\Delta TKE(z) = \left(\frac{TKE_C(z) - TKE_{WC}(z)}{TKE_{WC}(z)} \right) \times 100 \quad (6)$$

where the TKE_C is the TKE measured at z with the presence of canopy model, and the TKE_{WC} is the TKE measured at z without the presence of canopy model. Negative ΔTKE indicate a reduction of TKE, while positive values of ΔTKE imply TKE generation.

2.5. Sediment characteristics

For each experiment, the bottom of the flume was covered with sediment by uniformly seeding the same amount of sediment over the entire bottom of the flume, resulting in a homogeneous sediment bed of 3–5 mm height. The seeding was performed manually using a tube connected to a container with the sediment mixture. The tube was moved 1 cm above the bed along the bottom of the flume through the vegetation and also in the region without vegetation. The seeding resulted in an homogeneous bottom cloud of ~ 5 cm in height, whose particles were left to deposit by gravity. Therefore, experiments commenced 1 day after

Table 1

Wave and vegetation parameters for the experiments carried out: solid plant fraction, number of stems per unit area, wave frequency, the corresponding wavelengths calculated from the dispersion equation (Dean and Dalrymple, 1991) and the A_w/S parameter measured at $z/h_v=1.1$, where $A_w=U_w/(2\pi F)$ and S is the plant-to-plant distance.

Run	Canopy model	SPF (%)	n_s (stems/m ²)	F (Hz)	λ (m)	A_w/S ($z/h_v=1.1$)
Without vegetation						
WP1				0.6		
WP2				0.8	2.65	
WP3				1.0	1.86	
WP4				1.2	1.37	
WP5				1.4	1.03	
WP6				1.6	0.78	
					0.61	
Submerged rigid vegetation model						
SRV1		1	128	0.6		0.04
SRV2		5	640	0.6	2.65	0.09
SRV3		7.5	960	0.6	2.65	0.18
SRV4		10	1280	0.6	2.65	0.18
SRV5		1	128	0.8	1.86	0.05
SRV6		5	640	0.8	1.86	0.23
SRV7		7.5	960	0.8	1.86	0.19
SRV8		10	1280	0.8	1.86	0.32
SRV9		1	128	1.0	1.37	0.11
SRV10		5	640	1.0	1.37	0.17
SRV11		7.5	960	1.0	1.37	0.35
SRV12		10	1280	1.0	1.37	0.46
SRV13		1	128	1.2	1.03	0.07
SRV14		5	640	1.2	1.03	0.19
SRV15		7.5	960	1.2	1.03	0.30
SRV16		10	1280	1.2	1.03	0.45
SRV17		1	128	1.4	0.78	0.08
SRV18		5	640	1.4	0.78	0.23
SRV19		7.5	960	1.4	0.78	0.31
SRV20		10	1280	1.4	0.78	0.41
SRV21		1	128	1.6	0.61	0.06
SRV22		5	640	1.6	0.61	0.18
SRV23		7.5	960	1.6	0.61	0.24
SRV24		10	1280	1.6	0.61	0.34
					0.61	
Submerged flexible vegetation model						
SFV1		1	128	0.6	2.65	0.03
SFV2		5	640	0.6	2.65	0.08
SFV3		10	1280	0.6	2.65	0.20
SFV4		1	128	0.8	1.86	0.07
SFV5		5	640	0.8	1.86	0.38
SFV6		10	1280	0.8	1.86	0.36
SFV7		1	128	1.0	1.37	0.07
SFV8		5	640	1.0	1.37	0.32
SFV9		10	1280	1.0	1.37	0.66
SFV10		1	128	1.2	1.03	0.10

Table 1 (continued)

Run Canopy model	SPF (%)	n_c (stems/m ²)	F (Hz)	λ (m)	$A_{w/S}$ ($z/h_v=1.1$)
SFV11	5	640	1.2	1.03	0.32
SFV12	10	1280	1.2	1.03	0.48
SFV13	1	128	1.4	0.78	0.09
SFV14	5	640	1.4	0.78	0.25
SFV15	10	1280	1.4	0.78	0.44
SFV16	1	128	1.6	0.61	0.07
SFV17	5	640	1.6	0.61	0.19
SFV18	10	1280	1.6	0.61	0.34
Submerged real vegetation model					
SREV1	1	128	0.6	2.65	0.03
SREV2	1	128	0.8	1.86	0.07
SREV3	1	128	1.0	1.37	0.07
SREV4	1	128	1.2	1.03	0.10
SREV5	1	128	1.4	0.78	0.10
SREV6	1	128	1.6	0.61	0.08

the seeding. Bedforms at the bottom were not observed and it was not necessary to flatten the surface.

The concentration of suspended sediment, without the canopy, C_{WC} , or with the canopy, C_C , was measured at the same longitudinal position where velocity was measured at three points in the vertical (Fig. 1), at one point well inside the canopy ($z/h_v=0.4$) and at two vertical positions above the canopy ($z/h_v=1.1$ and $z/h_v=1.6$). Between experiments a lag time of 8 h was considered, so as to minimize the effect of residual sediment concentration in suspension in the flume. This time was calculated as 5 times the time needed for the sediment to settle through the whole water column based on the settling speed considering the diameter of the smallest particles. The sediment concentration was measured at $t=0$ for each experiment, and subtracted from the sediment concentration measured at the steady state, $t=t_{ss}$, at all depths of measurements.

Three turbidity sensors (Seapoint Turbidity Meter, Seapoint Sensors Inc., NH, USA) and a Laser in Situ Scattering and Transmissometry probe, LISST-100 (Sequoia Scientific, Inc., WA, USA), were used to measure the suspended sediment concentration. Turbidity meters were located at 5, 15 and 21 cm above the bed and measured at a frequency of 10 Hz. The 3 time turbidity series analyses were used to determine the time needed for the sediment resuspension to attain the steady state, which was ~15 min after the initiation of the wave generation. Oguz et al. (2013) also found the same time lag for a case of sediment resuspension in a wave dominated regime. In this study, experiments lasted for a period of 120 min, when sediment samples were collected from the water column. When the steady state was reached, water samples were collected at different depths and at different times. Samples were collected with a pipette for being afterwards analyzed by the LISST-100 to obtain the particle size distribution. The LISST-100 consists of a laser beam and an array of 32 detector rings to analyze the light received, from which it determines the particle volume concentration, C_i , of particles for 32 size classes logarithmically distributed in the range of 2.5–500 μm , by using a procedure based on the laser diffraction theory. By integrating the whole spectra of size classes, the total particle volume concentration of the suspension was obtained (Serra et al., 2002, 2005). C_i was measured at $t=0.5$, 1 and 2 h, and the mean of the last hour measurements is given as the particle volume concentration at the steady state.

The sediment to seed the tank bottom was taken from four field sites in the Empordà Marshes Natural Park, located at the North-East of Spain, and is characterized by a mixture of clays silts and very fine sands. Given the range analysis of the particle analyzer, and based on the classification by van Rijn (2007) and Blott and

Pye (2012), the sediment presented a bimodal shape with the first range between 2.5 and 6.0 μm , i.e. corresponding to clay and very fine silts (very cohesive), and the second range between 6.0 and 100 μm ; i.e., mainly corresponding from fine to coarse silts and small sand particles (weakly cohesive) (Fig. 2). From Fig. 2, the peak in the particle volume concentration distribution of the largest diameters above 100 μm was assumed to represent the role of just a few particles with a large volume. For this reason, these large particles were not considered in the analysis.

The same procedure was followed to ensure the same sediment characteristics for each run. The natural sediment mixture of sediments was sift to separate the coarse particles and root fragments, and then was kept in a tank in its hydrated form. A constant volume of 0.3 L of the dense homogeneous sediment mixture was taken, added to a container with 4 L of water, and agitated during a time lapse of 30 min to obtain a completely homogeneous mixture. Afterwards, the whole mixture was immediately introduced on the bottom of the flume.

3. Results

3.1. Physical basis of hydrodynamics within a canopy under progressive waves

Previous studies using rigid and flexible vegetation models have successfully described the turbulence structure for submerged vegetation subjected to unidirectional flows (Nepf and Vivoni, 2000; Infantes et al., 2012), however, a few of them explore the turbulent structure in a canopy dominated by progressive waves (Pujol et al., 2013). In this section we present the results of the wave velocities and the TKE for different values of the canopy density and the wave frequency.

The wave velocity, U_w , at $z/h_v=0.4$ increased with the frequency for $F \leq 1.2$ Hz for both rigid (Fig. 3A) and flexible canopy models (Fig. 3B) and also for experiments without plants, decreasing afterwards for $F \geq 1.2$ Hz. This result for U_w was also predicted by linear wave theory (Fig. 3A and B), where U_w increased with the frequency for $F \leq 1.2$ Hz. For frequencies $F \geq 1.2$ Hz, the linear wave theory also suggests that the wave attenuation increases with the wave frequency (Wiberg and Sherwood, 2008; Hansen and Reidenbach, 2012). The theoretical model for U_w at $z=5$ cm was calculated from Eq. (4), a in Eq. (4) was calculated by fitting the linear wave theory solution to the measurements obtained at the highest measurement location ($z/h_v=1.6$).

For rigid plants, the wave attenuation ratio, defined as the proportion of the wave velocity with plants and the velocity

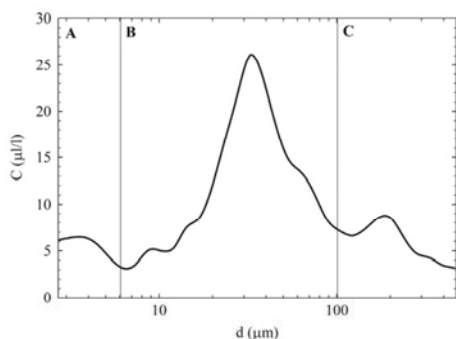


Fig. 2. Particle size distribution for the salt marsh sediment used in the experiments. Vertical dashed lines in the figure represent the classification by van Rijn (2007) where range A (small particles) corresponds to the particle range of clay and very fine silts (very cohesive sediment), range B (large particles) corresponds to the particle range of fine, coarse silts and fine sands (weakly cohesive sediment) and range C corresponds to fine sands.

without plants was in the range from 0.91 to 0.75 for SPF between 1% and 10%, respectively. For the flexible vegetation, the wave attenuation was lower than for the rigid vegetation and it was in the range from 0.96 to 0.85 for SPF between 1% and 10%, respectively. Despite this wave attenuation, results show that the wave penetrated into the canopy for all the cases studied.

Wave orbital excursion lengths $A_w (= U_w / 2\pi F)$, calculated at $z/h_v = 1.1$ were between 0.24 and 1.10 cm. An estimate of the wave penetration could be inferred from the parameter A_w/S , where S is the edge-to-edge distance (Lowe et al., 2005a). Values of this parameter are shown in Table 1. $A_w/S < 1$ for all the experiments indicated that the penetration of the wave in the canopy corresponded to the inertial force dominated regime, as described by Lowe et al. (2005a).

Fig. 4 shows the vertical distribution of ΔTKE at $z/h_v = 1.6$, 1.1 and 0.4, for comparison between runs of rigid (Fig. 4A, C, and E), and flexible models (Fig. 4B, D and F), respectively, as well as the results for the ‘natural’ case of *R. maritima* (thick black line in all figures). For measurements carried out above the submerged rigid vegetation, the percentage difference of TKE with and without plants (ΔTKE) was always found to be positive for all the frequencies studied (Fig. 4A and C); also, ΔTKE was found to increase with the frequency. For a canopy density of 1%, ΔTKE was the lowest, indicating that turbulent kinetic energy was similar to that without plants, especially for frequencies below 1.2 Hz, with $\Delta TKE \sim 0$ (Fig. 4A). Larger canopy densities produced a larger ΔTKE , especially for larger frequencies ($F \geq 1.2$ Hz). However, for densities of 1% and 10%, ΔTKE for larger frequencies was 2 to 3 times lower than those found for the densities of 5% and 7.5% (Fig. 4A).

Above the submerged flexible canopy (Fig. 4B and D), ΔTKE was found to be slightly positive for the density of 1%. It varied from ~ 0 for the lowest frequency and increased to 35% for the largest frequency. When the canopy density increased, ΔTKE followed the same pattern, that is, ΔTKE increased with frequency. Above the submerged flexible canopy, at both depths studied (Fig. 4B and D), ΔTKE increased with the wave frequency and decreased with increasing the canopy density. Positive ΔTKE (Fig. 4D) was found only for the canopy density of 1% (all frequencies) and for high wave frequencies ($F \geq 1.2$ Hz) for the experiments with SPF=5%. For SPF=5% and frequencies below 1.2 Hz, ΔTKE was always

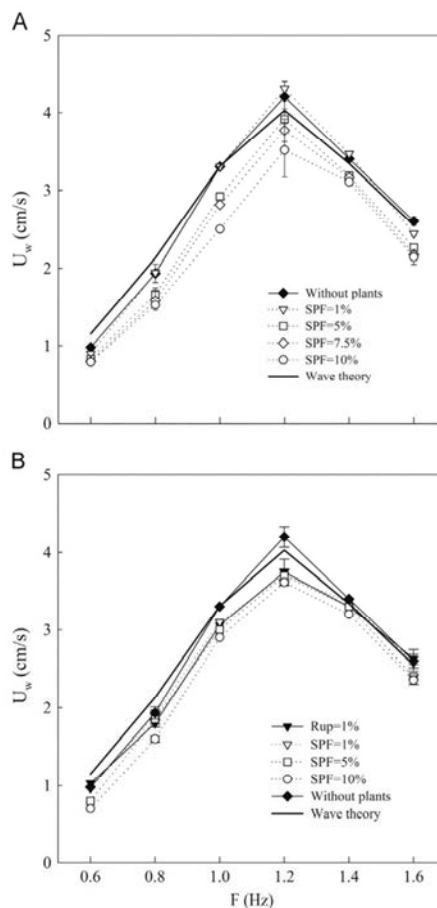


Fig. 3. Wave velocities at $z/h_v = 0.4$ for the different SPF studied and for rigid (a) and flexible (b) canopies. The solid line represents the theoretical value predicted for the no canopy case by the linear wave theory and calculated from Eq. (4) for the range of the wave frequencies studied.

negative. For the largest canopy density of 10%, ΔTKE was always negative for all frequencies.

Well inside the rigid canopy model (5 cm above the bottom), ΔTKE was found to be positive for frequencies up to 1.2 Hz (Fig. 4E). For the lowest canopy density of 1%, ΔTKE was constant and positive for all the frequencies. However, larger canopy densities resulted in negative ΔTKE for frequencies above 1.2 Hz. For low canopy densities (1% and 5%) and low frequencies (below 1.2 Hz), ΔTKE was nearly constant with frequency with percentages below 25%. For higher canopy densities (7.5% and 10%) ΔTKE increased with frequencies up to 1.0 Hz, to ΔTKE of $\sim 50\%$ up to 100%. For higher frequencies of 1.4 and 1.6 Hz, ΔTKE was negative, reaching a value of -25% for canopy densities of 5% and 7.5%, and -50% for canopy densities of 10% (Fig. 4E).

Well inside the flexible canopy model (Fig. 4F), ΔTKE was negative for all the frequencies and plant densities, with

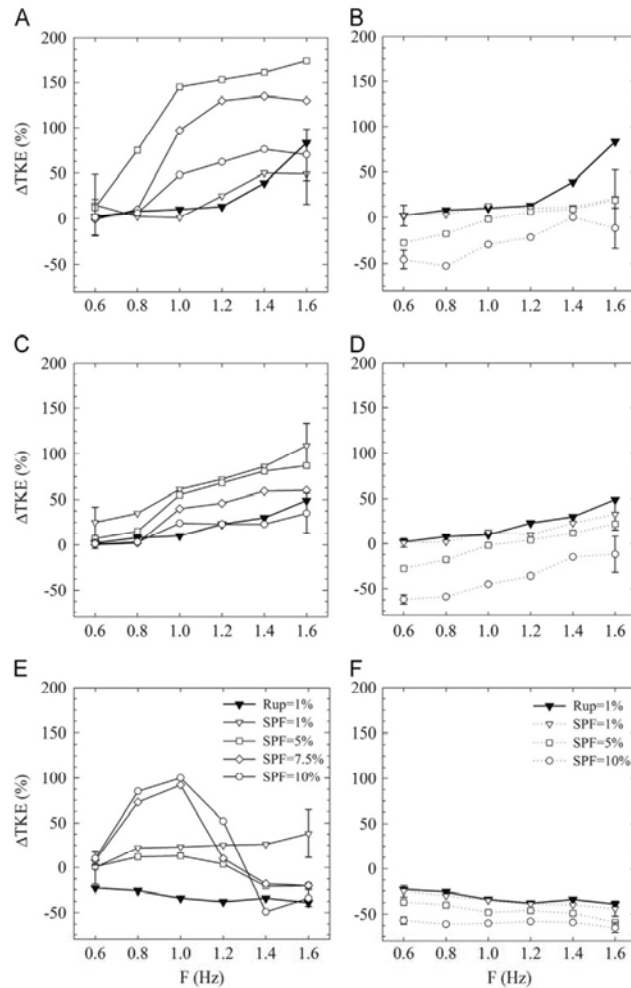


Fig. 4. Relation between ΔTKE (%), calculated using eq. 6, with the wave frequency for different canopy densities (SPF). Results for submerged rigid canopy models (SRV) are presented in the left hand panels ((A), (C) and (E)), while results for submerged flexible canopy models (SFV) are presented in the right hand panels ((B), (D) and (F)). Top panels ((A) and (B)) correspond to the results for $z/h_c = 1.6$, middle panels ((C) and (D)) correspond to the results for $z/h_c = 1.1$ and bottom panels correspond to the results for $z/h_c = 0.4$. Results for *R. maritima* (Rup) were included in all the plots. Vertical error bars are presented for the lowest and largest frequencies and for 1% and 10% canopy densities. (a) SRV, $z/h_c = 1.6$, (b) SFV, $z/h_c = 1.6$, (c) SRV, $z/h_c = 1.6$, (d) SFV, $z/h_c = 1.1$, (e) SRV, $z/h_c = 0.4$ and (f) SFV, $z/h_c = 0.4$.

percentages below -25% . Larger negative ΔTKE was attained for the largest canopy density. Contrary to that found above and close to the canopy top (Fig. 4B and D), ΔTKE slightly decreased with frequency.

To make comparisons, the experiments with the *R. maritima* canopy were represented in both schemes: submerged rigid vegetation (Fig. 4A, C and E) and submerged flexible vegetation (Fig. 4B, D, and F). Well above the *R. maritima* canopy (Fig. 4A and B) ΔTKE was low and positive for frequencies up to 1.2 Hz. For higher frequencies (1.4 and 1.6 Hz), ΔTKE increased considerably, reaching

percentages of 80%. Just above the real plant canopy, ΔTKE increased with frequency (Fig. 4C and D), but at a lower rate than that found well above the canopy (Fig. 4A). The percentage of ΔTKE attained at the highest frequency was lower, $\sim 50\%$, than that found well above the canopy, $\sim 100\%$ (Fig. 4A). Well inside the *R. maritima* canopy, ΔTKE was negative for all the frequencies (Fig. 4E and F). As the frequency increased, ΔTKE decreased slightly with percentages below -25% . Well inside the *R. maritima* canopy, the dependence of ΔTKE on frequency, was found to be similar to that of the flexible canopy, for the same canopy density of SPF=1%.

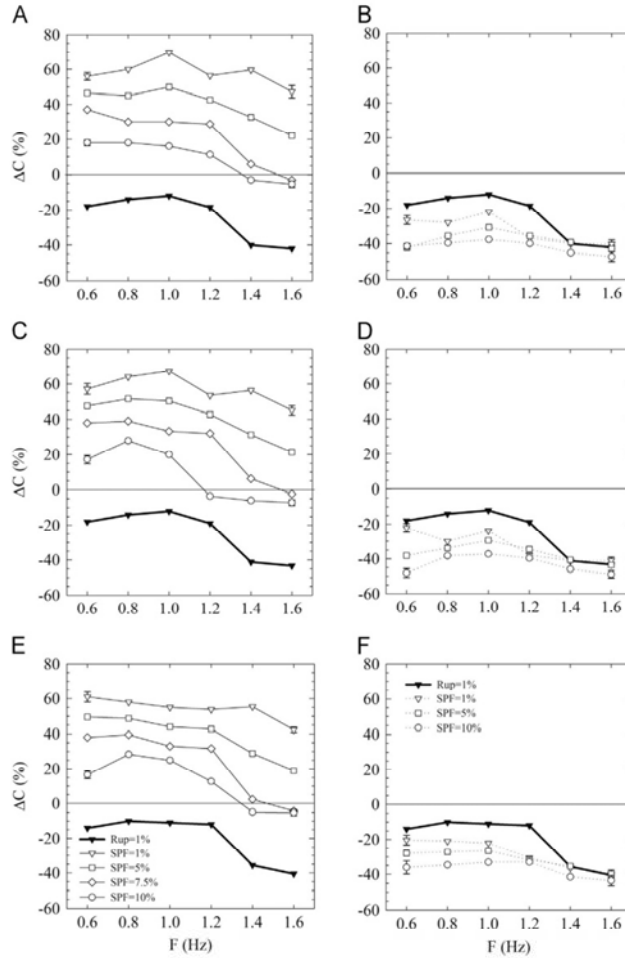


Fig. 5. Relationship between ΔC (%), calculated using Eq. (7), for the particle range of diameters from 2.5 to 6.0 μm with the frequency for the different canopy densities (SPF). The representation of the results was the same like that used in Fig. 4. (a) SRV, $z/h_v=1.6$, (b) SFV, $z/h_v=1.6$, SRV, $z/h_v=1.6$, (c) SRV, $z/h_v=1.1$, (d) SFV, $z/h_v=1.1$, (e) SRV, $z/h_v=0.4$ and (f) SFV, $z/h_v=0.4$.

3.2. Sediment resuspension within canopy models

Different regimes of turbulent flow inside and outside the vegetation area change the TKE and the transport rate of suspended sediment (Lopez and Garcia, 1998; Houwing, 1999). The bottom shear stress plays an important role in fine sediment movement and the morphology of bed form (Venier et al., 2012). It has been reported that plants can cause the increase of the shear stress of the bottom of the tidal flat or the reduction of vertical shear (Leonard et al., 2002) and the resuspension of bottom sediment (Widdows et al., 2008). The parameter ΔC was chosen to compare the concentration of the vegetated case to the concentration of the non-vegetated case and calculated

according to

$$\Delta C(z) = \left(\frac{C_C(z) - C_{WC}(z)}{C_{WC}(z)} \right) \times 100 \tag{7}$$

where C_C is the particle volume concentration at the steady state in the canopy experiments and C_{WC} is the equivalent in the non-canopy experiments.

Fig. 5 shows the vertical distribution of ΔC , for the range of small particles (2.5 to 6.0 μm), at the vertical heights $z/h_v=1.6$, 1.1 and 0.4, for comparison between runs of rigid (Fig. 5A, C, and E), and flexible models (Fig. 5B, D and F), respectively, as well as the results for the 'natural' case of *R. maritima* (thick black line in all figures). The vertical distribution of ΔC above the rigid canopy was

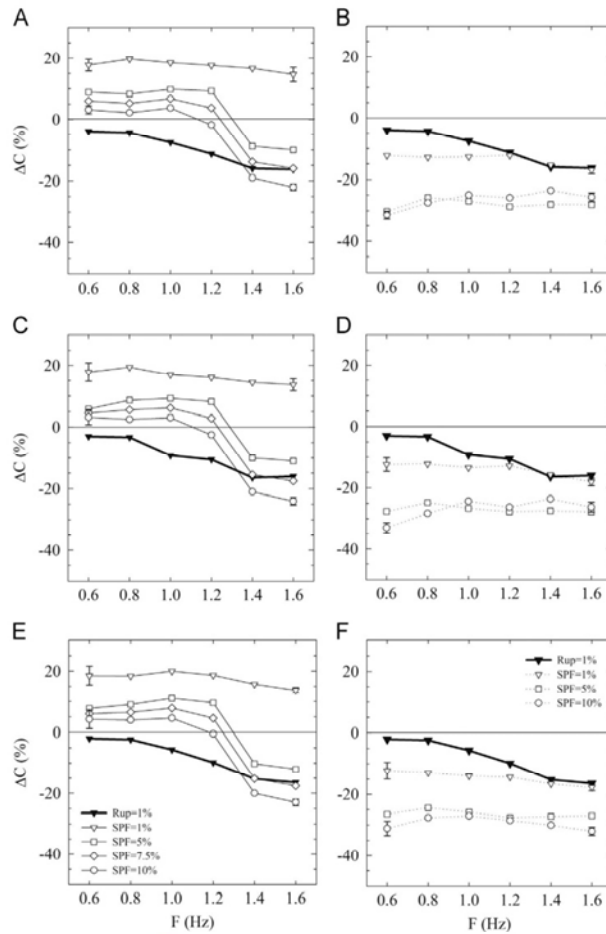


Fig. 6. Relationship between ΔC (%), calculated using Eq. (7), for the particle range of diameters from 6.0 to 100 μm with the frequency for the different canopy densities (SRP). The representation of the results was the same like that used in Fig. 4. (a) SRV, $z/h_v=1.6$, (b) SFV, $z/h_v=1.6$, SRV, $z/h_v=1.6$, (c) SRV, $z/h_v=1.1$, (d) SFV, $z/h_v=1.1$, (e) SRV, $z/h_v=0.4$ and (f) SFV, $z/h_v=0.4$.

found to be positive, except for canopy densities of 7.5% and 10%, which at very high frequencies presented negative ΔC . The lower the canopy density, the higher the resuspension of particles, at both $z/h_v=1.6$ (Fig. 5A) and $z/h_v=1.1$ (Fig. 5C). In addition, ΔC exhibited a tendency to decrease as frequencies increased. Inside the canopy the results presented the same tendency (Fig. 5E), with ΔC increasing with decreasing canopy density but declining at increasing wave frequencies. On the contrary, and as shown in Fig. 5B, D and F, for the flexible canopy experiments, ΔC above and within the canopy was always negative, and with a slight decrease of ΔC at increasing frequencies, for frequencies above 1 Hz. ΔC for the real plant model (*R. maritima*), was closer to ΔC obtained for the flexible canopy than to ΔC obtained for the rigid canopy, at the same 1% density of flexible vegetation.

Fig. 6 shows the same results as Fig. 5, but for large particles in the range between 6.0 and 100 μm . The resuspension of the 6.0 to 100 μm particles was found to be larger for the rigid vegetated experiments with the lowest density of 1% (Fig. 6A) and also, for the experiments with densities of 5%, 7.5% and 10% for wave frequencies ≤ 1.2 Hz, at all depths. In contrast, for the higher canopy densities, ΔC was found to be negative for the highest frequencies of 1.4 and 1.6 Hz, i.e. the higher the density, the higher the ΔC . Fig. 6A, C and E show that these results were found both above and inside the canopy bed. For the flexible canopies, the largest negative values of ΔC were found for the largest SRP 5% and 10%. As was also found for the small particles (Fig. 5B, D and F), ΔC was found to be largely negative when increasing the density of the canopy bed. No significant differences of ΔC were found with

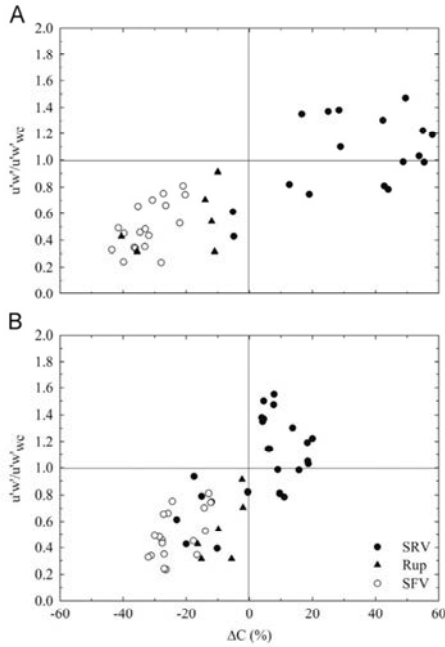


Fig. 7. Ratio between $u'w'$ for vegetated experiments and $u'w'$ for the vegetation-free experiments against ΔC , for experiments carried out with the three canopy models: (a) 2.5 to 6.0 μm particles and (b) 6.0 to 100 μm particles.

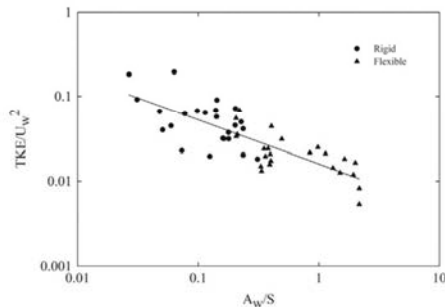


Fig. 8. TKE/U_w^2 vs. A_w/S , calculated at $z/h_c=0.4$ for both rigid and flexible vegetation.

depths, indicating a homogeneous vertical distribution of particles. ΔC for the real canopy (*R. maritima*) also mimicked the results obtained in the flexible canopy, at the same canopy density of flexible vegetation of 1%.

ΔC for the 2.5 to 6.0 μm particles (Fig. 7A) and for the 6.0 to 100 μm particles (Fig. 7B), was then compared to the ratio between the Reynolds stress ($u'w'$) with the presence of a canopy, and the Reynolds stress ($u'w'_{wc}$) for experiments without a canopy at $z/h_c=0.4$ for all the experiments carried out. For both particle size ranges, $u'w'/u'w'_{wc}$ below 1 resulted in negative ΔC (Fig. 7A and B),

showing that a low concentration of particles in suspension was found compared to the vegetation-free canopy experiments. In contrast, for the case with $u'w'/u'w'_{wc}$ above 1, ΔC was positive. A larger ΔC (up to 60%) was found for the smaller particle range (Fig. 7A), compared to the ΔC for the largest particle range, up to 20% (Fig. 7B), for the same $u'w'/u'w'_{wc}$. In general, experiments with flexible and natural canopies presented $\Delta C < 0$, i.e. a lower resuspension in the vegetated experiments than with the vegetation-free experiments. In contrast, the rigid vegetation was the only one with $\Delta C > 0$ for the majority of experiments.

4. Discussion

4.1. Canopy scale turbulence distribution

Developing models to predict flows inside natural canopies is challenging due to the difficulties in incorporating the complexity of the canopy geometry and the broad range of length scales. While some models approximate vegetation with higher bottom friction factors (Möller et al., 1999), the majority implement an empirical drag coefficient to estimate drag forces along the plant (Mendez and Losada, 2004). Taking into account that Lowe et al. (2005, 2005b) showed that A_w/S was the most relevant parameter affecting the attenuation of the flow inside the canopy, we hypothesize that the TKE inside the canopy can be written in the following form:

$$\frac{TKE}{U_w^2} = k \left(\frac{A_w}{S} \right)^a \quad (8)$$

Fig. 8 shows the best fit of the data with $k=0.016$, $a=-0.0519$ ($R^2=0.6114$, 99% confidence), where it can also be seen that highest values of the TKE correspond to the rigid plants. Here the TKE at $z=5$ cm was considered representative for the behaviour of the TKE within the canopy.

Although several studies have pointed out that canopies provide sheltering, showing a decrease in the TKE compared to canopy-free environments, our results show that sheltering was attained for all cases in the flexible canopy, while the net effect on rigid cylinders was dependent on both canopy density and wave frequency. Inside the rigid canopy the TKE was larger compared to the equivalent experiments without vegetation, for the cases of $SPF=1\%$ (i.e. 128 shoots/ m^2) for all frequencies, and for the higher densities (5%, 7.5% and 10%) and the lower frequencies from 0.6 to 1.2 Hz (Fig. 4). We attributed the increase in TKE to the generation of stem-wake turbulence, in accordance with the results obtained by Pujol et al. (2013). Fig. 9 shows the plant Reynolds number calculated as $Re_p=DU_w/\nu$, where D is a stem parameter scale (the diameter of the cylinders for the rigid canopy or the blade width for the flexible canopy) and ν is the kinematic viscosity. Experiments with $Re_p > 250$ and $\Delta TKE > 0$ corresponded to the rigid canopy environments with low wave frequencies and high SPF canopies.

For the rigid canopy there were also cases where $\Delta TKE < 0$ (Fig. 4) indicating that these canopy configurations might provide sheltering depending on both the wave velocity and the SPF . These cases correspond to the highest plant densities ($SPF=5\%$, 7.5% and 10%, i.e. 640, 960 and 1280 shoots/ m^2) and highest wave frequencies ($F=1.4$ and 1.6 Hz). In these cases maximum values of ΔTKE were found at the top of the canopy corresponding to a zone characterized by maximum shear as described by Pujol et al. (2013). As pointed out by Hendriks et al. (2008), in the region of the canopy-water interface, turbulent vertical transport of momentum is enhanced due to augmented turbulent shear stresses. Koftis et al. (2013) found that for a *Posidonia oceanica* meadow of 360 stems/ m^2 , at the positions above the top of the

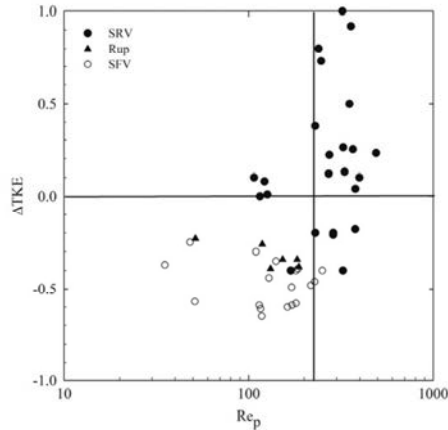


Fig. 9. Relationship between ΔTKE and the stem Reynolds number (Re_p) for the different canopy models used at $z/h_v=0.4$.

seagrass ($z/h_v=1.09$ and 1.45), the energy at the peak frequencies of the spectrum were amplified, revealing the effects attributed to the movement of the plant leaves.

For the flexible canopies $Re_p < 250$, and no TKE production was observed. Therefore, all the energy in the mean flow was dissipated without turbulence production. Indeed, results showed that inside the flexible vegetation canopy, ΔTKE decreased with canopy density, with no minimum threshold required to initiate wave velocity attenuation through a reduction in the TKE compared with the non-vegetated case, in accordance with other studies that found that the canopy density enhanced wave height reduction and therefore wave attenuation (Gambi et al., 1990; Fonseca and Cahalan, 1992; Granata et al., 2001; Neumeier and Ciavola, 2004; Bouma et al., 2005; Manca et al., 2012; Koftis et al., 2013).

4.2. Sediment resuspension within canopies

Studies show that resuspension is controlled by the bottom shear stress, that can be computed by estimates of $\langle u'w' \rangle$ within the constant stress region of the bottom boundary layer and extrapolated to the bed, which is normally well correlated with the TKE (Hansen and Reidenbach, 2012, 2013). Computation of the current shear stress within vegetation is not well described, especially in the presence of wave activity, but under unidirectional currents, a useful parameterization is through estimates of the near-bottom TKE (Widdows et al., 2008). In the present study, a linear correlation ($\langle u'w' \rangle = -0.033TKE$ with $r^2=0.5676$ (99% confidence) was found.

Our results showed that rigid canopies were not always effective in promoting the protection against resuspension. Cases with $\Delta C > 0$ corresponded to rigid canopies where resuspension was enhanced. Only a few cases for rigid canopies had $\Delta C < 0$ (higher frequencies and higher SPF). On the contrary, for all the flexible canopies and for the *R. maritima* $\Delta C < 0$, showing that flexible plants were able to reduce the sediment resuspension.

In the cases with $\Delta C > 0$, the energy from the main flow is dissipated via the production of the TKE ; however for flexible canopies energy from the main flow dissipates without producing TKE .

Observations made by MacVean and Lacy (2014) indicate that wave shear stresses at the bed led to high resuspension and sediment-induced stratification, and the Stokes drift velocity as well as wind stress at the water surface increased mean shear within the water column. The correlation between wave attenuation and resuspension of particles was also reported by Gruber and Kemp (2010). These authors linked an amount of wave attenuation, 37% in a submerged bed of *Stuckenia pectinata*, with a 60% reduction of total suspended solids, during a period of peak plant biomass. In the present study, the mean wave attenuation through the range of frequencies studied was 20% for the densest rigid vegetation model and 15% for the densest flexible vegetation model.

5. Conclusions

In summary, this study showed that the resuspension of sediments in submerged canopies under progressive waves was reduced for both the flexible and *R. maritima* vegetation canopies (encompassing both sparse and dense canopies) at all the wave frequencies studied. This reduction also coincided with a reduction in TKE and bottom shear stress well inside the canopy.

In contrast, the net effect on resuspension due to rigid cylinders depends on the SPF . Rigid cylinders enhanced sediment resuspension for all wave conditions within sparse vegetation (1% SPF) via an increase of TKE . For denser cases ($SPF=5, 7.5$ and 10%), enhancement in resuspension occurred for wave frequencies lower than 1.2 Hz, while resuspension was damped at higher frequencies. We attribute such a difference to the turbulent wake generation at $Re_p > 250$. Flexible canopies along with the densest rigid canopies at high frequencies, showed the ability to diminish sediment resuspension and therefore, their ability to diminish the erosion of the sediment at the bottom of the bed. In these cases the energy from the main flow dissipates without producing TKE .

The results presented in this paper were obtained in a laboratory using monochromatic waves and in the absence of currents. Further experimental investigations are needed to corroborate our main results to field conditions where the combination of currents and waves of varying frequencies can add considerable complexity to the problem. Also, although the generation of the TKE for rigid cylinders at $Re_p > 250$ has been documented, the physical mechanisms involved in the way that flexible plants dissipate the energy from the main flow is still not understood; because of this, vegetation models of the flexible plants do not take into account the movement of the stems. Further work is needed to understand this movement, which is crucial to evaluate the way in which the plants dissipate the energy.

Acknowledgments

This research was funded by the Ministerio de Economía y Competitividad of the Spanish Government, through grant CGL 2010-17289, and by the Biodiversity Foundation through grant AIN2011B to the Group of Environmental Physics of University of Girona. Àlex Ros was supported by the research fellowship BR2012/39 from the University of Girona.

References

- Blott, S.J., Pye, K., 2012. Particle size scales and classification of sediment types based on particle distributions: review and recommended procedures. *Sedimentology* 59, 2071–2096.
- Bouma, T.J., De Vries, M.B., Low, E., Peralta, G., Tancoz, C., Van de Koppel, J., Herman, P.M.J., 2005. Trade-offs related to ecosystem engineering: a case study on stiffness of emerging macrophytes. *Ecology* 86, 2187–2199.
- Dean, R.G., Dalrymple, R.A., 1991. *Water Wave Mechanics for Engineers and Scientists*, 1st ed. World Scientific Publishing, Singapore.

- Folkard, A.M., 2005. Hydrodynamics of model *Posidonia oceanica* patches in shallow water. *Limnol. Oceanogr.* 50, 1592–1600.
- Fonseca, M.S., Cahalan, J.A., 1992. A preliminary evaluation of wave attenuation by four species of seagrass. *Estuarine Coast. Shelf Sci.* 35, 565–576.
- Gambi, M.C., Nowell, A.R.M., Jumars, P.A., 1990. Flume observations on flow dynamics in *Zostera marina* (eelgrass) beds. *Mar. Ecol. Prog. Ser.* 61, 159–169.
- Ghisalberti, M., Nepf, H.M., 2002. Mixing layers and coherent structures in vegetated aquatic flows. *J. Geophys. Res.* 107, C2(3–1–3–11).
- Granata, T.C., Serra, T., Colomer, J., Casamitjana, X., Duarte, C.M., Gacia, E., 2001. Flow and particle distributions in a nearshore seagrass meadow before and after a storm. *Mar. Ecol. Prog. Ser.* 218, 95–106.
- Gruber, R.K., Kemp, W.M., 2010. Feedback effects in a coastal canopy-forming submersed plant bed. *Limnol. Oceanogr.* 55 (6), 2285–2298.
- Hansen, J., Reidenbach, M., 2012. Wave and tidally driven flows in eelgrass beds and their effect on sediment suspension. *Mar. Ecol. Prog. Ser.* 448, 271–287.
- Hansen, J., Reidenbach, M., 2013. Seasonal growth and senescence of a *Zostera marina* seagrass meadow alters wave-dominated flow and sediment suspension within a coastal bay. *Estuaries Coasts* 36, 1099–1114.
- Hendriks, I.F., Sintes, T., Bouma, T.J., Duarte, C.M., 2008. Experimental assessment and modeling evaluation of the effects of the seagrass *Posidonia oceanica* on flow and particle trapping. *Mar. Ecol. Prog. Ser.* 356, 163–173.
- Houwing, E.J., 1999. Determination of the critical erosion threshold of cohesive sediments on intertidal mudflats along the Dutch Wadden sea Coast. *Estuarine Coast. Shelf Sci.* 49, 545–555.
- Infantes, E., Orfila, A., Simarro, G., Terrados, J., Luhar, M., Nepf, H., 2012. Effect of seagrass (*Posidonia oceanica*) meadow on wave propagation. *Mar. Ecol. Prog. Ser.* 456, 63–72.
- Koch, E.W., 2001. Beyond light: physical, geological, and geochemical parameters as possible submersed aquatic vegetation habitat requirements. *Estuaries* 24, 1–17.
- Koftis, T., Prinos, P., Stratigaki, V., 2013. Wave damping over artificial *Posidonia oceanica* meadow: a large-scale experiment study. *Coastal Eng.* 73, 71–83.
- Leonard, L.A., Wren, P.A., Beavers, R.L., 2002. Flow dynamics and sedimentation in *Spartina alterniflora* and *Phragmites australis* marshes of the Chesapeake Bay. *Wetlands* 22, 415–424.
- Lopez, F., Garcia, M., 1998. Open-channel flow through simulated vegetation: Suspended sediment transport modeling. *Water Resour. Res.* 34, 2341–2352.
- Lowe, R.J., Koseff, J.R., Monismith, S.G., 2005a. Oscillatory flow through submerged canopies. Part 1. Velocity structure. *J. Geophys. Res.* Oceans 110, C10016(1–17).
- Lowe, R.J., Koseff, J.R., Monismith, S.G., Falter, J.L., 2005b. Oscillatory flow through submerged canopies. Part 2. Canopy mass transfer. *J. Geophys. Res.* Oceans 110, C10017(1–14).
- Luhar, M., Coutu, S., Infantes, E., Fox, S., Nepf, H., 2010. Wave-induced velocities inside a model seagrass bed. *J. Geophys. Res.* 115, C12005(1–15).
- MacVean, L.J., Lacy, J.R., 2014. Interactions between waves, sediment, and turbulence on a shallow estuarine mudflat. *J. Geophys. Res.* Oceans 119, 1534–1553.
- Manca, E., Cáceres, I., Alsina, J.M., Stratigaki, V., Townend, I., Amos, C.L., 2012. Wave energy and wave-induced flow reduction by full-scale model *Posidonia oceanica* seagrasses. *Cont. Shelf Res.* 50–51, 100–116.
- Mendez, F.J., Losada, I.J., 2004. An empirical model to estimate the propagation of random breaking and nonbreaking waves over vegetation fields. *Coastal Eng.* 51, 103–118.
- Möller, I., Spencer, T., French, J.R., Leggett, D.J., Dixon, M., 1999. Wave transformation on salt marshes: a field and numerical study from Norfolk, England. *Estuarine Coast. Shelf Sci.* 49, 411–426.
- Monismith, S., 2007. Hydrodynamics of coral reefs. *Annu. Rev. Fluid Mech.* 39, 37–55.
- Nepf, H., Vivoni, E.R., 2000. Flow structure in depth-limited, vegetated flow. *J. Geophys. Res.* Oceans 105, 28547–28557.
- Nepf, H., Ghisalberti, M., White, B., Murphy, E., 2007. Retention time and dispersion associated with submerged aquatic canopies. *Water Resour. Res.* 43, W04422(1–10).
- Neumeier, U., Ciavola, P., 2004. Flow resistance and associated sedimentary processes in a *Spartina maritima* salt-marsh. *J. Coast. Res.* 20, 235–447.
- Neumeier, U., Amos, C.L., 2006. Turbulence reduction by the canopy of coastal *Spartina* salt-marshes. *J. Coast. Res.* 1 (39), 433–439.
- Neumeier, U., 2007. Velocity and turbulence variations at the edge of saltmarshes. *Cont. Shelf Res.* 27, 1046–1059.
- Oguz, E., Elginöz, N., Koroglu, A., Kabdasli, M.S., 2013. The effect of reed beds on wave attenuation and suspended sediment concentration. *J. Coast. Res.* 65, 356–361.
- Paul, M., Bouma, T.J., Amos, C.L., 2012. Wave attenuation by submerged vegetation: combining the effect of organism traits and tidal current. *Mar. Ecol. Prog. Ser.* 444, 31–41.
- Pujol, D., Colomer, J., Serra, T., Casamitjana, X., 2010. Effect of submerged aquatic vegetation on turbulence induced by an oscillating grid. *Cont. Shelf Res.* 30, 1019–1029.
- Pujol, D., Serra, T., Colomer, J., Casamitjana, X., 2013. Flow structure in canopy models dominated by progressive waves. *J. Hydrol.* 486, 281–292.
- Serra, T., Casamitjana, X., Colomer, J., Granata, T.C., 2002. Observations of the particle size distribution and concentration in a coastal system using an in situ laser analyzer. *Mar. Technol. Soc. J.* 36, 59–69.
- Serra, T., Colomer, J., Julià, R., Soler, M., Casamitjana, X., 2005. Behaviour and dynamics of a hydrothermal plume in lake Banyoles, Catalonia, NE Spain. *Sedimentology* 52, 795–808.
- Terrados, J., Duarte, C.M., 2000. Experimental evidence of reduced particle resuspension within a seagrass (*Posidonia oceanica* L.) meadow. *J. Exp. Mar. Biol. Ecol.* 243, 45–53.
- Türker, U., Yagci, O., Kadbasli, M.S., 2006. Analysis of coastal damage of a beach profile under the protection of emergent vegetation. *Ocean Eng.* 33, 810–828.
- van Katwijk, M.M., Bos, A.R., Hermus, D.C.R., Suykerbuyk, W., 2010. Sediment modification by seagrass beds: mudification and sandification induced by plant cover and environmental conditions. *Estuarine Coast. Shelf Sci.* 89, 175–181.
- van Rijn, L.C., 2007. Unified view of sediment transport by currents and waves. I: Initiation of motion, bed roughness, and bed-load transport. *J. Hydraul. Eng.* 133, 649–667.
- Venier, C., Figueiredo da Silva, J., McLelland, S.J., Duck, R.W., Lanzoni, S., 2012. Experimental investigation of the impact of macroalgal mats on flow dynamics and sediment stability in shallow tidal areas. *Estuarine Coast. Shelf Sci.* 112, 52–60.
- Ward, L.G., Kemp, W.M., Boynton, W.R., 1984. The influence of waves and seagrass communities on suspended particulates in an estuarine embayment. *Mar. Geol.* 59, 85–103.
- Wiberg, P.L., Sherwood, C.R., 2008. Calculating wave-generated bottom orbital velocities from surface wave parameters. *Comput. Geosci.* 34, 1243–1262.
- Widdows, J., Pope, N.D., Brinsley, M.D., Asmus, H., Asmus, R.H., 2008. Effects of seagrass beds (*Zostera noltii* and *Z. marina*) on near-bed hydrodynamics and sediment resuspension. *Mar. Ecol. Prog. Ser.* 358, 125–136.